PROFILING THE MULTI-OMIC RESPONSE TO MITOCHONDRIAL PROTEASE CLPP ACTIVATION IN TRIPLE-NEGATIVE BREAST CANCER CELLS

Emily M.J. Fennell

A dissertation submitted to the faculty at the University of North Carolina at Chapel Hill in partial fulfillment of the requirements for the degree of Doctor of Philosophy in the Department of Pharmacology in the School of Medicine.

Chapel Hill
2022

Approved By:

Lee M. Graves

Channing J. Der

Henrik G. Dohlman

Jonathan C. Schisler

Nathaniel J. Moorman

ABSTRACT

Emily M.J. Fennell: Profiling the Multi-omic Response to Mitochondrial Protease ClpP Activation in Triple-Negative Breast Cancer Cells
(Under the direction of Lee M. Graves)

ONC201 and structural analogs (TR compounds) have been recently discovered as novel pharmacological activators of the mitochondrial protease ClpP. We were the first to publish the target of these compounds, as well as the ClpP-dependent induction of the integrated stress response (ATF4, CHOP). We have shown that the novel TR compounds are more potent than ONC201 at both *in vitro* activation of ClpP and growth inhibition in triple-negative breast cancer (TNBC) cells. Identification of significant mitochondrial effects following ONC201 treatment led us to investigate the effects of ONC201 and TR compounds on mitochondrial protein expression and oxidative phosphorylation, which we found to be significantly downregulated by pharmacological ClpP activation. Additionally, *in vivo* TR compound studies indicate a similar mechanism to effects observed *in vitro* (e.g., mtDNA and TFAM loss) while also being a well-tolerated treatment with optimized pharmacokinetic profiles, indicating potential for future clinical use. To investigate (1) the complete mechanism of action of ClpP activators leading to growth inhibition and (2) potential metabolic vulnerabilities generated by ClpP activation, multi-omic (proteomic, transcriptomic, and metabolomic) data was collected for TNBC cells following pharmacological ClpP activation. The multi-omic profile of these cells was analyzed using MetaCore, which revealed significant up- and downregulation across all three -omics datasets. Significantly perturbed pathways included amino acid, pyrimidine, citrulline, and heme biosynthesis, as well as tricarboxylic acid (TCA) cycle function. Identification of these perturbations confirms the multi-nodal effects of ClpP activation, as well as identifies potential metabolic vulnerabilities to be utilized in TR compound co-treatment development. This data can be further utilized in the future, as well as expanded upon, to elucidate the complete mechanism of action of ClpP activators on cell proliferation.

ACKNOWLEDGEMENTS

First and foremost, I would like to thank Dr. Lee Graves for his constant encouragement, invaluable advice, and his unwavering belief that I have the intelligence, work ethic, and critical thinking skills to be a scientist. Thank you for challenging me to be a well-rounded scientist and allowing me to pursue research directions that were unknown to both of us, and for encouraging me to be a well-rounded person outside of lab and reminding me to take time off to foster my creative endeavors and pursue my hobbies. Lee, having you as an advisor has been a wonderful experience that I would not change. To members of the Graves Lab, both past and present, I owe a huge debt of gratitude. You were all so welcoming to a brand-new graduate student, and I appreciate your willingness to help me regardless of how many obvious questions I asked. Coming to work every day would not have been as easy as it was without your advice, collaboration, and friendship. Ed Iwanowicz and Madera Therapeutics, thank you for giving myself and the Graves Lab the exciting opportunity to work on the TR compounds—without these compounds, we would not have much of this work. To my committee—Channing, Henrik, Schis., and Nat—I am incredibly grateful to have had you all on my committee. The support and advice that I received from you all in committee meetings or through collaborations on research projects is so appreciated and will always be remembered. To the Department of Pharmacology: I could not have chosen a better department. I am forever grateful for the comradery, the laughs, the endlessly fun events, and the learning environment that was essential for cultivating my skills as a scientist.

To my friends: thank you for everything from the coffee dates and board game nights to practice talks and late-night study sessions. Thank you for every time you attended a trivia night with me, even if it wasn't really your thing. Thank you for the constantly supply of jokes and memes to brighten up my day. Thank you for your unwavering support, even though you may not have been sure of what exactly I was doing for the last five years. Linda's Bar and Grill: thank you for late night tater tots, incredible trivia nights, and all the friends I made here. I'm not sure if any of you will ever read this, but I will always cherish the memories we made. To the Brody Family: thank you for taking me in as one of your own

during these past four years. I am eternally grateful for your hospitality, friendship, and support that you have so generously given to me. You are all a second family to me.

Leo, I am so lucky to have had you as a support during this stage of my life. You always celebrated my accomplishments and offered advice and encouragement during difficult times. You listened to every time I complained about a failed experiment or every time I was stressed over a deadline and always offered solutions and kind words. Thank you for making me watch more movies, read more books, and go to Raleigh more often (and for being my GPS while we're there). Thank you for being the taste-tester for all the baked goods I made when I was stressed and listening to me talk about my houseplants and my garden. There is nobody else I could imagine going through graduate school with—I love you endlessly.

To my family, thank you for everything you have done for me throughout my life. Michael, thanks for being a great younger (but taller) brother. Thanks for providing tons of laughs and always being up for baking something or going to Schenck Forest with me when I needed to do something fun. A very special thank you to my parents, Susan and Tim. Thank you for being such incredible parents for 27 years. You have both been amazing role models, both as scientists and human beings, for my whole life. Many folks would assume that I got my love for science early on from two parents that approached every situation with the scientific method, and they would be correct. All the times we made crystals out of sugar, vinegar and baking soda volcanoes, compasses out of paperclips and magnets, and other science experiments just for fun was another step towards me pursuing a Ph.D. I would not be here today without your guidance and support.

TABLE OF CONTENTS

LIST OF TABLES

LIST OF FIGURES

LIST OF ABBREVIATIONS

ACO2	Aconitase, mitochondrial
ADEP	acyldepsipeptide
Akt/PKB	Ak strain transforming kinase/protein kinase B
AML	Acute myeloid leukemia
ATF4	Activating transcription factor 4
ATF5	Activating transcription factor 5
ATP	Adenosine triphosphate
AUC	Area under the curve
BCL-2	B-cell lymphoma 2
BSA	Bovine serum albumin
cDNA	Complementary DNA
CHOP	C/EBP homology protein
ClpP	Mitochondrial matrix caseinolytic protease, proteolytic subunit
ClpX	Mitochondrial matrix caseinolytic peptidase, chaperone subunit X
ClpXP	Mitochondrial matrix ClpX-ClpP complex
Cmax	Maximal plasma concentration
CRISPR	Clustered regularly interspaced short palindromic repeats
CRISPRi	CRISPR interference
DMEM	Dulbecco’s Modified Eagle Medium
DMEM:F-12	1:1 DMEM: Nutrient Mixture F-12
DMSO	Dimethylsulfoxide
DPBS	Dulbecco’s phosphate buffered saline
DR4	Death receptor 4
DR5	Death receptor 5
DRD2	Dopamine receptor D2
DRD3	Dopamine receptor D3
DTT	Dithiothreitol

ECAR	Extracellular acidification rate
ECL	Enhanced chemiluminescence
EDTA	Ethylenediaminetetraacetic acid
EGTA	Ethylene glycol-bis(β-aminoethyl ether)-*N,N,N',N'*-tetraacetic acid
eIF2α	Eukaryotic translation initiation factor 2α
ER	Estrogen receptor
ETC	Electron transport chain
F%	Oral bioavailability
FBS	Fetal bovine serum
FCCP	Trifluoromethyoxy carbonylcyanide pheylhydrazone
HER2	Human epidermal growth factor receptor 2
HMBC	heteronuclear multiple-bond correlation
HSP60	Heat shock protein 60
IC_{50}	Inhibitory concentration 50
IDH1/2	Isocitrate dehydrogenase 1/2
ISR	Integrated stress response
K_d	Equilibrium dissociation constant
KD	Knockdown
KO	Knockout
LC	Liquid chromatography
LONP	Lon protease homolog, mitochondrial
MALDI	Matrix-assisted laser desorption/ionization
MCL	Mantle cell lymphoma
mRNA	Messenger RNA
mtDNA	Mitochondrial DNA
MS	Mass spectrometry
NCI	National Cancer Institute
NEM	Nuclear encoded mitochondrial

NMR	Nuclear magnetic resonance
OCR	Oxygen consumption rate
OXPHOS	Oxidative phosphorylation
p53	Tumor protein 53
PAGE	Polyacrylamide gel electrophoresis
PARP	Poly(ADP-ribose) polymerase
PCR	Polymerase chain reaction
PK	Pharmacokinetic
POLRMT	DNA-directed RNA polymerase, mitochondrial
PR	Progesterone receptor
PVDF	Polyvinyl difluoride
RIPA	Radioimmunoprecipitation assay
RNA	Ribonucleic acid
RNAi	RNA interference
RU	Response units
RT	Reverse transcription
RT	Room temperature
SAR	Structure-activity relationship
SDHA/B	Succinate dehydrogenase A/B
SDS	Sodium dodecyl sulfate
SEM	Standard error of mean
sgRNA	Single guide RNA
siRNA	Small interfering RNA
STS	Staurosporine
$t_{1/2}$	Elimination half-life
TBST	Tris buffered saline, Tween-20
TCA	Trichloroacetic acid
TCA Cycle	Tricarboxylic acid Cycle

TFAM	Transcription factor A, mitochondrial
TNBC	Triple-negative breast cancer
TOF	Time-of-flight
TRAIL	TNF-related apoptosis-inducing ligand
TUFM	Elongation factor Tu, mitochondrial
UPR^{mt}	Mitochondrial unfolded protein response
WT	Wildtype

CHAPTER 1: INTRODUCTION

1.1 Discovery of Imipridone Compounds

Current Cancer Therapies

Cancer is the second leading cause of death in the United States at an estimated 21% of total deaths in 2019[1]. In women, breast cancer accounts for the most new cases (31%) and the second most cancer-related deaths (15%)[2]. The current first line therapies for many cancers include surgery, radiation, and traditional chemotherapies, though targeted treatments are becoming more widely used due to their increased selectivity and reduced systemic side effects[3–5]. Targeted therapies include antibodies conjugated to anticancer drugs (e.g., trastuzumab for HER2+ breast cancers), prodrugs that are converted to active forms by cancer cells, and small molecules with specific targets whose function are essential to cancer cell survival, and hormone therapies that inhibit estrogen receptor (ER) and progesterone receptor (PR) (e.g., tamoxifen)[3,5–8]. However, triple-negative breast cancer (TNBC), characterized by the lack of ER, PR, and HER2, is considered the most aggressive and difficult to treat subtype due to increased rates of metastasis and a dearth of available targeted treatments[3,9].

Identification and Proposed Mechanisms of Action

The structure of ONC201, the parent compound of the imipridone group, was first described by Stähle et al as an imidazolinopyrimidinone containing a linear tricyclic core in 1973[10]. In 2013, as part of a TNF-related apoptosis-inducing ligand (TRAIL) induction screen by using the National Cancer Institute (NCI) Diversity Set II of small molecules, TIC10 was identified to significantly upregulate TRAIL induction[11]. TRAIL induction as an anti-cancer therapy has been of significant recent interest due to its ability to act as a Death Receptor 4/5 (DR4/DR5) agonist, inducing apoptosis[12]. TIC10 was selected for further investigation due to its ability to upregulate TRAIL expression independent p53, a positive regulator of TRAIL, due to the potential to avoid cancer cell resistance through inactivation of p53[11]. The proposed mechanism of ONC201 induction of TRAIL was through inhibition of Akt and ERK, which in turn prevents the phosphorylation of FOXO3a, allowing it to translocate to the nucleus to upregulate TRAIL

production (Fig. 1.1A). In 2014, Jacob et al. attempted to synthesize ONC201 to further investigate its effects on TRAIL induction. Interestingly, synthesis following methods reported for the linear structure of ONC201 rendered an inactive compound. However, ONC201 obtained from the NCI was able to induce TRAIL mRNA expression in RAW 264.7 cells. Heteronuclear multiple-bond correlation (HMBC) nuclear magnetic resonance (NMR) spectroscopy and X-ray crystallographic analysis of the active ONC201 identified an angular tricyclic core[13] (Fig. 1.1).

ONC201 was also predicted to be a dopamine receptor type D2/D3 (DRD2/DRD3) antagonist through *in silico* and *in vitro* experiments[14] (Fig. 1.1B). This is further supported by the identification of prolactin stimulation in human clinical trial participants[15]. The mechanism by which ONC201-mediated DRD2 antagonism inhibits cell growth or induces apoptosis has been proposed to be through the observed inhibition of ERK and AKT[16]. However, dopamine receptor expression is variable across cell lines (including those responsive to ONC201 treatment), and knockout of DRD2/DRD3 did not alleviate effects of ONC201 in treated cells[17]. Further investigation into the mechanism of ONC201 revealed that ONC201 treatment somehow activates the integrated stress response (ISR), classified by the induction of activating transcription factor 4 (ATF4) and C/EBP homology protein (CHOP)[18,19](Fig. 1.1C). Canonical activation of the integrated stress response (ISR) occurs through activation of eIF2α kinases (PERK, PKR, GCN2, HRI) and eIF2α[20,21] and ONC201 treatment demonstrated activation of PKR and HRI activity in HCT116 cells[18], however, activation of eIF2α was not observed in hematological malignancy cell lines[19].

While these compounds showed evidence of mechanisms involving p53-independent TRAIL induction, evidence of a TRAIL and DR4/5-independent mechanism came to light in TNBC and HER2-positive breast cancer cells[22]. Greer et al. demonstrated ONC201 treatment inhibited cell growth in multiple models of breast cancer, however, significant induction of TRAIL or DR4/5 mRNA was not detected following treatment, consistent with previously reported data in hematological malignancies[19]. While others have reported caspase-induction following ONC201 treatment, this study demonstrated that the pan-caspase inhibitor zVAD-FMK did not alleviate ONC201 induced toxicity[22]. However, ONC201 treatment was identified to induce CHOP mRNA expression in TNBC cells. Further, Greer et al. showed DRD2 mRNA was not detected in tested breast cancer cells, indicating that DRD2 may not be the target

shared amongst ONC201-sensitive cancer types[22]. While evidence for some previously reported mechanisms was not evident in breast cancer models, Greer et al. showed ONC201 resulted in decreased mitochondrial respiration and increased sensitivity to drug when cultured in galactose, indicating that ONC201 treated TNBC cells were reliant on glycolysis for ATP generation. These cells showed significant loss of mitochondrial DNA (mtDNA), mitochondrial fragmentation, and loss of nuclear-encoded mitochondrial (NEM) genes (e.g., TFAM) that are required for stabilization of mtDNA[22]. This demonstrates a clear disruption of mitochondrial function in cancer cells, however, these same phenotypes were not reported in normal fibroblast cells[22].

Efficacy in Clinical Trials

Before the target of ONC201 was discovered, its potent anticancer activity resulted in an FDA fast-track designation to clinical trials. The initial discovery of ONC201's anticancer potential identified the compound as a surface TRAIL inducer in multiple cancer cell lines, including the $p53^{-/-}$ HCT116 colorectal cell line[11]. Additionally, this study identified an increase in sub-G_1 DNA accumulation and decreased colony formation in cancer cell lines, but growth was not inhibited in normal fibroblasts, indicating that this anticancer effect is specifically targeting cancer cells[11]. Further, this study showed ONC201 as inducing tumor stasis or regression in *in vivo* models, while also observing little toxicity across multiple doses. This provided evidence of a therapeutic window for ONC201, increasing its validity as a clinical candidate.

To date, ONC201 has been in several clinical trials for aggressive cancers including glioblastoma, breast, ovarian, and hematological malignancies[23]. The first published Phase I clinical trial data of ONC201 showed significant loss of tumor burden in participants with refractory solid tumors on a low-frequency dosing schedule (once per 21 days) while also exhibiting few reported side effects. Additional clinical trial data for refractory solid tumors and neuroendocrine tumors confirm that ONC201 is well tolerated at multiple doses and in more frequent dosing schedules (up to twice per 7 days)[23–26] while showing partial response to treatment in some patients. Clinical trials of ONC201 have also shown increased immune stimulatory activity in patients, as indicated by increases in markers such as infiltration of granzyme B+ and CD56+ cells, serum perforin, and circulating natural killer (NK) cells in refractory solid tumors malignancies[23,27]. Additionally, Phase II clinical trials of ONC201 in wildtype IDH1/2

glioblastoma have identified ONC201 as a potential efficacious treatment for H3 K27M-mutant glioblastoma, with one patient showing a 96% reduction in overall tumor size[15,23].

1.2 Discovery of Imipridone and Analog Compounds' Target

The development of ONC201 analogs (called TR compounds) by Madera therapeutics created more potent inhibitors of cell growth compared to ONC201[28]. Further, the development of the ONC201 analog TR-80 enabled the immobilization of a structurally similar compound to an agarose bead that could be used to identify ONC201 binding partners. Mass spectral analysis of proteins from whole cell lysates identified to bind to TR-80 in the absence, but not presence, of free TR-80 lead to the discovery of mitochondrial caseinolytic protease P (ClpP) as the target of ONC201 and related analogs[28] (Fig. 1.1D). ONC201 binding to and activating ClpP was further confirmed through a compound screen for *in vitro* ClpP activation[29]. Following the identification of ONC201 and TR compounds as ClpP binding partners, we investigated how these compounds affected ClpP and found that the proteolytic activity of purified recombinant human ClpP was activated by ONC201 or TR compound treatment, as measured by FITC[28]. Further, direct binding of ONC201 to ClpP was confirmed through co-crystallization of ONC201 and purified ClpP[29].

1.3 Role of ClpP

Structure

ClpP is a mitochondrial serine protease that serves as the proteolytic subunit of the complex ClpXP, which also consists of the ATP-dependent unfoldase ClpX[30–32]. ClpX acts by opening the axial pore of ClpP and unfolding mitochondrial proteins that are misfolded for degradation before they enter the catalytic core of ClpP. The crystal structures of ClpP, ClpX, and ClpXP have been solved and it is widely understood that ClpX binds to hydrophobic pockets between ClpP monomers and facilitates the widening of the axial pore of ClpP from the compacted to the extended state, thus allowing unfolded proteins to interact with the catalytic domain[30,31]. Previously known pharmacological activators of ClpP, such as acyldepsipeptides (ADEPs) or D9, have been shown to bind to these same hydrophobic pockets in ClpP, thus activating ClpP in the absence of ClpX and allowing nonspecific entry of proteins into the axial pore of ClpP[33–36].

Canonical Function

The canonical function of ClpP is widely understood to be regulation of mitochondrial protein homeostasis through degradation of misfolded proteins. Mitochondrial ClpP is also known to play a role in regulation of the electron transport chain (ETC), mitophagy, and mitochondrial dynamics[36,37]. Lists of putative substrates of ClpP have been identified and include mitochondrial proteins involved in bioenergetic processes (e.g., tricarboxylic acid (TCA) cycle, ETC), translation, protein import, and chaperones[37–40]. The ClpXP complex has also been implicated in the regulation of heme biosynthesis, mitophagy, and mitochondrial dynamics[41]. Interestingly, ClpP has also been shown to be involved in the UPR^{mt} in *C. elegans*, and it has been hypothesized that the activation of ClpP proteolytic function results in increased peptide fragment release from the mitochondrial to the cytosol, resulting in UPR^{mt} activation[42,43].

ClpP in Cancer

ClpP has been identified as overexpressed in multiple cancer types, including lung, breast, thyroid, and liver[41]. As a regulator of protein homeostasis, loss of ClpP proteolytic function has been shown to lead to accumulation of misfolded mitochondrial proteins, including the ETC Complex II[38,41]. Accumulation of misfolded proteins can lead to loss of OXPHOS, as well as an induction of oxidative stress. Loss of ClpP expression has been shown to reduce proliferation in some cell lines but not others, indicating a cancer and/or cell line specific dependence on ClpP expression[38,44]. Inhibition of ClpP proteolytic activity was identified as a potential anticancer therapy for cells dependent on ClpP for proliferation and has shown success in hematological cell lines highly expressing ClpP[44]. On the other hand, activation of ClpP was identified to have potent cell growth inhibitory activity across a wide variety of cell lines, indicating potential for anticancer effects regardless of whether cancer cells depend on ClpP for proliferation[41].

1.4 Metabolic Processes and Cancer

Normal vs. Cancer Cell Metabolism

The Warburg effect, also known as aerobic glycolysis, was identified in the 1920s as increased glycolytic dependence of cancer cells in aerobic conditions[45,46]. The role of aerobic glycolysis has been highly debated through the years, however, it is frequently hypothesized that glycolysis not only provides

a rapid method of ATP synthesis but reserves mitochondrial biosynthetic intermediates (e.g., TCA cycle intermediates and NAD+) for anabolic processes required for rapid cell proliferation, including nucleotide and amino acid biosynthesis[47–50]. Cancer cell dependence on metabolic reprogramming has been heavily investigated and has identified dependencies including serine biosynthesis, glutaminolysis, and nicotinamide adenosine dinucleotide (NAD+) biosynthesis in cancer metabolism[48,49,51–53].

Metabolic Processes as Therapeutic Targets

Metabolic reprogramming in cancer cells has been classified into three categories: transforming, enabling, and neutral[54]. Transforming activities have been defined as directly contributing to cell transformation and that their inhibition may prevent tumorigenesis. Examples of these activities include IDH1/2 mutations that result in the formation of 2-hydroxyglutarate, an oncometabolite that contributes to epigenetic dysregulation in cancer. Enabling activities include those that are altered in cancer cells but do not drive transformation, including oncogenic KRAS and loss of arginine synthesis. These mutations do not necessarily contribute to tumorigenesis but result in metabolic reprogramming to increase cell proliferation. Neutral activities are those that are altered but not required for tumor growth and are not likely to be effective anticancer targets[54].

Targeting metabolic reprogramming in cancer is not a novel idea—many current anticancer therapies target metabolic dependencies in cancer, including OXPHOS (e.g., metformin), TCA cycle (e.g., CPI-613), and glutaminolysis (e.g., CB-839)[51,54]. However, anticancer therapies must target the transforming or enabling activities to be as effective as possible. Targeting metabolic dependencies or vulnerabilities in cancer may also be dependent on interactions with the tumor microenvironment and immune system, providing increased complexity to identification of these enabling activities[54].

1.5 Multi-Omics as an Analytical Approach

Large omics datasets profiling vast numbers of changes following specific treatments or cellular state has been a valuable tool in identifying changes across the genome for decades[55]. More recently, the field of omics research has encompassed proteomics, transcriptomics, and metabolomics, and the integration of these datasets as a tool to identify causal relationships between protein-, transcript-, and metabolite-level changes has recently come to light as a challenge in the field of omics analysis[55–58]. Not only do these analyses provide information on the individual datasets, but they also allow for the potential

identification of relationships between changes in transcript and protein level, as well as the relationships between protein level of enzymes and the metabolites in those enzymatic pathways. This analytical technique can be used to identify potential metabolic vulnerabilities in cancer cells that can be further exploited for cancer treatment. In Chapter 4, the goal of the multi-omic study was to utilize proteomic, transcriptomic, and metabolomic changes in TNBC cells to identify potential metabolic vulnerabilities that arise following pharmacological activation of ClpP. These vulnerabilities could then be further studied to determine if they could be utilized to identify responders to treatment, as well as identify metabolic dependencies in ClpP-activated cancer cells that could be further disrupted to reduce cell proliferation and increase response to drug.

1.6 Figures

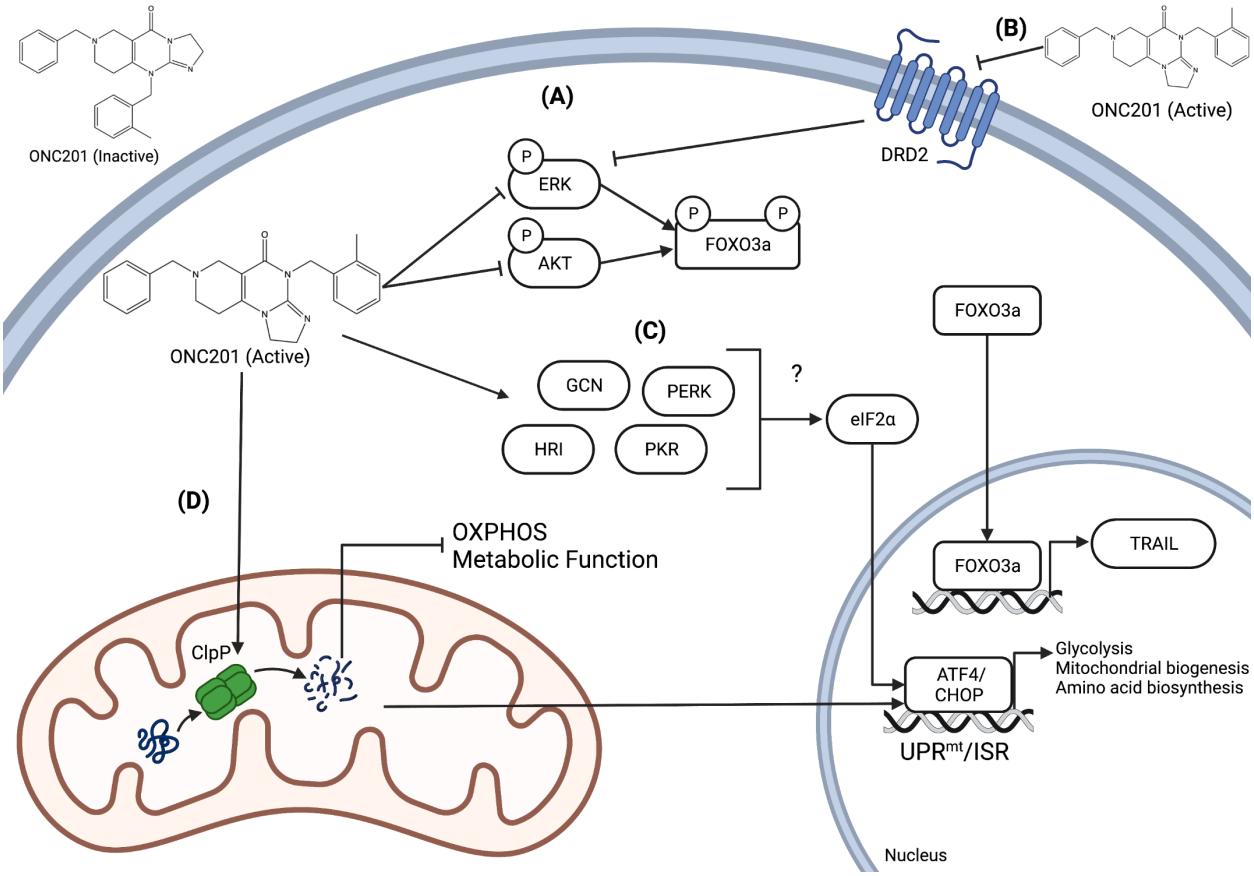

Figure 1.1 Schematic of proposed mechanisms of ONC201 action. ONC201 has been proposed to (A) induce TRAIL through inhibition of ERK and AKT and subsequent ability of FOXO3a to translocate to the nucleus to induce TRAIL expression, (B) DRD2 antagonism and subsequent ERK and AKT inhibition, (C) activation of the ISR through eIF2α kinases and other atypical mechanisms, and (D) activation of ClpP activity to result in mitochondrial dysfunction and activation of the UPR^{mt}.

CHAPTER 2: MITOCHONDRIAL PROTEASE CLPP IS A TARGET FOR THE ANTICANCER COMPOUNDS ONC201 AND RELATED ANALOGUES[1]

2.1 Introduction

ONC201 (also known as TIC10) was originally identified from an NCI chemical library screen for its ability to induce TRAIL (tumor necrosis factor-alpha-related apoptosis-inducing ligand) gene transcription in a human colon cancer cell line (HCT116)[11]. ONC201 has shown growth inhibitory effects in multiple cancer cell lines and antitumor activity in animal models of glioblastoma, colorectal, non-Hodgkins lymphoma, and pancreatic cancer (reviewed in ref[14]). As a result of these promising preclinical studies, its drug-like properties, its low toxicity in animals, and its penetration of the blood–brain barrier, ONC201 has rapidly advanced and is currently in 15 clinical trials (ClinicalTrials.gov identifier: NCT02863991)[14,15]. In 2018, ONC201 was granted Fast Track Designation for the treatment of adult recurrent H3 K27 M mutant high-grade gliomas.

Despite significant preclinical promise[15,27,59], no defined mechanism of action for ONC201 has been established. While TRAIL was found to be induced by ONC201 in some cell types[11,60], this was not consistently observed in all studies. Specifically, TRAIL was not increased in breast cancer cell lines even though ONC201 strongly reduced cell viability[22]. ONC201 was also effective against TRAIL-resistant breast cancer cells8 and hematological malignancies independently of TRAIL[19]. Although ONC201 has been reported to increase the DR5 death receptor[14], Greer et al. did not observe increased DR4 or DR5 expression after ONC201 treatment, nor did knockdown of DR4 or DR5 affect the inhibitory activity of ONC201[22].

ONC201 has been reported to inhibit Akt and ERK activity, potentially providing a mechanism to explain TRAIL induction through FOX3a[14,61,62]. Again, this was not observed by others despite significant

[1] This chapter has previously appeared as an article in *ACS Chem. Biol.* The original citation is as follows: Graves PR, Aponte-Collazo LJ, Fennell EMJ, Graves AC, Hale AE, Dicheva N, Herring LE, Gilbert TSK, East MP, McDonald IM, Lockett MR, Ashamalla H, Moorman NJ, Karanewsky DS, Iwanowicz EJ, Holmuhamedov E, Graves LM. Mitochondrial Protease ClpP is a Target for the Anticancer Compounds ONC201 and Related Analogues. *ACS Chem. Biol.* 2019; 14(5) doi: 10.1021/acschembio.9b00222

effects of ONC201 on cell growth[22]. Finally, it was also reported that the dopamine receptors (DRD2 and DRD3) may be targets of ONC201[17]. However, direct evidence for this interaction has been sparse, and siRNA-mediated knockdown of these receptors did not reduce ONC201's inhibitory effect[17].

Recently, ONC201 was shown to kill breast cancer cells by targeting mitochondria and mitochondrial metabolism[22]. Consistent with multiple previous reports[14], Lipkowitz and colleagues reported that ONC201 induced an integrated stress response (ISR) as shown by the induction of ATF4 and the C/EBP homology protein (CHOP)[22]. Although a specific mechanism was not elucidated, there was a direct correlation observed between the antiproliferative activity of ONC201, reduced oxidative phosphorylation, and the number of viable mitochondria. Moreover, ONC201 was shown to be ineffective in Rho0 cells (cells with impaired mitochondrial function due to chemical depletion of mitochondrial DNA)[22].

Taken together, these studies indicated the necessity to investigate and identify the potential targets for ONC201 and related compounds. The SAR of the ONC201 chemical series has been investigated though an iterative process of chemical optimization and subsequent testing in cell viability assays[61]. Importantly, the initial chemical structure for the compound was determined to be incorrect by Janda and colleagues[13], spurring a series of synthetic efforts leading to the identification of novel chemical entities based on this newly discovered pharmacophore[63]. Madera Therapeutics created a series of novel highly potent analogues of ONC201 and defined a new chemical series collectively known as TR compounds[64–66]. To investigate potential targets for ONC201 and the related TR compounds, we applied an unbiased affinity proteomics approach to identify potential targets. In this study, we report human mitochondrial ClpP as a key protein that binds ONC201 and related compounds in a direct and specific manner. In addition, we show that pretreatment of isolated recombinant ClpP with ONC201 and the TR compounds significantly increases the activity of ClpP. We show that ClpP activation by ONC201 and related compounds in vitro correlates directly with their biological potency in cells. Finally, we demonstrate that these compounds act through ClpP activation to induce the ISR, inhibition of protein synthesis, and mitochondrial events related to inhibition of cell growth.

2.2 Results

ONC201 Analogues are Highly Potent Inhibitors of TNBC Growth

Madera Therapeutics synthesized a number of novel chemical analogues of ONC201 known as the TR compounds. TR-31, first published by Nanjing Gator Meditech, is identical to ONC212.11,16−18 TR-42, TR-65, and TR-57 were designed to address limitations of ONC201, including modest cell activity and dose-dependent pharmacokinetics. Madera also synthesized additional amine-containing analogues (TR-79, TR-80, and TR-81) for the purpose of creating affinity ligands to capture TR binding proteins (Fig. 2.1A).

We compared ONC201 and the TR compounds for effects on growth inhibition of two established models of TNBC (MDA-MB-231, SUM159 cells). Cells were incubated with ONC201 or the TR compounds for 24–72 hours, and cell viability was measured using MTS assay. The TR compounds were all significantly more potent compared to ONC201, with IC_{50} values ~100-fold lower than ONC201 in these cells (Fig. 2.1 B). Growth inhibition was confirmed by crystal violet colony formation assays (Fig. 2.1C) and cell counting experiments (Fig 2.1D).

ONC201 and analogues have been shown to induce an ISR in multiple cancer cell lines[11,18,19,22]. CHOP and ATF4 proteins are common markers of the ISR response and ER stress[67], and we compared the ability of ONC201 and the TR compounds to induce CHOP and ATF4. Incubation of SUM159 or MDA-MB-231 cells with ONC201 or TR-57 strongly induced dose- and time-dependent increases in ATF4 as measured by immunoblotting. The amount of ONC201 or TR-57 required to increase ATF4 closely reflected the IC_{50} values for growth inhibition in these cells. While the effects on CHOP were more modest and peaked earlier than ATF4 (Fig. 2.1E), these data confirmed the activation of the ISR by these compounds. Under the same conditions, we observed increased ERK and Akt phosphorylation (Fig. S2.1).

ONC201 was shown to increase PARP cleavage and apoptosis in some cancer models[14,68] but not others[22]. We tested the effects of ONC201 and select TR analogues on caspase activity in SUM159 cells using a fluorogenic Ac-DEVD-AMC substrate. No significant increase in caspase activity was detected by either fluorogenic assays or immunoblotting for PARP cleavage, even at the highest concentrations of ONC201 or TR-57 tested. By contrast, staurosporine, an established apoptosis inducer,

increased Ac-DEVD-AMC cleavage as expected (Fig S2.1). Cell counting experiments confirmed that these compounds did not reduce the total number of cells below the initial value, even after 72 hours incubation (Fig. 2.1D). Thus, these compounds, at the concentrations tested, are having cytostatic effects but not increasing caspase-dependent cell death in SUM159 cells.

Affinity Chromatography Identifies the Mitochondrial Protease ClpP as a Target of ONC201 and the TR Compounds

To identify protein targets of ONC201, we coupled modified ONC201 analogues (TR-79, TR-80, and TR-81 (Fig. 2.1A) to agarose beads. Addition of the spacer arm and primary amine did not significantly reduce the potency of TR-79 to inhibit TNBC growth (Fig. 2.1B). To control for nonspecific interactions, we compared our TR-80 affinity column protein binding results to agarose alone or agarose coupled to an unrelated drug, PQ. HeLa cell lysates were mixed with control beads, PQ-beads, or TR-80 beads in the absence or presence of excess free TR-80. Following incubation of beads with lysate, the beads were washed and boiled in sample buffer to release bound proteins, and the samples were resolved by SDS-PAGE and silver stained. A distinct protein band of ~24 kDa was observed that did not bind the control beads or the PQ-beads and only bound TR-80 beads in the absence of free TR-80. The protein, indicated by the arrow (Fig. 2.2A), was excised, trypsin digested, and subjected to MALDI TOF/TOF mass spectrometry. MASCOT analysis identified this protein as the human mitochondrial protease, ClpP (Methods and Table S2.1).

To confirm the mass spectrometry results, the experiment was repeated as above except the samples were immunoblotted with anti-ClpP antibodies. ClpP was only detected bound to TR-80 beads in the absence of free TR-80 (Fig 2.2B). Because total cell lysate was applied to TR-81 beads, we sought to determine if ClpP binding to TR-81 was direct or mediated by other proteins. To this end, TR-81 beads were charged with HeLa cell lysates, washed to remove nonspecific proteins, and eluted with 50 μM free TR-57. The eluant was resolved by SDS-PAGE and silver stained or immunoblotted with ClpP antibodies. A single protein band at 24 kDa was observed upon silver staining of the eluate (Fig. 2.2C), and immunoblotting confirmed the protein to be ClpP (Fig. 2.2D). Because ClpP was the only protein detected in the eluate (Fig. 2.2C), it suggests that ClpP binds directly to TR-81 and that TR-81 is highly specific for

ClpP. Confirmation of direct binding between TR-81 and ClpP was shown by incubation of pure recombinant human ClpP with TR-81 beads (Fig. 2.2E).

To compare the relative ability of ONC201 or TR compounds to bind ClpP *in vitro*, we used TR-81 beads in a competition assay. Increasing concentrations of ONC201, TR-31 (ONC212),11 or TR-57 were mixed with HeLa cell lysates or added directly to HeLa cells in culture. These lysates were applied to TR-81 beads and the amount of ClpP bound assessed by immunoblotting. ONC201, TR-57, and TR-31 all reduced ClpP binding to TR-81 beads in a dose-dependent manner whether mixed with HeLa cell lysates (Fig 2.2F,G) or added to cell culture media (Fig 2.2H). Importantly, both TR-57 and TR-31 exhibited a ~10-fold greater potency over ONC201 in reducing ClpP binding whether applied to cell lysates or cell cultures. To determine if TR-81 bound ClpP from other cancer cell lines, we generated cell lysates from breast cancer (SUM159, MCF7), lung (A549), prostate (PC3), or pancreatic (PANC1) cells and performed similar experiments. ClpP bound immobilized TR-81 from all cell lines tested, and this binding could be prevented with TR-57 (Fig. S2.2), indicating that the interaction between TR compounds and ClpP was not restricted to HeLa cells but was observed from multiple different cancer cell types.

ONC201 and TR Compounds Activate ClpP Peptidase and Protease Activity

We next tested the effects of these compounds on ClpP enzymatic activity. Using purified, recombinant human ClpP protein and a select ClpP peptide fluorogenic substrate (Ac-WLA-AMC), we measured the peptidase activity of ClpP in the presence or absence of ONC201 and TR compounds. As shown in Figure 2.3A, incubation of ClpP with ONC201 or TR-57 strongly increased ClpP peptidase activity in a dose- and time-dependent manner. We then compared the effects of other TR compounds on ClpP activity. TR-27, 65, 66, and 79 all activated ClpP in a dose-dependent manner similarly to that observed with TR-57 and ONC201. All of the TR compounds were observed to be more potent activators of ClpP than ONC201. We also tested the effects of the recently reported ClpP activator D9[35]. D9 also increased ClpP activity albeit at much higher concentrations (EC_{50} ~ 110 μM), compared to that observed for ONC201 or the TR compounds (Fig. S2.4).

ONC201 and TR-57 were tested for their effects on ClpP protease activity. We preincubated recombinant ClpP with DMSO, ONC201, or TR-57 and then assayed for casein proteolysis. ONC201 and TR-57 increased ClpP activity toward casein proteolysis with an observed half maximal dose of ~1.25 μM

and ~200 nM for ONC201 and TR-57, respectively (Fig. 2.3B). These results demonstrate that ONC201 and the TR compounds increase ClpP activity toward unstructured proteins (casein) and peptide substrates.

ClpP Knockdown Reduces the Effects of ONC201 and TR-57 on the ISR and Cell Growth

To investigate if ClpP was a biological target for ONC201 and the TR compounds, siRNA knockdown of ClpP was performed in SUM159 cells. ClpP knockdown was verified by immunoblotting, and ClpP expression was almost completely eliminated by this treatment (Fig. 2.4A). Next, the effect of ClpP knockdown on CHOP/ATF4 induction by ONC201 and TR-57 was examined. Incubation of WT SUM159 cells with ONC201 or TR-57, increased the amount of CHOP protein after 24 hours. By contrast, no increase in CHOP was observed after ONC201/TR-57 treatment of the ClpP knockdown cells (Fig. 2.4A). Similar results were observed with ATF4 (Fig. S2.3).

The mitochondrial transcription factor A (TFAM) was recently shown to be reduced by ONC201 treatment[22]. From a global proteomics analysis, we observed that the mitochondrial protein elongation factor Tu (TUFM) and other mitochondrial proteins were strongly reduced by ONC201 and TR-57 treatment of SUM159 cells (E.M.J. Fennell, unpublished observations). The effects of ONC201 and TR-57 on the reduction of TFAM and TUFM were compared by immunoblotting control or ClpP knockdown cells. Interestingly, the ONC201/TR-57-stimulated reduction of these proteins was prevented in the ClpP knockdown cells (Fig. 2.4A). Moreover, the less potent ClpP activator D9, also decreased TFAM and TUFM in a ClpP-dependent manner (Fig. S2.3).

ONC201 has been shown to activate the protein synthesis inhibitory eIF2a kinases[18]. Using 35S-methionine incorporation into proteins[69,70], we measured the effects of ONC201 and TR-57 on protein synthesis in SUM159 cells. Both compounds significantly inhibited total protein synthesis (>50%) after 24 hours (Fig. 2.4B) with TR-57 much more potent than ONC201. Knockdown of ClpP strongly inhibited this response, consistent with activation of ClpP being required. Thus, these results support the importance of ClpP activation by ONC201 or TR-57 as essential for the inhibition of protein synthesis by these compounds.

Lastly, the effects of ClpP knockdown on growth inhibition by ONC201 and TR-57 were examined. ClpP knockdown cells were incubated with or without ONC201 or TR-57, and cell proliferation

was measured. The results of these studies demonstrated that the growth inhibitory effects of ONC201 or TR-57 were significantly reduced in the ClpP knockdown cells as compared to WT cells. Thus, these studies demonstrate that the cytostatic effects of ONC201 and TR-57 are in part dependent on ClpP, providing further evidence that this protein is an important target for these compounds (Fig. 2.4C).

2.3 Discussion

In conclusion, the rapid clinical advance of ONC201 has preceded a detailed understanding of the molecular mechanism of drug action[15]. We now demonstrate that highly potent chemical agents related to ONC201 may be prepared and that the mitochondrial protein ClpP is a novel target for ONC201 and the related TR compounds. Our data provide evidence for direct binding and activation of the peptide and protease activity of ClpP. Furthermore, through knockdown experiments, we demonstrate that ClpP is essential for the activation of the ISR and subsequent events, including protein synthesis inhibition and ultimately mitochondrial changes initiated by these compounds (Fig. 2.5).

While multiple mechanisms of ONC201 action have been proposed, our results support the importance of ClpP activation to the ISR and subsequent mitochondrial events. This includes ClpP-dependent reduction of the mitochondrial proteins TFAM and TUFM in cells treated with ONC201 or the TR compounds. In this way, our findings are in agreement with Greer et al., who identified reduced TFAM and mitochondrial metabolism as part of the ONC201 response. Interestingly, they observed TFAM protein levels decreased prior to a change in RNA levels[22]. Our data showing inhibition of protein synthesis by ONC201 and TR-57, in a ClpP-dependent manner, further supports this observation (Fig. 2.4).

The ATP-dependent CLP protease (ClpP) is a highly conserved serine protease found in species ranging from bacteria to humans[32,71,72]. In humans, ClpP is localized to the mitochondrial matrix and is important for regulating responses to cell stresses, including heat shock, nutrient deprivation, and other cellular insults[73,74]. ClpP has been linked to the mitochondrial unfolded protein response (UPR), where it is involved in the regulation of protein homeostasis[42]. ClpP is overexpressed in some leukemias, and human ClpP has recently been recognized as a potential target for cancer chemotherapy[75,76]. Activators of ClpP, including the acyldepsipeptides (ADEPs) and other compounds, are currently being investigated as novel anticancer or antimicrobial treatments[33,35,76].

The mechanism of ClpP activation by ONC201 and TR compounds remains to be established. In cells, the ClpP complex is composed of two components, the ATP-binding chaperone protein (ClpX) and the barrel-shaped ClpP peptidase[77]. Other known activators of human and bacterial ClpP (i.e., ADEPs) are believed to displace ClpX and open the central substrate cavity. Elegant structural studies demonstrated that opening this cavity may increase the peptidase activity of ClpP independently of the protein unfolding activity of ClpX[78]. Wong et al. demonstrated that the ADEPs bound to a hydrophobic cleft between the monomers in the heptamer structure of purified ClpP[33].

Our data are consistent with the effects of ONC201 and the TR compounds being mediated through direct binding to ClpP. This thesis is supported by affinity column binding assays and biochemical assays where we used isolated, purified ClpP in the absence of ClpX to assess the effects on enzyme activity. While we only tested activity on peptides and a protein lacking significant structure (casein), the effects on intact proteins remains to be determined. However, our proteomics analysis after ONC201 or TR-57 treatment indicates a significant reduction in multiple mitochondrial proteins, suggesting that ClpP activation in cells is leading to the degradation of intact mitochondrial proteins (E.M.J. Fennell, unpublished observations).

In all studies, we observed that the TR compounds were more potent binders and activators of ClpP than ONC201 or the recently reported compound D9. While we were unable to prevent binding of ClpP to TR-81 beads with ADEP or D9 (Fig. S2.2), whether or not ONC201 or the TR compounds bind to the same pocket as these compounds or compete with ClpX binding in intact cells remains to be determined. Importantly, the potent effects of the TR compounds on ClpP directly paralleled the effects of these compound on ISR induction, protein synthesis, and growth inhibition.

The mechanisms by which ONC201 and the TR compounds inhibit cell growth or induce cell death also remains to be determined. The ADEPs affect mitochondrial morphology and inhibit oxidative phosphorylation after extended exposure. We confirmed that ONC201 and the TR compounds induce changes in mitochondrial morphology, inhibition of oxidative phosphorylation, and increased lactic acid formation as reported by others (E. Holmuhamedov, unpublished observations). While we observed primarily cytostatic responses in our studies, these results may be cell type-dependent, as others have observed apoptotic responses. We also did not observe a complete elimination of the cytostatic effects of

these compounds in ClpP knockdown cells, suggesting that additional mechanisms of action may also contribute to the growth inhibitory effects of these compounds.

In summary, ONC201 as an unoptimized screening hit has displayed remarkable clinical activity in a range of difficult-to-treat cancers. We propose that the clinical response observed by treatment with ONC201 underscores the importance of a common biological mechanism of action that explains its broad efficacy against multiple cancer types. Our studies demonstrate that ClpP is the common target for both ONC201 and the TR compounds, and activation of ClpP results in modulation of the integrated stress response pathway. Thus, the TR compounds, based on the pioneering work of Janda and colleagues[13], are novel and highly potent activators of ClpP and represent the future direction of ClpP activators as anticancer agents.

2.4 Materials and Methods

Chemical Compounds

ONC201 was obtained from SelleckChem (S7963). The TR compounds and D9 were supplied by Madera Therapeutics, LLC and Nanjing Gator Meditech, Ltd. ADEP was obtained from Cayman Chemical (A-54556A). All compounds were dissolved in DMSO unless otherwise stated.

Synthetic Chemistry

The compounds were prepares as described previously[64–66]. For additional clarity, we have provided synthetic details below for TR-79, TR-80, and TR-81. 2-(3-iodopropyl)isoindoline-1,3-dione is available from multiple vendors including Sigma-Aldrich (CPR-R465674). In addition, 2-(4-iodobutyl)isoindoline-1,3-dione is available from multiple vendors, including Sigma Aldrich (CPR-R260312).

Example 1

Synthesis of TR-79

3-((1-(3-aminopropyl)-2,4-dioxo-3-(4-(trifluoromethyl)benzyl)-1,2,3,4,7,8-hexahydropyrido[4,3-d]pyrimidin-6(5H)-yl)methyl)benzonitrile

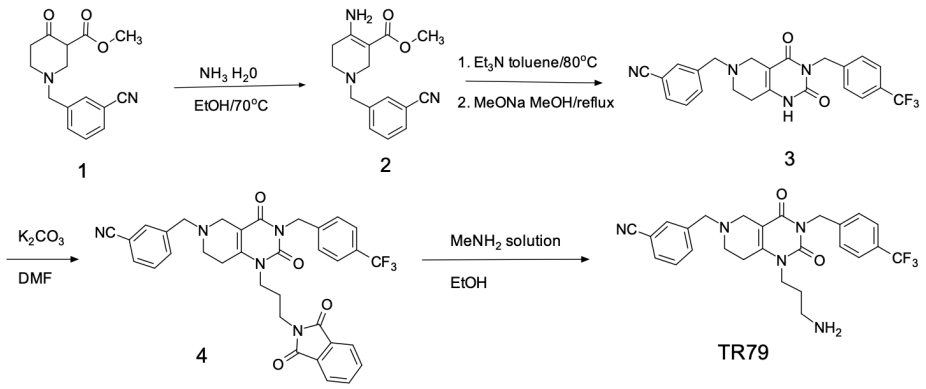

Step 1: A mixture of 1-(3-cyanobenzyl)-4-oxopiperidine-3-carboxylate **1** (8.55 g, 31.4 mmol), and ammonia solution (7 mL, 25%) in ethanol (110 mL) was heated at 70°C for 5 hours. The solution was concentrated, extracted with DCM (2 x 300 mL) and washed with brine. The extracts were dried over Na_2SO_4 and evaporated under reduced pressure to give 8 g of 2-((4-amino-3-(methoxycarbonyl)-5, 6-dihydropyridin-1(2H)-yl) methyl)-4- cyanobenzen-1-ide 2 (oil), which was directly used for next step.

Step 2: To a solution of 2-((4-amino-3-(methoxycarbonyl)-5, 6-dihydropyridin-1(2H)- yl) methyl)-4-cyanobenzen-1-ide (**2**, 2 g, 7.4 mmol) in toluene 20 mL was added 1-(isocyanatomethyl)-4-(trifluoromethyl)benzene (1.6 g, 7.5 mmol) and triethylamine (1.1 g, 10.4 mmol). The solution was heated to 80°C for 8 hours. The reaction solution was cooled to RT and concentrated *in vacuo*. The formed white solid was filtered and dissolved in MeOH (20 mL). NaOMe (350 mg) was added and the mixture was refluxed overnight. Then ca 10-15mL of methanol was removed and the precipitate was filtered. The desired product 3-((2,4-dioxo-3-(4-(trifluoromethyl)benzyl)-1,2,3,4,7,8-hexahydropyrido[4,3-d]pyrimidin-6(5H)-yl)methyl)benzonitrile (**3**) was obtained as a pale yellow solid (0.8 g, 25%).

Step 3: To a solution of 3-((2,4-dioxo-3-(4-(trifluoromethyl)benzyl)-1,2,3,4,7,8- hexahydropyrido[4,3-d]pyrimidin-6(5H)-yl)methyl)benzonitrile (**3**, 200 mg) in DMF (2 mL) was added potassium carbonate (150 mg) and 2-(3-iodopropyl)isoindoline-1,3-dione (150 mg). The mixture was heated at 100°C for 12 hours. Water (ca 3 mL) was added and the solution was extracted with EtOAc (3 x 5 ml). The combined extracts were washed with brine 3 times (ca 5 mL), dried over Na_2SO_4, filtered, and concentrated *in vacuo* to yield the crude product. The purified product (**4**) was obtained by preparative TLC, 100 mg, Yield 35%.

Step 4: To a solution of product (**4**) (100 mg) in EtOH (3 mL) was added methylamine solution (0.25 mL, 30%). The mixture was heated at 80°C for 4 hours. The water was added and the solution was extracted

with DCM (3 x 3 mL). The combined organic extracts were dried over Na_2SO_4, filtered, and concentrated *in vacuo* to yield the crude product, TR-79. The final product (TR-79) was obtained by preparative HPLC, 15 mg, Yield 19%.

^{1}HNMR (400MHz, CD_3OD) 2.03 (t, J = 7.2Hz, 2H), 2.99 (t, J = 6.8Hz, 2H), 3.18 (s, 2H), 3.67 (s, 2H), 4.01 (t, J = 6.8Hz, 2H), 4.07 (s, 2H), 4.62 (s, 2H), 5.17 (s, 2H), 7.5-7.57 (m, 4H), 7.69 (t, J = 8Hz, 1H), 7.86-7.93 (m, 2H), 7.99 (s, 1H); LC-MS: m/z = 498.1(M+1).

Example 2

Synthesis of TR-80

3-((1-(4-aminobutyl)-2,4-dioxo-3-(4-(trifluoromethyl)benzyl)-1,2,3,4,7,8-hexahydropyrido[4,3-d]pyrimidin-6(5H)-yl)methyl)benzonitrile

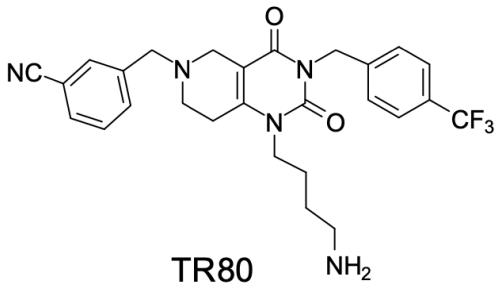

TR80

TR-80 is prepared in a similar fashion as Example 1. ^{1}HNMR (400MHz, CD_3OD) 1.7 (s, 4H), 2.95 (s, 2H), 3.16 (s, 2H), 3.64 (s, 2H), 3.9 (s, 2H), 4.03, (s, 2H), 4.59 (s, 2H), 5.15 (s, 2H), 7.49-7.57 (m, 4H), 7.67-7.7 (m, 1H), 7.88 (t, J = 8Hz, 2H), 7.98 (s, 1H); LC-MS: m/z 5.12.2(M+1).

Example 3

Synthesis of TR-81

3-((1-(4-aminobutyl)-3-(4-chlorobenzyl)-2,4-dioxo-1,2,3,4,7,8-hexahydropyrido[4,3-d]pyrimidin-6(5H)-yl)methyl)benzonitrile

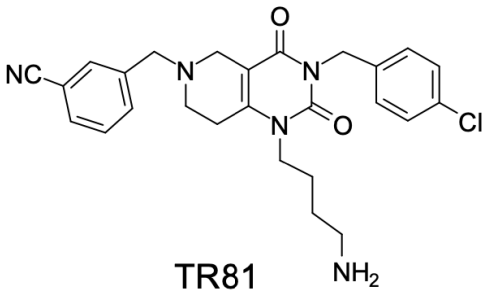

TR81

TR-81 is prepared in a similar fashion as Example 1. ^{1}HNMR (400MHz, CD3OD) 1.72 (s, 4H), 2.98-2.99 (d, 2H), 3.15-3.17 (d, 2H), 3.61 (t, J=5.6Hz, 2H), 3.91-3.93(d, 2H), 4.01 (s, 2H), 4.57 (s, 2H), 5.08 (s, 2H), 7.28-7.3 (d, 2H), 7.35-7.37 (d, 2H), 7.71 (t, J=7.6Hz, 1H), 7.9-7.92 (d, 2H), 7.99 (s, 1H).

Preparatory HPLC conditions

Column	Waters T3 Prep C18, 5 µm 19*100mm		
PREP	Gilson 215		
Mobile Phase (A)	0.1% FA/Water		
Mobile Phase (B)	Acetonitrile		
Flow Rate	20 mL/minute		
Detection	220 nm		
Run Time	12 minutes		
Injection Volume	100 µL		
Dilutant	Methanol		
Gradient	Time	A (%)	B (%)
	0.00	90	10
	8.00	50	50
	8.50	5	95
	10.00	5	95
	10.50	90	10
	12	stop	

Cell Culture

Human Triple Negative Breast Cancer (TNBC) cell lines SUM159 and MDA-MB-231 were a generous gift from Dr. Gary Johnson at UNC CH. SUM159 cells were cultured in Dulbecco's modified Eagle's medium: Nutrient Mixture F-12 (DMEM/F12, 0565-018, Thermo Fisher Scientific) supplemented with 5% fetal bovine serum (FBS, TMS-013-B, Millipore), 5 µg/mL insulin, 1 µg/mL hydrocortisone, and 1% mixture of antibiotic–antimycotic (15240062, Thermo Fisher Scientific). MDA-MB-231 cells were cultured in RPMI 1640 media (11875-093, Thermo Fisher Scientific) supplemented with 10% FBS and 1% antibiotic–antimycotic. Cells were incubated at 5% CO2 and 37°C. HeLa, A549, Panc1, PC3, and MCF-7 cells were obtained from ATCC and maintained in DMEM with 10% FBS and 1% antibiotic.

Viability Assays

Resazurin Assay

Cell viability assays were performed by plating SUM159 (1000 cells/well) on a Cellstar 96-well plate (655-180, Griener) in supplemented DMEM:F12 and allowed to incubate/adhere overnight. After adherence, the media in each well was aspirated and replaced with 50 µL of pure media and 50 µL of media containing the drug at twice the final concentration. The concentrations of drugs used are shown in the figure legends and discussed in the text. Cells treated with DMSO (vehicle only) were used as a negative control in all experiments. The final concentration of DMSO (vehicle) was kept under 1% in all experiments.

Cells treated with appropriate concentrations of selected compounds for 72 hours in 100 µL of incubation media were supplemented with 20 µL of resazurin (0.6 mM, Acros Organics 62758-13-8) and incubated for 30 minutes at 37°C. Cells were incubated to allow metabolism to resorufin, at which point 75 µL of each sample was transferred to a Costar black 96-well plate (CLS3915, Millipore Sigma), and the relative fluorescence of resorufin across samples was determined using a PHERAstar (BMG Labtech) with fluorescent module FI: 540-20, 590-20. The results were analyzed using GraphPad Prism 7 software which was used to generate the dose-dependence curves and to calculate IC_{50} values.

Total Cell Counting

Total cell counting assays were performed by plating SUM159 (50 cells/well) on a 96-well Greiner plate in supplemented DMEM:F12, allowing them to incubate/adhere overnight, and treating with drug as described above. At a predetermined time point (0, 24, 48, or 72 hours), media was aspirated, and 100 µL of Hoechst stain (1 µg/mL, H3570, Thermo Fisher Scientific) was added to each well and then allowed to incubate for 30 minutes at 37 °C. Total cell number was then quantified using the Celigo Imaging Cytometer (Nexcelom).

Crystal Violet Assays

Crystal violet assays were performed by plating SUM159 (1000 cells/well) on a 6-well Costar plate (CLS3506, Millipore Sigma) and allowing them to incubate/adhere overnight. Media was aspirated and replaced by media containing the drug at the desired concentration. Cells were allowed to incubate for 48 h, and the media was either replaced by fresh media with drug or media without drug. Cells were

then allowed to incubate until one well was 100% confluent, changing media as needed. Once confluent, cells were stained using 0.5% crystal violet in 20% methanol, allowed to incubate for 10 minutes at RT, then rinsed 3 times and allowed to dry overnight. Staining was quantified by dissolving crystal violet stain in Sorenson's buffer (0.1 M sodium citrate, 50% ethanol, pH 4.2) and measuring the absorption of dissolved crystal violet at 570 nm using a BMG Polarstar Omega.

Immunoblotting

For Western blotting, SUM159 or MDA-MB-231 cells were plated and treated with compounds as described above for cell viability assays. Following treatment, cells were rinsed 3 times with 2 mL of cold PBS and lysed using RIPA buffer (no SDS) supplemented with 2 mM $Na(VO_3)_4$, 10 mM NaF, 0.0125 µM calyculin A, and complete protease inhibitor cocktail (11873580001, Roche Diagnostics). Cell lysates were clarified and immunoblotted as described earlier[79]. Membranes were incubated with the following primary antibodies: [TUFM (PA5-27511), IDH2 (PA5-79436) from Invitrogen]; [ClpP (CS-14181), ATF4 (CS-11815), LONP (CS-28020), Aconitase (CS-6922s) from Cell Signaling Technologies]; [β-actin (SC-47778), CHOP (SC-575), TFAM, (SC-376672), ClpP (SC-271284) from Santa Cruz Biotechnologies] diluted 1:1000 in 5% TBST/BSA + 0.02% NaN_3) overnight at 4°C, removed, washed 3 x 5 minutes in TBST, and placed in their respective 2° antibodies (1:10 000 dilution in 5% milk/TBST) for 1 hour. Membranes washed 3 x 5 minutes in TBST were embedded in 2 mL of each ECL reagent and imaged using a Chemidoc MP (BioRad) or developed with film. Acquired images were processed/quantified using Image Lab software (BioRad).

siRNA Transfections

Approximately 5 x 10^4 SUM159 cells were seeded in 6-well plates and allowed to adhere overnight. Cells were then mock transfected or transfected with human ClpP siRNA (siGENOME, Dharmacon, 8192, GAAGGACCUGUAGAAGCA) at a final concentration of 33 nM according to the standard Dharmacon protocol. Dharmafect was used at a dilution of 1:50. Cells were incubated with siRNA for 48 hours and then additional 24 hours in the presence of drug before harvesting.

Reverse Transfection

All siRNA stocks were ordered from Dharmacon at 2 nmol/siRNA and resuspended in 100 µL 1X siRNA reconstitution buffer (Dharmacon) to create a 20 µM stock. Dharmafect I was diluted 1:266 in

OptiMEM media and divided into 250 µL aliquots. Individual siRNAs were added to Dharmafect aliquots for a final concentration of 125 nM, incubated at RT for 30 minutes, and then added to 6-well or 96-well plates. SUM159 cells were washed with PBS and trypsinized at 37 °C for 5 minutes. Cells were resuspended to a final concentration of 1 x 10^5 cells/mL (6-well) or 1 x 10^4 cells/mL (96-well) in 1:1 DMEM:F-12 supplemented with 5% FBS, 5 µg/mL insulin, and 1 µg/mL hydrocortisone. Cells (1.0 mL/well, 100 µL/well) were added to each well containing siRNA and incubated for 24 hours.

Caspase and Apoptosis Assays

Caspase 3/7 activity was analyzed using a fluorescent peptide substrate (7-amido-4-methylcoumarin)[79]. The cells were plated at 8 x 10^5 cells per plate (6 cm plate) and treated for 24 hours with 3, 30, and 300 nM TR57 and TR31; 300 nM, 3 µM, and 30 µM ONC201, as well as 0.1% DMSO and 10 nM staurosporine (IC_{25} on SUM159 cells determined by MTS cell viability assay (data not shown)). The samples were harvested by mechanical scraping of the cells into 400 µL of lysis buffer (50 mM HEPES (pH: 7.4), 5 mM CHAPS, and 5 mM DTT), and caspase activity was measured as described earlier[79].

Affinity Capture of Protein Targets

To generate TR-80 or TR-81 affinity resins, we coupled free TR-80 or TR-81 to NHS-activated agarose (Thermo Scientific catalog #26200). Briefly, NHS-agarose beads were allowed to react with TR-80 or TR-81 at a final concentration of 5 mM in coupling buffer (PBS with 20% DMSO) for 4 hours at RT. Following washing with PBS to remove unbound ligand, the beads were blocked for an additional hour with 1 M Tris-HCl, pH 7.5. Control agarose beads were generated by blocking uncoupled NHS-agarose beads with 1 M Tris-HCl, pH 7.5. Primaquine (PQ)-agarose was generated by coupling NHS-agarose with 20 mM primaquine in phosphate buffered saline, pH 8.0.

To identify TR-80 interacting proteins, approximately 50 x 10^6 HeLa cells were homogenized in cell lysis buffer (50 mM Tris-HCl, pH 7.5, 150 mM NaCl, 2 mM EDTA, 0.5% NP-40) and clarified by centrifugation (15 min at 13 000*g*). The resultant supernatant was divided into 1 mL aliquots and mixed with ~50 µL packed beads of control agarose, PQ-agarose, or TR-80 agarose in the presence of 2% DMSO or 1.25 mM free TR-80 and rotated for one hour at RT. Beads were then collected by centrifugation and washed 3 times, 1 mL each wash, with cell lysis buffer. Beads were boiled in SDS

sample buffer, resolved by SDS-PAGE using 11% polyacrylamide gels, and silver stained as described[80]. A protein band, indicated by the arrow, was excised, destained, trypsin digested, and subjected to mass spectrometry for identification (see below).

TR-81 Elution

To determine the specificity of protein interactions with TR-81 beads, ~ 30 µL of TR-81 agarose was mixed with 1 mL of HeLa cell lysate generated as described above. After washing the beads to remove nonspecific interactions, the beads were incubated with 100 µL of elution buffer (50 mM Tris-HCl, pH 7.5, 150 mM NaCl) containing 2% DMSO or 50 µM TR-57 for 30 minutes at RT. The eluant was collected, resolved on an 11% polyacrylamide gel and silver stained or immunoblotted with ClpP antibodies.

In Vitro Drug Competition Assays

To compare the relative binding ability of different compounds to ClpP, ~200–400 µL of HeLa cell lysate (generated as described above) was mixed with vehicle (2% DMSO final) or different concentrations of ONC201 or TR compounds. After mixing for 15 minutes, the lysate was combined with ~20 µL packed TR-80 beads and rotated for 1 hour at RT. The supernatant was discarded, and beads were washed briefly 3 times, 1 mL each wash, with cell lysis buffer before boiling in SDS sample buffer. Samples were then resolved by SDS-PAGE and immunoblotted with ClpP antibodies. To compare the ability of the compounds to compete for ClpP binding within live cells, HeLa cells in culture were treated with DMSO (final concentration 0.1%) or various concentrations of ONC201 or TR compounds for 30 minutes. Cells were then snap frozen, and lysates were subsequently prepared and analyzed in a similar manner as described above.

MALDI TOF/TOF Analysis

The resultant tryptic peptides obtained from the silver-stained band were desalted using a C18 Zip-Tip and applied to a MALDI target plate with α-cyano-4-hydroxycinnamic acid as the matrix. The sample was analyzed on an AB Sciex 5800 MALDI TOF/TOF mass spectrometer. MS/MS spectra were searched against a Uniprot human database using Mascot version 2.3 (Matrix Science) within ProteinPilot software version 3.0 (AB Sciex). A significance score threshold was calculated in Mascot, and an ion score above 36 was considered a significant identification ($p < 0.05$).

Measurement of Human ClpP Activity

Measurement of *in vitro* activity of recombinant human caseinolytic peptidase ClpP (Cat # MBS204060, MyBioSource) was based on monitoring the release of fluorescent coumarin from the fluorogenic substrate Ac-WLA-AMC (Cat #S330, Boston Biochem, Inc.) as described previously[81–83] with minor modifications. Briefly, the activity of recombinant ClpP proteolytic subunit (1 µg/mL) was measured in assay buffer composed of 50 mM Tris, 10 mM $MgCl_2$, 100 mM KCl, 1 mM DTT, 4 mM ATP, 0.02% Triton X-100, and 5% glycerol, pH 8.0 (HCl) using 10 µM of fluorogenic Ac-WLA-AMC substrate as described[83,84]. Two different protocols were used to investigate the effects of ONC201 and the TR compounds on ClpP activity. Using the first protocol (Protocol #1), the reaction was initiated instantly by direct mixing of ClpP enzyme and substrate in the presence of indicated concentrations of compounds. Applying a second protocol (Protocol #2), the enzyme and compounds were mixed and incubated in assay buffer for 60 min before initiating the reaction by adding Ac-WLA-AMC substrate. The kinetics of the free coumarin fluorescence was monitored using black, µ-CLEAR 96-well flat bottom plates (Cat # 655090, Greiner), and the fluorescence of released coumarin was recorded at 350 nm excitation and 460 nm emission using BMR PHERAstar plate reader equipped with appropriate FI module (BMG LABTECH). The slope of the linear portion of the fluorescence signal over time used as a measure of the activity of ClpP. Measurements were carried out in triplicate and presented as the rate of fluorescence change at given concentrations of ClpP and substrate in the presence or absence of ONC201 or the TR compounds. Dose-dependence of ClpP activation with different compounds was used for determination of EC_{50} for each compound, and the activity of samples treated with DMSO (vehicle) measured as background and subtracted from experimental data and the activity of ClpP expressed as RFU/µg of ClpP/h.

To measure ClpP protease activity *in vitro*, assays were conducted using Protocol #2 as described above. Recombinant ClpP was preincubated for 1 hour at 37 °C with DMSO or the indicated compounds in assay buffer and then an additional hour at 37 °C in the presence of substrate. The reaction volume was 50 µL with a final concentration of 10 ng/µL ClpP, 5 µM α-casein, and 1% DMSO. Samples were boiled in SDS sample buffer, resolved by 12% SDS-PAGE, and silver stained[80].

Metabolic Labeling of Nascent Proteins

Nascent proteins were metabolically labeled and quantified as described previously[69,70]. Briefly, cells were incubated in methionine- and cysteine-free medium (Sigma) containing relevant concentrations of compounds tested for 15 minutes. ^{35}S-labeled methionine and cysteine (125 µCi; PerkinElmer EasyTag Express Labeling Mix) were added and allowed to incorporate for 30 minutes. Cells were then washed twice in ice-cold PBS, scraped, and collected by centrifugation. Cell pellets were lysed in RIPA medium containing protease inhibitors (Roche), and protein concentrations were determined by the Bradford assay (Amresco). Trichloroacetic acid (TCA) was added to a final concentration of 20%, and precipitated proteins were captured on glass microfiber filters by filtration under vacuum. The filters were washed twice with 20% TCA and once with 100% ethanol and allowed to air-dry. The filters were then transferred to vials containing scintillation fluid (EcoScint), and radioactivity was quantified using a scintillation counter. The amount of radioactivity was normalized to the protein concentration for each sample.

2.5 Figures

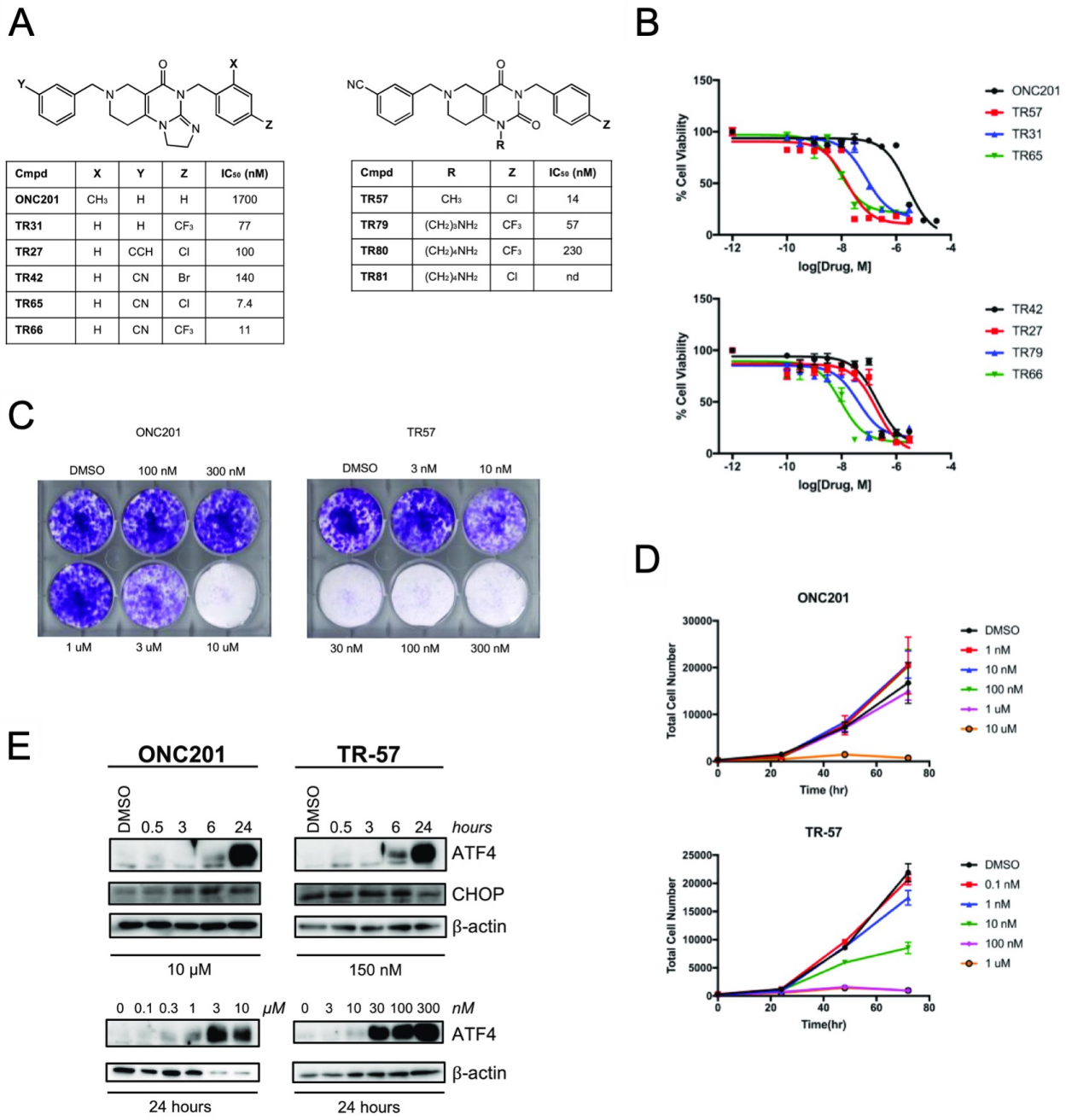

Cmpd	X	Y	Z	IC_{50} (nM)
ONC201	CH_3	H	H	1700
TR31	H	H	CF_3	77
TR27	H	CCH	Cl	100
TR42	H	CN	Br	140
TR65	H	CN	Cl	7.4
TR66	H	CN	CF_3	11

Cmpd	R	Z	IC_{50} (nM)
TR57	CH_3	Cl	14
TR79	$(CH_2)_3NH_2$	CF_3	57
TR80	$(CH_2)_4NH_2$	CF_3	230
TR81	$(CH_2)_4NH_2$	Cl	nd

Figure 2.1 ONC201 and TR analogs inhibit cell growth and induce ATF4 and CHOP activation. A) Chemical structures of ONC201 and TR compounds B) Cell viability of ONC201 and TR compounds using MTS assay in SUM159 cells. IC_{50} values are shown in table to the left (A). Values represent mean ± SEM, representative of N=4. C) Growth of SUM159 cells determined by crystal violet assay, representative of N=3. D) Changes in cell number determined by Hoechst stain, representative of N=2. E) Immunoblots of SUM159 lysates for ATF4, CHOP, and β-actin.

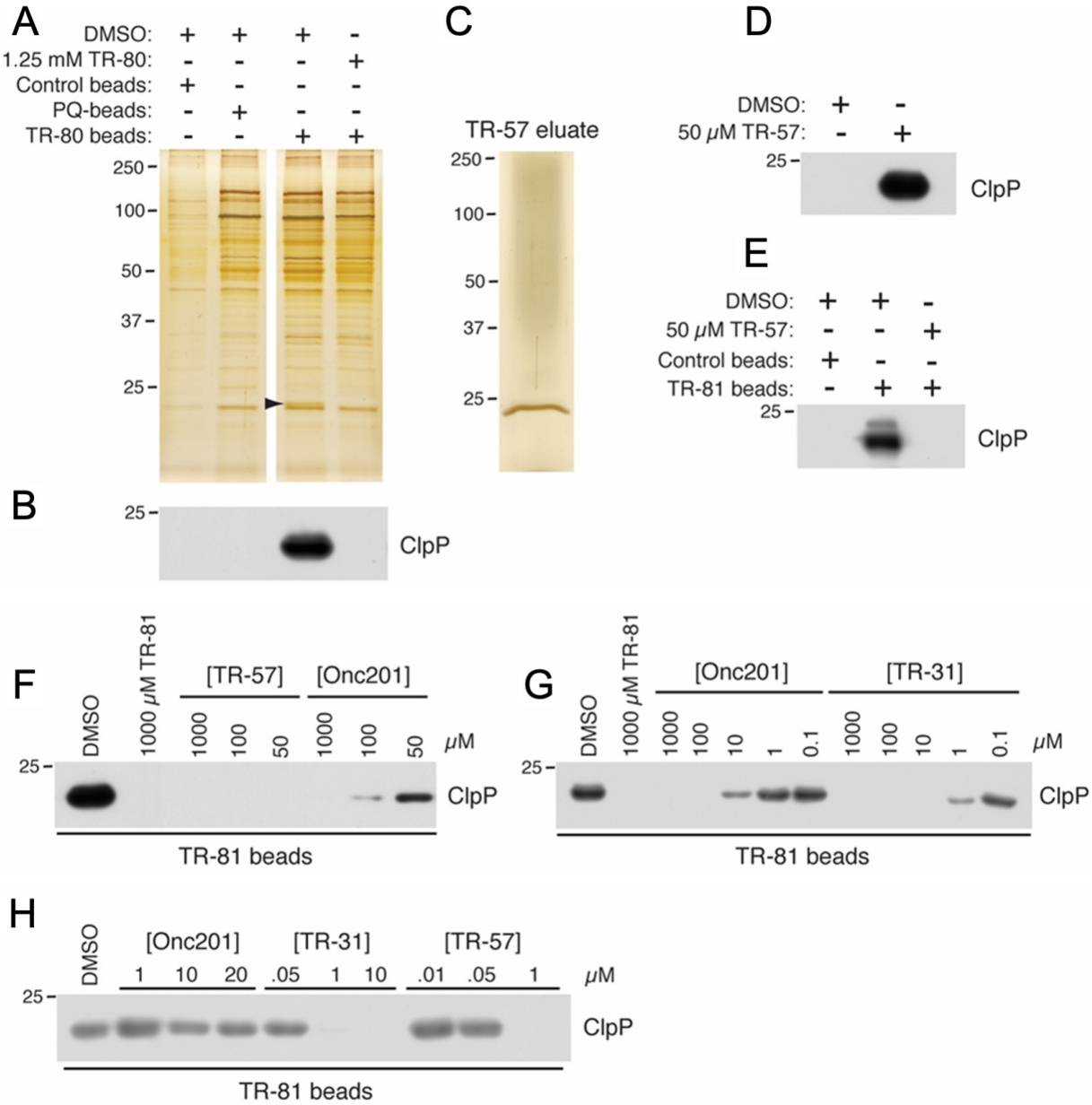

Figure 2.2. Identification of ClpP as an ONC201 and TR compound binding protein. A) HeLa cell lysate was mixed with the indicated beads in the presence or absence of free TR-80. A Silver-stained gel is shown, and the band indicated by the arrow was excised and subjected to mass spectrometry for identification. B) Replicate samples from panel A were immunoblotted with anti-ClpP antibody. TR-81 beads were charged with HeLa lysate and eluted with 50 μM TR-57. A portion of the eluant was silver stained (C) or immunoblotted for ClpP (D). (E) Pure, recombinant human ClpP was mixed with the indicated beads in the presence or absence of 50 μM TR-57 and immunoblotted for ClpP. (F,G) HeLa cell lysates were mixed with TR-81 beads in the presence of the indicated compounds and immunoblotted for ClpP. (H) HeLa cell lysates were treated with the indicated compounds for 30 minutes and lysates were mixed with TR-81 beads and immunoblotted for ClpP.

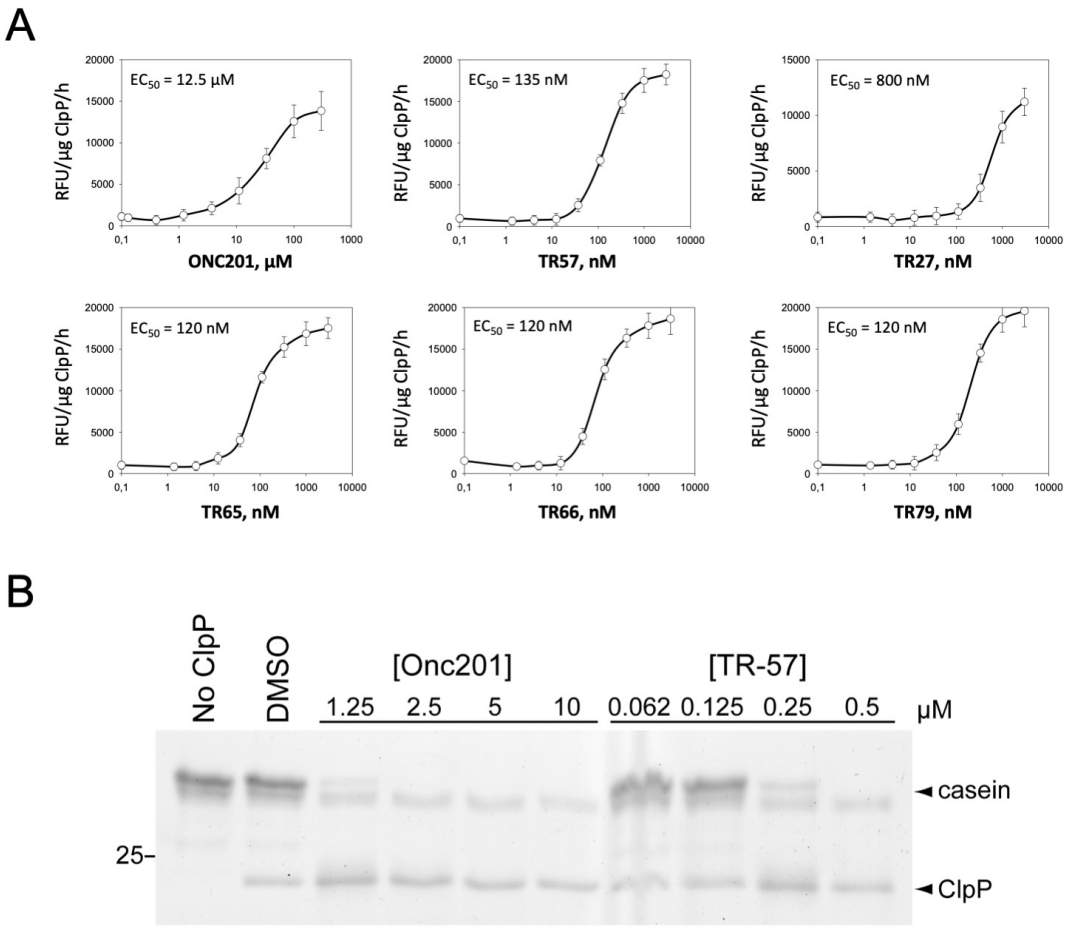

Figure 2.3 Activation of ClpP by ONC201 and the TR Compounds. A) Purified recombinant human ClpP was incubated with the indicated concentrations of each compound and ClpP peptidase activity was measured. B) Recombinant human ClpP was pre-incubated for 1 hour at 37°C with the indicated compounds and then for an additional 1 hour at 37°C in the presence of casein. Reaction products were resolved by SDS-PAGE and silver stained.

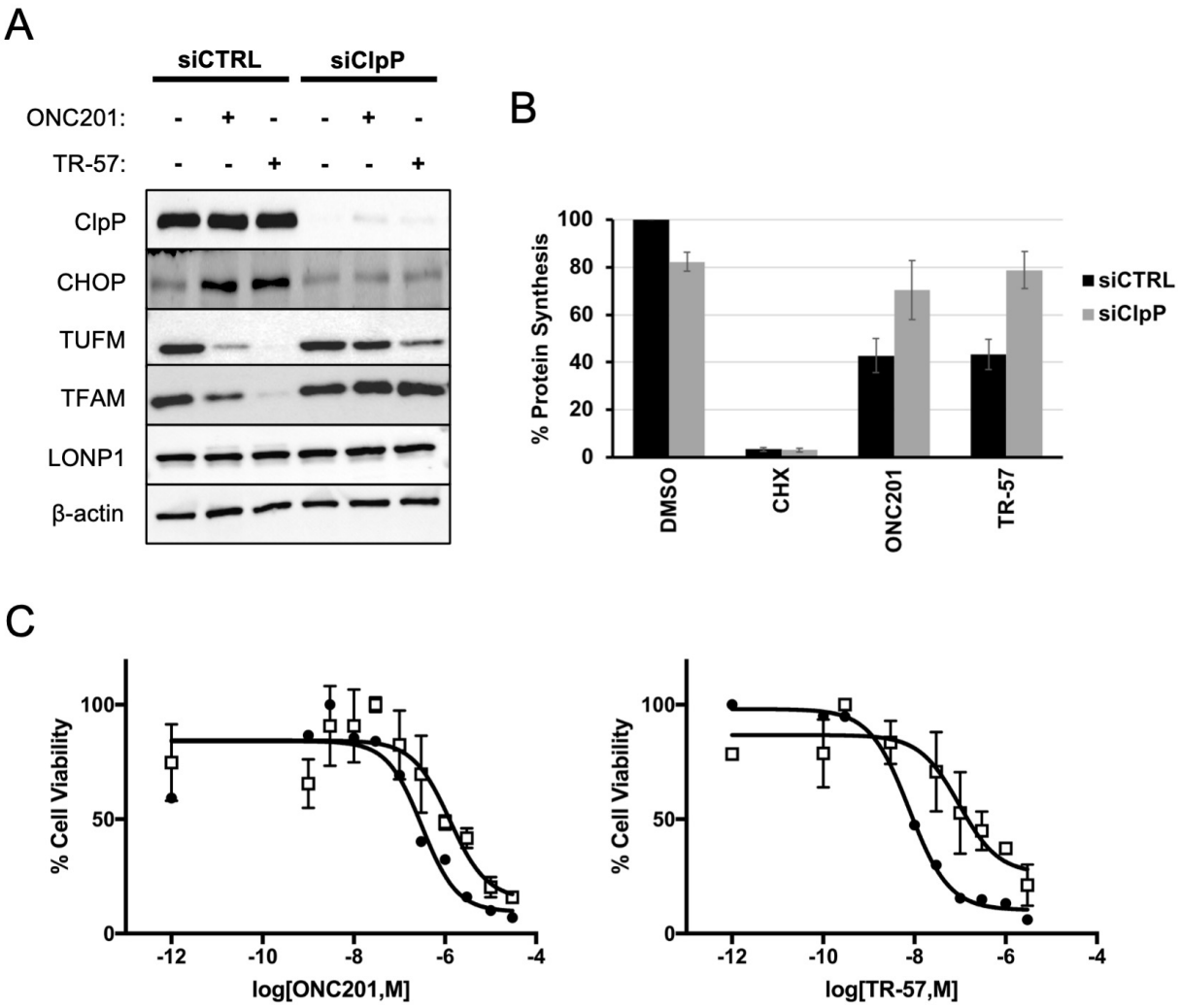

Figure 2.4 Effects of ONC201 and TR-57 are prevented by ClpP knockdown in SUM159 cells. A) Immunoblot of lysates from SUM159 cells transfected with a nontargeting siRNA (siCTRL) or siRNA targeting ClpP (siClpP) and treated with either 10 μM ONC201, 150 nM TR-57, or 0.1% DMSO for 24 hours. Representative of N=3. B) Total protein synthesis measured in SUM159 cells transfected with siCTRL (black circles) or siClpP (white squares) using Hoechst stain for total cell counting after 48 hour treatment with OCN201 or TR-57 at indicated concentrations. Graphs shown in (B) and (C) are representative of N=2. Values represent mean ± SEM.

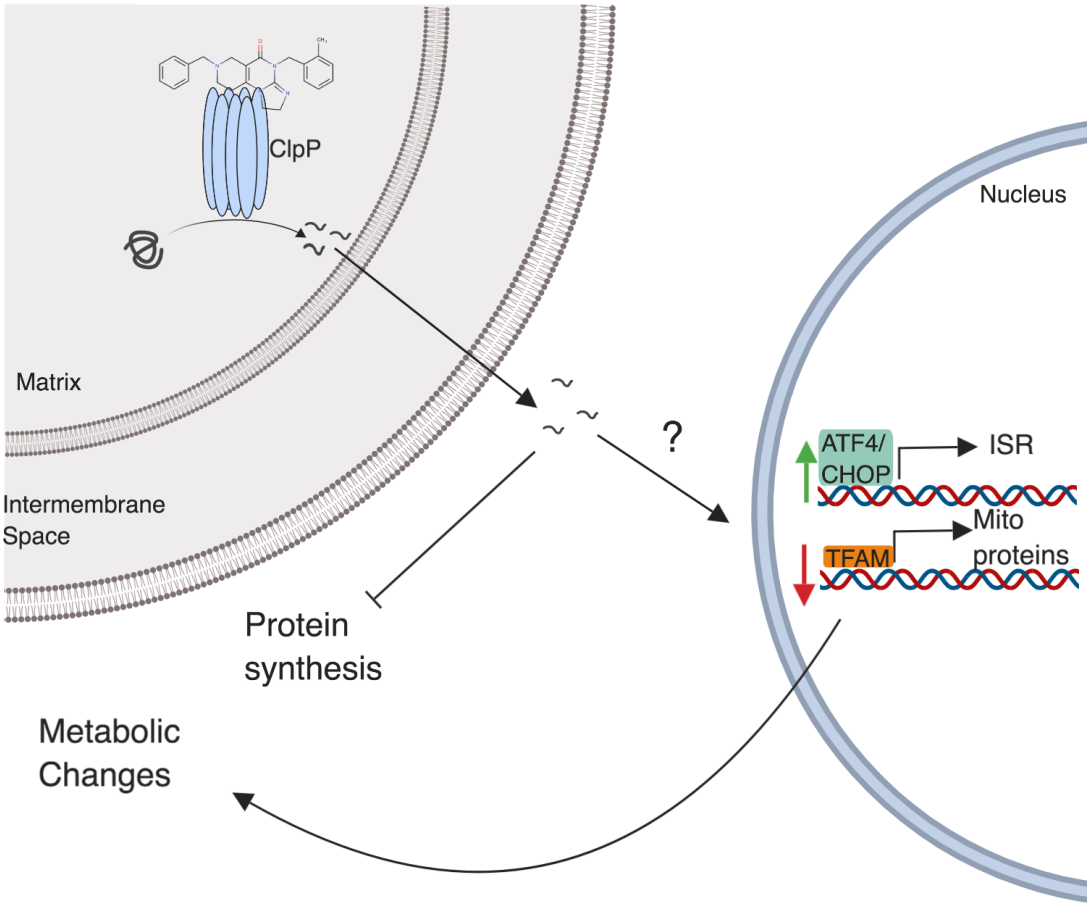

Figure 2.5 Model for the regulation of ClpP and the ISR by ONC201 and TR compounds. ClpP, a mitochondrial protease, is activated by ONC201 and TR analogues to degrade mitochondrial proteins. Protein fragments are exported from the mitochondria and activate the unfolded protein response (ATF4, CHOP), decrease TFAM activity, and inhibit protein synthesis. ClpP-mediated changes in ATF4, CHOP, and TFAM leads to alterations in metabolism.

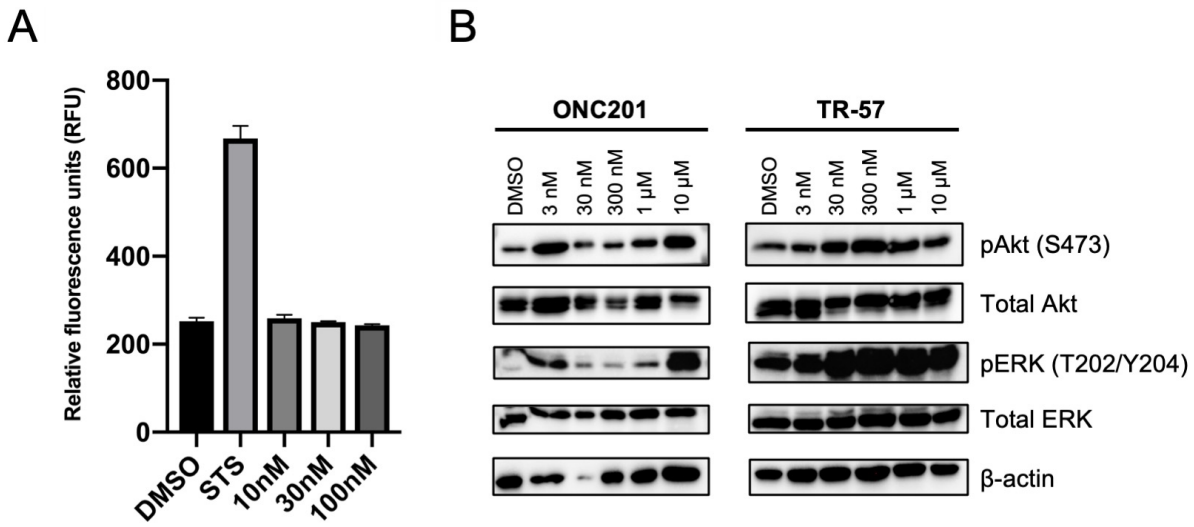

Figure S2.1 ONC201 and TR-57 do not activate caspase or inhibit ERK/AKT in SUM159 cells. A) Measurement of caspase-3/7 activity in SUM159 cells after 24 hour treatment with 20 nM staurosporine (STS), 10, 30, or 100 nM of TR-57, or 0.1% DMSO. Values indicate mean ± SEM, N=2. B) Immunoblot showing changes in phosphorylation of indicated proteins in SUM159 cells following 24 hour treatment with either 0.1% or indicated concentrations of ONC201 or TR-57.

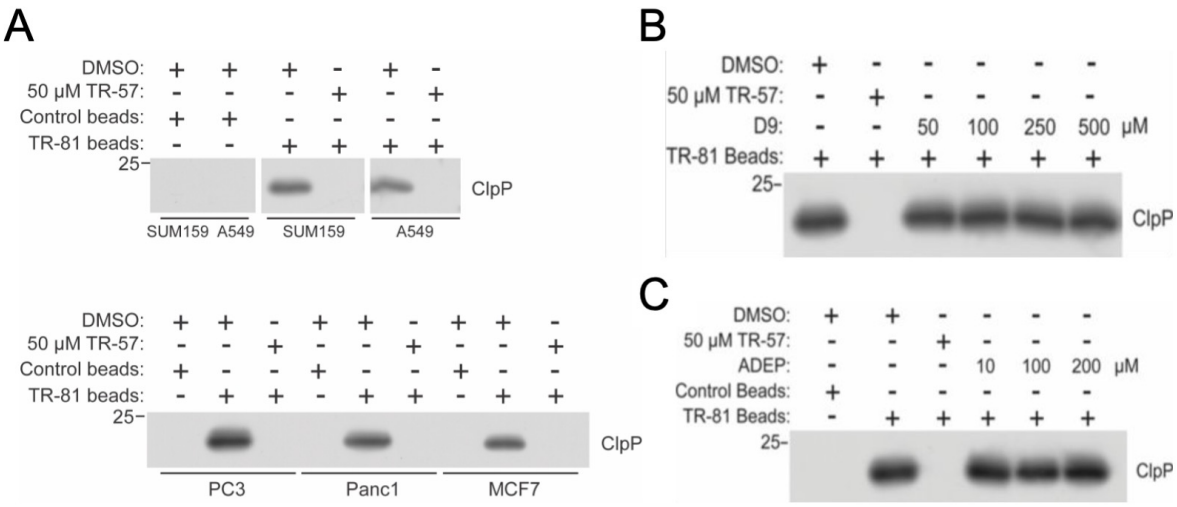

Figure S2.2 TR-57, but not D9 and ADEP compete for ClpP binding. A) Lysates from indicated cell lines were mixed with Control or TR-81 beads in the presence or absence of TR-57 and ClpP was detected by immunoblot. B) SUM159 cell lysates were incubated in TR-81 beads in the presence or absence TR-57 or indicated concentrations of D9 and ClpP was detected by immunoblot. C) HeLa cell lysates were incubated with Control or TR-81 beads in the presence or absence of TR-57 or indicated concentrations of ADEP and ClpP was detected by immunoblot.

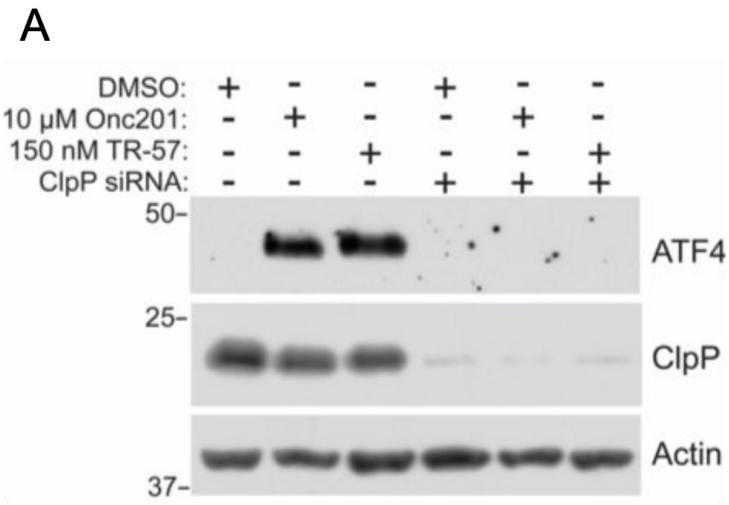

Figure S2.3 ATF4 induction by ONC201 and TR-57 is prevented by ClpP knockdown. A) SUM159 cells were mock or ClpP siRNA transfected and treated with 0.1% DMSO, 10 µM ONC201 or 150 nM TR-57 for 24 hours and immunoblotted for indicated proteins. Representative of N=3.

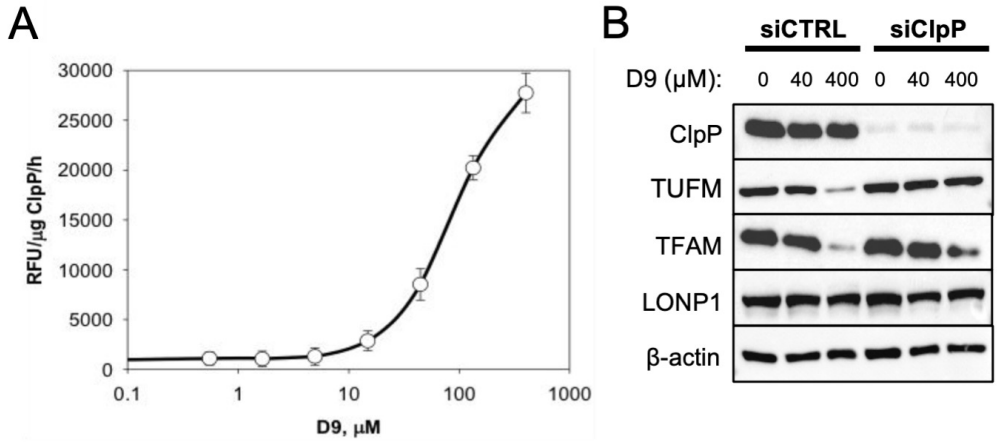

Figure S2.4 Effects of D9 are prevented by ClpP knockdown in SUM159 cells. A) Purified recombinant human ClpP was incubated with indicated concentrations of D9 and ClpP peptidase activity was measured. B) Immunoblot of lysates from SUM159 cells transfected with siCTRL or siClpP and treated with 0.1% DMSO or indicated concentrations of D9 for 24 hours. Representative of N=3.

Table S2.1 Identification of ClpP through PID Analysis. Mass spectrometry protein identification from HeLa cell lysate after incubation with TR-80 beads and TR-57 elution.

Protein Name	Database Accession ID	MW (Da)	Peptide Count	Ion Score
ATP-dependent Clp protease proteolytic subunit OS=Homo sapiens GN=CLPP PE=1 SV=1	CLPP_HUMAN	30161	8	435
Peroxiredoxin-1 (Fragment) OS=Homo sapiens GN=PRDX1 PE=1 SV=1	A0A0A0MSI0_HUMAN	18964	2	47

CHAPTER 3: CHARACTERIZATION OF TR-107, A NOVEL CHEMICAL ACTIVATOR OF THE HUMAN MITOCHONDRIAL PROTEASE CLPP[2]

3.1 Introduction

Triple-negative breast cancer (TNBC) is the most aggressive breast cancer subtype and is associated with poor prognosis, shorter progression-free and overall survival compared to other breast cancer subtypes[9,85,86]. Unlike other subtypes, targeted therapies (e.g., tamoxifen and trastuzumab) are ineffective against TNBC leaving patients with limited options of systemic chemotherapy, surgery or radiation[85] or more recently immunotherapy[87,88]. As an alternative, considerable interest has developed in targeting mitochondrial metabolism as a potential approach to treat recalcitrant cancers[89,90]. Multiple studies now support the feasibility of targeting essential mitochondrial processes such as oxidative phosphorylation (OXPHOS), mitoribosomal activity and TCA cycle function as a unique strategy to inhibit cancer cell proliferation[91,92]. This has led to the development of small molecule inhibitors of OXPHOS, TCA cycle enzymes (isocitrate dehydrogenases (IDH1/2), a-ketoglutarate dehydrogenase), as well as modifiers of mitochondrial transcription (POLRMT) and lipid metabolism[93,94]. Included in this class of molecules are metformin and other clinical agents (BAY 87-2243, IACS-010759) designed to inhibit mitochondrial multimeric complex I enzyme that comprises the first step in the electron respiratory chain[95–97]. While these have shown promising activities in preclinical studies, the clinical application of these agents has yet to be realized[92].

The small molecule imipridone ONC201 was initially identified in a screen for TRAIL inducers and later shown to have antagonistic effects on the dopamine receptors D2/D3[60,98]. While the direct target was unresolved, multiple studies showed that ONC201 exhibited anti-cancer responses in diverse cancer models including breast, pancreatic, leukemia and others[11,14,16,18,19,99–101] leading to the clinical

[2] This chapter has previously appeared as an article in *Pharmacol. Res. Perspect.* The full citation is as follows: Fennell EMJ, Aponte-Collazo LJ, Wynn JD, Drizyte-Miller K, Leung E, Greer YE, Graves PR, Iwanowicz AA, Ashamalla A, Holmuhamedov E, Lang H, Karanewsky DS, Der CJ, Houry WA, Lipkowitz S, Iwanowicz EJ, Graves LM. Characterization of TR-107, a novel chemical activator of the human mitochondrial protease ClpP. *Pharmacol. Res. Perspect.* 2022; 10(4) doi: 10.1002/prp2.933.

advancement of ONC201. The unexpected finding that ONC201 potently affected OXPHOS and mitochondrial metabolism in models of TNBC suggested an alternative mechanism of action[22]. Importantly, the development of the chemically-related TR compounds, (Madera Therapeutics), including immobilizable analogs, facilitated the discovery of the mitochondrial matrix protease ClpP as the major target[28]. Additional studies confirmed these findings and demonstrated that activation of ClpP was essential for the anti-cancer properties of ONC201 and related analogs[29,102].

Modifiers of ClpP activity have previously shown anti-cancer properties[35,103], with both inhibitors and activators of ClpP demonstrating anti- tumor efficacy for acute myelogenous leukemia[41,44]. Chemical activators of ClpP include diverse chemical structures such as the macrocyclic acyldepsipeptides (ADEPs) and D9 (Fig S3.1A). ADEP and D9 were both described in 2018 as human ClpP activating agents prior to the discovery of a similar mechanism of action for ONC201 and the TR compounds[35]. Madera was the first to prepare a number of highly potent, cell permeable ClpP activators through modifications of peripheral functionality on the chemical core of ONC201, and later through changes to the chemical core[28]. Detailed crystal structure analysis of ClpP and ONC201 further validated ClpP as a direct and specific binding partner[29].

ClpP is a component of the ClpXP protein complex localized in the mitochondrial matrix. ClpP is a tetradecameric serine protease that forms a complex with hexameric AAA+ ClpX, an ATP-dependent protein unfoldase that enables substrate recognition and unfolding prior to its degradation by ClpP[37,38,41,71]. The crystal structure of ClpXP has been solved from a number of species providing detailed insight into how this proteolytic protein complex is regulated. ClpX binds to a hydrophobic pocket in ClpP thereby facilitating the opening of the axial pore and passage of unfolded proteins into the central barrel of ClpP. Pharmacological activators of ClpP, such as the ADEPs, were the first small molecules shown to bind to this hydrophobic pocket and open the axial pore of ClpP in the absence of ClpX, allowing for nonspecific entry of proteins into the active site of ClpP[103–105].

As part of the mitochondrial unfolded protein response, ClpXP canonically targets misfolded proteins to prevent formation of protein aggregates in the mitochondria[43,71]. ClpXP also has regulatory roles in heme biosynthesis[106–108], mitophagy[109,110], and reduction in reactive oxygen species levels following mitochondrial depolarization[38]. ClpP is overexpressed in breast cancer[111], providing the potential

for utilizing highly selective and potent ClpP activators as a novel approach to disrupt mitochondrial metabolic processes required for TNBC proliferation.

In this study, we present data on the characterization of a novel class of highly potent and selective ClpP activators. We focused on one compound, TR-107, and show that it induces the downregulation of select mitochondrial proteins, impairs OXPHOS and inhibits TNBC growth in a ClpP-dependent manner, with markedly improved potency compared to the imipridones (ONC201, 206, 212). Analysis of the pharmacokinetic properties of TR-107 demonstrated high systemic drug levels following oral administration. Furthermore, the efficacy of TR-107 in mouse xenograft models of MDA- MB-231 TNBC cells showed that TR-107 was well tolerated, and inhibited tumor growth and increased animal survival in a manner consistent with ClpP activation. In summary these studies identify TR107 as one of the most potent and selective ClpP activators with anti-cancer potential.

3.2 Results

New TR Chemical Scaffolds are Highly Potent Inhibitors of TNBC Growth

Madera Therapeutics synthesized multiple small molecules containing modifications to the multi-ring core system using the optimized peripheral functionality from TR-65 and similar analogs. This included modification of the core imipridone structure with the appropriate addition of nitrile, halide and trifluoromethyl groups to the two benzyl moieties. The structures of these compounds and other established ClpP agonists (i.e. ADEPS and D9) are shown in Fig. 3.1A, Fig. S3.1A, or a previous publication[28].

We tested the TR compounds' ability to inhibit the growth of two commonly studied TNBC cell lines. Many of these new compounds showed significantly enhanced potency of cell growth inhibition in the MDA-MB-231 and SUM159 cell models compared to ONC201 and ONC206. Of these, TR-98 and TR-107 demonstrated the greatest growth inhibitory potency, comparable to the previously reported TR-57 and TR-65[28]. For example, TR-107 inhibited cell growth with an IC50 of 12 nM and 23 nM in SUM159 and MDA-MB-231 cells, respectively (Fig. 3.1B). By contrast, TR-109 and TR- 122, devoid of a key nitrogen atom of the 6 membered 3-piperideine system (X in structure A, Fig. 3.1A), were less potent, suggesting the importance of a reported hydrogen bond interaction with tyrosine 118 of ClpP[29]. This hydrogen bond is one of three hydrogen bonds observed in the human ClpP-ONC201 complex structure, involving

glutamate 82 and glutamine 107 (through a bridging water molecule) that anchor the molecule to the hydrophobic site of ClpP[29]. Taken together, our data with TR-97, TR-98 and TR-107 show that significant chemical modification of the imipridone core is tolerated and that the imidazoline moiety of the imipridone core is not required for high potency.

To confirm the ClpP dependence of the new TR compounds, the growth inhibitory effects of these compounds were compared in matched pairs of wild-type (WT) and ClpP- KO MDA-MB-231 and SUM159 cell lines. Compared to the dose-dependent inhibition observed in the WT cells, no significant growth inhibition was observed in the ClpP-KO cells, providing evidence that ClpP is the major target for these molecules (Fig. 3.1C). To compare the response to TR-107 in another model of TNBC, we examined the effects of TR-107 on C3(1)-Tag cells and compared the potency of growth inhibition to the tubulin inhibitor paclitaxel, an established therapeutic. The C3(1)-Tag model is a transgenic murine model of TNBC that shares many of the essential characteristics of human TNBC[112]. TR-107 potently inhibited C3(1)-Tag cell proliferation with an IC_{50} value (22 nM), similar to paclitaxel (14 nM) (Fig. 3.1D), which was also similar in potency to that observed with the MD-MBA-231 and SUM159 cells (23 and 12 nM, respectively).

Characterization of Novel Activators of ClpP

We examined the ability of the new TR compounds to bind and activate ClpP. Select TR compounds were incubated with purified recombinant human ClpP and ClpP proteolytic activity was determined using the *in vitro* activity assay described in Materials and Methods. All compounds showed dose-dependent increases in ClpP activity with the greatest potency of ClpP activation observed with TR-107, followed by TR-98 and TR-97 (EC_{50} = 140, 310, and 340 nM respectively). Consistent with reduced effects on cell growth, TR-109 and TR-122 were also weaker activators of ClpP *in vitro* (Fig. 3.2A). Direct binding of TR-107 to purified ClpP was also examined. Surface plasmon resonance (SPR) measurement of TR-107 binding to ClpP, revealed values equivalent to that observed for ClpP activation (K_d ~180 nM) (Fig. 3.2B). Higher concentrations of compound were required for ClpP activation or binding *in vitro,* compared to cell growth inhibition. However, compounds that potently activate ClpP *in vitro* also potently inhibited cell growth as observed above (Fig. 3.1) and as previously reported[28].

TR-107 Inhibits TNBC Growth without a Significant Increase in Apoptosis

Since TR-107 showed excellent potency in these assays, this compound was selected for further testing on cell growth inhibition and apoptosis. MDA-MB-231 or SUM159 cells were incubated with TR-107 and total cell counts determined every 24 hours for up to 72 hours following treatment at the indicated concentrations. As shown in Fig. S3.1B, TR-107 potently (at concentrations >10 nM), inhibited the increase in cell number compared to vehicle control in both cell lines. By comparison, cell growth was not inhibited in the ClpP- KO cells with TR-107 concentrations as high as 1 μM (Fig. S3.1B). Because the highest concentration of TR-107 tested in MDA-MB-231 or SUM159 cells did not reduce the total cell number below the initial seeded number, we tested for evidence of apoptosis.

Caspase-3/7 assays were performed on lysates from the MDA-MB-231 or SUM159 cells following 24-hour compound treatment at indicated concentrations. Caspase activity was quantified as described in Materials and Methods. Staurosporine (STS)-treated cells showed a strong increase in caspase-3/7 activity as expected, whereas no increase in caspase-3/7 activity was detected in lysates from ONC201, TR- 57, or TR-107 treated cells (Fig. S3.1C). Similarly, no increase in PARP cleavage after ONC201, TR-57 or TR-107 treatment was observed (data not shown). Taken together, these findings indicate that the TR compounds show growth inhibitory effects without substantially increasing apoptosis, consistent with previously reported results for ONC201 in MDA-MB-231 cells[22].

TR-107 Induces Time- and Dose-dependent Reduction of Multiple Mitochondrial Proteins

We and others reported that treatment of MDA-MB-231 or SUM159 cells with ONC201 or TR-57 resulted in the reduction of the mitochondrial proteins elongation factor Tu (TUFM) and transcription factor A (TFAM)[22,28]. Since ClpP is a mitochondrial matrix protease, we compared the time and dose-dependent effects of TR-107, TR-57 and ONC201 on additional mitochondrial proteins in MDA-MB-231 and SUM159 cells. As determined by immunoblotting, both TUFM and TFAM protein levels began to decline ~6 hours after treatment with 100 nM TR-107, 150 nM TR-57 or 10 μM ONC201 and showed a complete or near-complete loss by 24 hours (Fig. 3.3A-B; Fig. S3.2A).

We also observed the time- and dose-dependent loss of aconitase (ACO2) and isocitrate dehydrogenase (IDH2), two key TCA cycle enzymes beginning at ~12-24 hours following treatment (Fig. 3.3A-D; Fig. S3.2A-B). Succinate dehydrogenase A (SDHA) and complex I subunit NDUFS3, both

OXPHOS proteins, were observed to decline by 12 to 24 hours (Fig. 3.3A-B; Fig. S3.2A-C). ClpX, the ATPase subunit of the ClpXP complex, was previously observed to decline after 24 hours ONC212 treatment in pancreatic cancer models[113]. We observed ClpX to decline rapidly (~3 hours) after TR compound addition (Fig. 3.3A-B; Fig. S3.2A). The loss of all these proteins was dose- dependent and occurred at concentrations at or above the respective growth inhibitory (IC_{50}) value for each compound with TR-107 showing the most potent effects (Fig. 3.3C-D; Fig. S3.2B). By comparison, the levels of these proteins were not affected in the ClpP-KO cell lines, even at the highest concentration of compound tested (Fig. 3.3, Fig. S3.2).

Heat shock protein 60 (HSP60) is mitochondrial matrix chaperone required for maintaining the folding of imported proteins and HSP60 inhibitors are being investigated as potential anti-cancer compounds[114]. Immunoblotting for HSP60 protein after TR-107 treatment of MDA-MB-231 cells showed that HSP60 levels were significantly reduced in a time-dependent manner (Fig. S3.2D). DNA-directed RNA polymerase, mitochondrial (POLRMT) is a TFAM interacting protein involved in the replication of mitochondrial DNA. Recent studies have shown the efficacy of inhibiting POLRMT as a potential anti-cancer approach[93]. Because of the observed decline in TFAM, we investigated whether POLRMT was similarly affected by these treatments. Immunoblotting data showed that POLRMT followed a dose-dependent decline in full length protein level following TR compound treatment (Fig. S3.2E). Together, these results demonstrate significant effects of TR-107 on mitochondrial proteins involved in energetic and homeostatic processes in a time-, dose-and ClpP-dependent manner.

TR-107 Inhibits OXPHOS in MDA-MB-231 Cells

Because previous studies showed inhibition of OXPHOS by ONC201[22,29] and ADEP[33], we examined the effects of TR-107 on mitochondrial oxygen consumption and respiration using a Seahorse XF Analyzer. Incubation of MDA-MB-231 cells with TR-107 (25, 50 nM), resulted in a dose-dependent decline in oxygen consumption rate (OCR) (Fig. 3.4A). By contrast, this was not observed in ClpP-KO MDA-MB-231 cells (Fig. 3.4B). We observed significant dose-dependent decline in basal mitochondrial respiration, ATP production-linked oxygen consumption, maximal respiration, and spare respiratory capacity following TR-107 treatment in WT but not ClpP-KO cells (Fig. 3.4C). Correspondingly, TR107 incubation caused a dose- dependent increase in extracellular acidification (ECAR, Fig. 3.4C). Taken

together, our results demonstrate substantial disruption of OXPHOS by TR107 in a dose and ClpP-dependent manner.

As shown by Greer *et al*., ONC201 treatment resulted in a greater dependence on glycolysis for cell survival and switching media carbon sources from glucose to galactose enhanced cell growth inhibition by ONC201[22]. We similarly compared the effects of incubating cells in galactose instead of glucose on cell growth inhibition by TR-107. As expected for ONC201, galactose shifted the dose response curve for growth inhibition by ~5-fold (IC_{50} = 1.7 μM (glucose) and 350 nM (galactose)). While the effects on TR-107 on growth inhibition after galactose substitution were much less marked (~2- fold change; IC_{50} = 19 nM (glucose) and 9.8 nM (galactose)) (Fig. 3.4D), these results are consistent with OXPHOS inactivation and an increased reliance on glycolysis after TR- 107 treatment.

Pharmacokinetic Properties of TR-107

With TR-107 and other leading TR compounds showing significantly enhanced potency over ONC201 and functional effects indicative of specific ClpP activation, we compared the PK properties of a set of TR compounds, ONC201 and ONC212/TR-31. The PK studies were conducted by tail vein injection or oral gavage in ICR mice as described in Materials and Methods. Based on the enhanced potency of this set of TR compounds we anticipated an effective oral dose to be ~10 mg/kg or less in a murine model of breast cancer. Therefore, we chose to evaluate the oral exposure of these agents with a single dose of 10 mg/kg and in many cases a 2 mg/kg i.v dose allowing for a F% determination. Importantly, the results of our studies showed significant differences in PK properties among these compounds (Table 3.1).

Of the impridone analogs closely related to ONC201, TR-27, ONC212/TR-31 and TR-65 showed enhanced exposure over ONC201, increased F%, and half-lives ranging from ~0.95-1.68 hours. Our initial studies of ONC201 using either an intravenous dose of 2 mg/kg or oral dose of 10 mg/kg showed markedly different results than what has been previously reported for higher doses. Both arms of our study showed a short $t_{1/2}$ (0.26- 0.31 hours) and poor oral bioavailability (F% = 1.2%) vs. a reported $t_{1/2}$ of 6.4 hours in mouse[11]. Notably, a 25 mg/kg oral dose of ONC201 showed a 46X increase in exposure (AUC) vs the 10 mg/kg study. In addition, ONC212/TR-31 displayed a terminal half-life of 1.49 hours (10 mg/kg) whereas the reported $t_{1/2}$ of an oral dose of 125 mg/kg was 4.3 hours[61] (Table 3.1).

TR-57 and TR-107 displayed the highest exposure (AUC) of the tested agents when administered at 10 mg/kg orally (2710 and 2360 hr*ng/mL respectively, Table 3.1). Both compounds showed rapid absorption via oral administration with an F% of 61% (TR- 57). In addition, protein binding studies for TR-107 shows a serum free fraction of 10% (mouse, Fig. S3.3C). Because of the favorable PK characteristics observed with TR-107 and its efficient molecular design, this compound was selected for advancement into animal xenograft studies described below.

TR-107 Inhibits Tumor Growth in an MD-MBA-231 Mouse Xenograft Model

To determine the *in vivo* anti-tumor efficacy of TR-107, we examined dose-dependent responses using an MDA-MB-231 mouse xenograft model. MDA-MB-231 cells in Matrigel were orthotopically injected into the flank mammary fat pad of female NCr nu/nu mice (10/group) as described in Materials and Methods and Supplemental Information. Vehicle control (Group 1) and TR-107 treatments (4 mg/kg (Group 2), 8 mg/kg (Group 3)) were administered by oral gavage at frequencies described in Table S3.1.

The results of these studies demonstrated a dose- and time-dependent reduction in tumor volume. The mean tumor volume decreased for both treatment groups (G2, G3) with ~50% reduction in tumor volume observed at day 26 (Fig. 3.5A). Comparing the two different groups over the course of the study did not reveal significant advantages of one dosing regimen over the other in tumor volume reduction (Fig. 3.5A, B) or survival (Fig. 3.5C). A ~35% increase in median survival was also observed in mice treated with TR-107 for both groups (Fig. 3.5C). Consistent with ClpP activation, analysis of the tumor lysates from control and treated animals (G3), showed a substantial loss of mitochondrial DNA (Fig. 3.5D). TR-107 treatment was well tolerated and less than 5% weight loss was observed even at the highest dosing regimen (Fig. S3.3). Effects of ONC201 and TR compounds on ClpP activation *in vivo* were further interrogated through immunoblot of xenograft tumor lysates (Fig. 3.5E). These analyses demonstrated significant loss of TFAM consistent with our cell culture studies. Additionally, mitochondrial pyrroline-5-carboxylate reductase 2 (PYCR2) and 3-hydroxy-3-methylglutaryl-CoA synthase 1 (HMGCS1) protein levels were significantly reduced in these tumor lysates. Taken together, TR-107 showed significant efficacy in prevention of tumor growth, consistent with ClpP activation, in the MDA-MB-231 mouse xenograft model.

3.3 Discussion

ONC201, a screening hit with previously described CNS activity[16], was the first imipridone molecule shown to be effective against a variety of cancer models[14,16,18,59,98,113]. Chemically similar derivatives of ONC201 (ONC206 and ONC212/TR-31) were recently identified and both ONC201 and ONC206 are under evaluation in clinical trials. Despite evidence suggesting that ONC201 acts through effects on the dopamine receptor[17], the discovery of the mitochondrial protease ClpP as the target for ONC201 and chemically related compounds[28,29,102] has redefined our understanding of the anticancer mechanism of these agents. Moreover, the identification of ClpP as the major target has enabled the design and characterization of highly potent and specific ClpP activators. In this study, we describe the advancement of the chemically diverse TR compounds as selective ClpP activators, which includes molecules of different chemical scaffolds from which agents for preclinical assessment were selected. We characterize one of these compounds, TR-107, for effects on mitochondrial metabolism and protein turnover, PK properties and TNBC growth inhibition both *in vitro* and *in vivo*. Importantly, these studies further demonstrate the pivotal role for ClpP activation in the mechanism of TR-107 action.

From the collection of TR compounds, we were able to perform initial structure activity relationship (SAR) studies using cell growth inhibition and ClpP activation as determinants. Nanjing Gator Meditech was the first to accurately determine that for the imipridone scaffold, substitution at the V- and Z- positions by small lipophilic moieties was preferential to substitution at the W- position, yielding nM activity in cancer cells[64]. Our survey of residues for the other benzyl ring determined that the nitrile residue at position Y- was preferred. The combination of these two optimized benzyl residues on the imipridone scaffold (TR-65) resulted in markedly improved potency with regards to both ClpP activation and growth inhibition[28] compared to ONC201 and ONC206.

Two key chemical features of the imipridone chemical core are a basic nitrogen of the 3-piperidine moiety and an imbedded acylguanidine. The importance of the basic nitrogen of the piperidiene residue to activity is demonstrated through substitution of the nitrogen atom with carbon atom (e.g., X position, TR-109 and TR-122, Fig. 3.1A). Both TR- 109 and TR-122 are significantly less potent than TR-65 displaying μM IC_{50} values for TNBC cells. We previously reported the modification of the acylguanidine moiety to prepare TR-57 and the homologated analogs TR-79 and TR-80 for target

identification studies[28]. We now report that further modification of TR-57 removing the carbonyl oxygen and methyl residue (R group) gives TR-107, a compound of equal potency. In addition, expansion of the 5-membered ring of the imipridone scaffold by one methylene unit yields TR-98, a compound that is equipotent to TR-65. In summary, the additional modifications described here resulted in two of the most potent ClpP activators (TR-98 and TR-107) so far reported and further support that the imipridone chemical scaffold is not a requirement of potent ClpP activation.

Because of high potency in cell growth and ClpP activation assays, TR-107 was selected for further mechanistic, pharmacokinetic and animal model studies. Other attributes include a low molecular weight (<400 amu), highly potent and defined ClpP dependence, excellent PK properties and efficacy against TNBC models both *in vivo* and *in vitro.* Using two independent ClpP-KO cell lines, our studies confirm the mitochondrial protease ClpP as the key target for TR-107 and related compounds. This includes effects on cell growth, OCR, and mitochondrial protein level as determined by immunoblotting. While ONC201, at concentrations far higher than that is necessary to activate ClpP or inhibit cell growth, has shown effects on dopamine receptors D2/D3[17,115], our data[28] and that of others[22,29] strongly argues against a major role of the dopamine receptors in growth inhibition.

In strong support of a mitochondrial mechanism of action, we observed TR-107 treatment results in reduction of multiple mitochondrial proteins. Some of the most significantly affected proteins, in addition to TFAM and TUFM, included ACO2 and IDH2, which catalyze essential reactions in the TCA cycle. Similarly, respiratory chain proteins NDUFS3 and SDHA declined strongly. Lastly, we observed the ClpP-dependent loss of other essential mitochondrial proteins including POLRMT and HSP60, both of which are predicted to have significant effects on mitochondrial function through regulation of mitochondrial gene replication and protein chaperone functions. Both POLRMT and HSP60 have been shown to be viable drug targets for cancer research[93,114], and provide potential further explanation for the anticancer properties of these compounds. While this is a partial list of all mitochondrial proteins observed to decline following TR-107 treatment, based on these results we propose that inactivation of key mitochondrial functions is, in part, responsible for the growth inhibition observed in these studies.

Mitochondrial dysfunction and metabolic reprogramming are accepted hallmarks of cancer[47,90,116–118]. Inhibiting mitochondrial processes such as OXPHOS has gained interest as an alternative approach

to combatting cancer[51,96,119–123]. Our studies confirm the original findings of Greer *et al*. that ONC201 targets mitochondrial metabolism. In addition to TCA cycle enzymes, we observed proteins with essential roles in OXPHOS that were reduced after ONC201 and TR-107 exposure. The inhibition of OXPHOS was confirmed by mitochondrial respiration analysis and galactose experiments. Interestingly, substituting media glucose for galactose had a much greater effect on the IC_{50} values of ONC201 compared to TR-107. These data further illustrated the superior potency of TR-107 and suggests that the effects of TR-107 may be less dependent of nutritional conditions (e.g., glucose availability) compared to ONC201. Taken together, the results of our studies demonstrate an increased reliance on glycolysis as compensatory response to inhibition of mitochondrial metabolism by ClpP activation.

Previous attempts to inhibit OXPHOS or specific enzymes in the TCA cycle have met with limited success for cancer treatment. The repurposing of metformin [1,1- dimethylbiguanide] as an anticancer agent has been investigated in both research and clinical settings[119,122,124]. As a weak inhibitor of mitochondrial complex I, metformin appears to lack the potency and specificity to effectively treat cancer as a single agent or in combination via complex I inhibition. The complex I inhibitor, BAY 87-2243 is a highly potent inhibitor of complex I with a more complex chemical structure than metformin featuring lipophilic pharmacophores absent in metformin. Notably, clinical evaluation of BAY 87-2243 was terminated after treatment of patients (NCT01297530). A focused contemporary approach by Stuani *et al*. to target mutant forms of IDH 1 and 2 and thereby reducing the oncometabolite (R)-2- hydroxyglutarate (2-HG), led to agents that showed initial efficacy but lost their effectiveness with established disease[125].

As single agents, we observed that ONC201 and the TR compounds induced a growth stasis response in these TNBC models. Even at the highest concentrations tested, little evidence for apoptosis was observed. In this way our results are consistent with earlier studies in TNBC that showed a similar absence of apoptosis after treatment with ONC201[22,99]. Recent studies suggest that addition of TRAIL or TRAIL receptor agonists induces an apoptotic response in cells that have previously displayed a growth stasis response to ONC201[126–128]. Moreover, combination of imipridones with BCL-2 inhibitors has shown promise for increased cancer cell apoptosis[19,23]. Given the greatly improved potency of the TR compounds, it will be important to determine if low concentrations of TR compounds more effectively

sensitize cells to TRAIL treatment or synergize with TRAIL ligand or other agents to increase apoptosis[129].

Lastly, the development of potent and selective ClpP agonists addresses a key limitation for ONC201, ONC206, and ONC212/TR-31 series of compounds regarding the requirement of high doses (50-130 mg/kg) to achieve *in vivo* efficacy[61]. The enhanced potency of ONC206 and TR-31/ONC212 in cellular growth assays did not result in lower *in vivo* efficacious doses. The pharmacokinetic data reported herein, coupled with previously reported results, points to a complex picture of pharmacokinetic behavior of ONC201 and ONC212/TR-31 at therapeutically relevant doses.

TR-107 at an oral dose of 10 mg/kg results in similar $t_{1/2}$ and serum exposure (AUC) to an equivalent oral dose of TR-57. In addition to improved PK properties, TR- 107 effectively reduced tumor volume and increased median survival *in vivo* at 4 and 8mg/kg dosages. Further analysis of xenografts revealed decrease of TFAM protein levels and mitochondrial DNA following TR-107 administration. Similar results were observed with additional mitochondrial proteins (PYCR2), confirming ClpP activation *in vivo* and providing additional evidence for mitochondrial mechanism of action.

In summary, our studies show chemical optimization of ONC201 has resulted in novel ClpP activators with increased potency in both *in vitro* and *in vivo* studies. TR-107 showed excellent potency in TNBC cell growth inhibition and provide further evidence that ClpP activation inhibits growth through loss of mitochondrial metabolic functions. Our *in vivo* studies show that these compounds are highly orally bioavailable, well-tolerated, and effective at reducing tumor burden in an MDA-MB-231 murine xenograft model. In total, our observations support the clinical evaluation of TR-107 for the treatment of TNBC.

There are a number of limitations in our studies that should be mentioned. The characterization of the direct effects of these compounds on purified recombinant ClpP may not accurately replicate the ClpP activation kinetics in vivo. This may be a factor of the concentration of ClpP, the artificial substrates or the assay conditions used that underestimate the potency of ClpP activation by these compounds. In fact, our data from the cell-based analysis of dose-dependent ClpP activation, very closely parallels the effects observed on growth inhibition, for both ONC201 and the TR compounds. Therefore, we believe that the cell-based assays are a better indicator of ClpP activation efficacy and further reflect potential differences in compound cell permeability as well. While there are potential limitations with CRISPR-CAS generation

of knockouts, the fact that we obtained similar results with two completely different CLPP knockout lines, strongly supports the specificity of the compound effects on ClpP. As with any animal study, there are also limitations to our animal studies. We performed our analysis with the least number of animals to achieve a statistically-powered result. Given the fact that ONC201 has been extensively examined in other animal models, we only tested the effects of the TR compounds in these studies. While female mice were used exclusively in our experiments, we acknowledge that a similar study in male mice could be valuable. However, since the focus of our study was breast cancer, we believe that our rationale for this initial study was logical. Lastly, we acknowledge the limitations of studying a single xenograft model. Ideally additional studies will be performed in syngeneic models of breast cancer to fully characterize these important new compounds.

3.4 Materials and Methods

Cell Culture

Human TNBC cell line SUM159 was a generous gift from Dr. Gary Johnson (University of North Carolina at Chapel Hill). MDA-MB-231 (WT and CLPP-KO) cells were provided by Dr. Stanley Lipkowitz (National Cancer Institute). MDA-MB-231 cells were cultured in RPMI 1640 media (Gibco, 11875-093) supplemented with 10% fetal bovine serum (FBS; VWR-Seradigm, 97068-085), and 1% antibiotic–antimycotic (anti/anti; ThermoFisher Scientific, 15240062). SUM159 cells were cultured in Dulbecco's modified Eagle's medium: Nutrient Mixture F-12 (DMEM/F12; Gibco, 11330-032) supplemented with 5% FBS, 5 µg/mL insulin (Gibco, 12585014), 1 µg/mL hydrocortisone, and 1% anti/anti. Cells were maintained at 5% CO2 and 37°C and periodically tested for mycoplasma.

CRISPRi Cell Lines

sgRNA against human ClpP (Eurofins Genomics) was annealed and ligated into vector VDB783. This vector was transformed into DH5a cells and the presence of sgRNA was confirmed by colony PCR. Lentivirus was produced in HEK293T cells following transfection with plasmid and jetPRIME (PolyPlus) as previously described[130]. Clonal populations of SUM159 cells infected with dCas9-KRAB lentivirus were clonally isolated to ensure dCas9-KRAB expression. Isolated SUM159 cells were infected with ClpP sgRNA lentivirus followed by additional selection passage in growth media supplemented with 2.5 mg/ml puromycin.

Synthesis of Compounds

All TR compounds were prepared by Madera Therapeutics, LLC as previously described in the patent literature[131]. ONC201, ONC206, and ONC212/TR-31 were purchased from Selleck Chemicals, LLC (S7963, S6853, S8673, respectively).

Viability Assays

Total cell counting assays were performed by seeding MDA-MB-231 cells (WT and ClpP- KO; 4000 cells/well) or SUM159 (WT and ClpP-KO; 1000 cells/well) in a 96-well plate (Perkin Elmer, 6005050) and allowed to adhere overnight. Growth medium was then aspirated and replaced with 100 µL of growth medium supplemented with drug at concentrations indicated in the figure or figure legends. Cells treated with vehicle control (0.1% DMSO, Sigma-Aldrich D2650) were used as a negative control in all experiments and cells were incubated with drug-containing media for 24, 48, or 72 hours as indicated in figure legends. Media was then aspirated and replaced with 100 µL Dulbecco's phosphate buffered saline (DPBS Gibco, 14190-144) containing 1 µg/mL Hoechst stain (ThermoFischer Scientific, H3570) and allowed to incubate at 37°C for 30 minutes. Total cell number was then quantified using the Celigo Imaging Cytometer (Nexcelom).

Immunoblotting

MDA-MB-231 or SUM159 cells were plated (100,000 cells/well) on a 6-well Costar plate (Corning, 3516) and incubated with compounds as described above for cell viability assays. Following treatment, cells were rinsed three times with 2 mL of cold DPBS and lysed using RIPA buffer (20 mM Tris (pH 7.4), 137 mM NaCl, 10% glycerol, 1% Nonidet P-40, 0.5% deoxycholate, 2 mM EDTA) supplemented with 2 mM Na3VO4, 10 mM NaF, 0.0125 µM calyculin A, and complete protease inhibitor cocktail (Roche Diagnostics, 11873580001). Cell lysates were clarified and immunoblotted as described earlier[79]. Membranes were incubated with primary antibodies obtained from Cell Signaling Technologies (SHDA (5839), ClpP (14181), ACO2 (6922), TFAM (8076), HMGSC2 (36877)), Invitrogen (TUFM (PA5-27511), IDH2 (PA5-79436), POLRMT (PA5-28196)), Abcam (ClpX (168338), NDUFS3 (183733)), BD Transduction Laboratories (HSP60 (611562)), Sigma Aldrich (PYCR2 (HPA056873)), and Santa Cruz Biotechnologies (TFAM (sc-376672), Vinculin (sc-73614), HSC70 (sc-7298)), diluted 1:1000 in 1% fish gelatin (Sigma Aldrich, G7041)/TBST overnight at 4°C, removed, washed 3 x 5 minutes in TBST, and

placed in their respective 2° antibodies (Promega, W401B and W402B, 1:10,000 dilution in 5% milk/TBST) for 1 hour. Membranes washed 3 x 5 minutes in TBST then incubated in ECL reagent (BioRad, 170-5061) and imaged using a Chemidoc MP (BioRad) or Odyssey Fc (LI-COR). Acquired images were processed/quantified using Image Lab software (BioRad) or Image Studio Lite (LI-COR).

Caspase Activity Assay

Caspase-3/7 activity was analyzed using a fluorescent peptide substrate (Ac-DEVD- AMC, Cayman Chemical, 14986) as previously described[79]. Briefly, cells were plated at 1 x 10^5 cells per well (6 cm^2 plate, Corning, 430166) and treated for 24 hours with 10 μM ONC201, 150 nM TR-57, 100 nM TR-107 (10X IC_{50}) as well as 0.1% DMSO or 100 nM staurosporine. The samples were collected in lysis buffer (50 mM HEPES (pH: 7.4), 5 mM CHAPS, and 5 mM DTT), and caspase activity was measured by monitoring fluorescence (ex/em: 360 nm/ 460 nm) using a SpectraMax i3x (Molecular Devices).

ClpP Activity Assay

Measurement of in vitro activity of purified recombinant human ClpP was performed with a slight modification to the method previously described[34]. Briefly, ClpP activity was measured through degradation of casein-FITC (Sigma-Aldrich, C0528) in the presence of indicated compounds. The activity of ClpP proteolytic subunit (41 μg/mL (1.4 μM)) was measured in assay buffer (20 mM HEPES (pH 8.0), 100 mM KCl, 1 mM DTT, and 100 μM ATP) using 235 μg/mL fluorogenic casein-FITC substrate. Enzyme and compounds were mixed and incubated in assay buffer for 30 minutes before adding casein-FITC substrate. The kinetics of substrate degradation fluorescence was monitored in 96-well plates (PerkinElmer, 8059-21401), and fluorescence was recorded at 490 nm/ 525 nm (ex/em) using SpectraMax i3x (Molecular Devices). Linear slope of fluorescence signal was used to measure ClpP activity and normalized to DMSO control, expressed as RFU/hour.

Surface Plasmon Resonance (SPR)

For the SPR experiments, recombinant human ClpP was purified as previously described[34]. SPR measurements were performed on a Biacore X100 instrument (Cytiva Life Sciences, Marlborough, MA, USA) at 25°C in buffer (25 mM sodium phosphate, pH 7.5, 200 mM KCl, 0.05% Tween-20, and 0.004% DMSO). ClpP was immobilized onto flowcell 2 of a CM5 chip (Cytive Life Sciences, Marlborough, MA, USA) using the amine coupling wizard using Biacore X100 Control Software. A pulse of a mixture of NHS

and EDC activated the CM5 chip surface. ClpP was diluted to 100 µg/ml in 10 mM sodium acetate, pH 4.5 immediately prior to use and injected over the activated surface for 180 seconds. Remaining activated sites were blocked with a pulse of ethanolamine. 12000 RU of ClpP was captured using this procedure. Flowcell 1 was unmodified and served as a reference. For TR-107 binding to ClpP, a concentration series of TR-107 in DMSO was diluted into buffer to achieve 0.004% final DMSO concentration in all samples. Three replicates were injected for each concentration. Data were blank subtracted and analysis was performed in Biacore X100 Evaluation Software (Cytiva Life Sciences, Marlborough, MA, USA). The steady state response was calculated at 15 seconds before the end of injection with a window of 15 seconds. Data were fitted to a one-site Langmuir binding model.

Mitochondrial Respiration Analysis

Cellular oxygen consumption and extracellular acidification rates (OCR and ECAR, respectively) were measured using Seahorse XFe96 (Agilent, Santa Clara, CA, USA). MDA-MB-231 cells were plated (15,000 cells/well) in Seahorse XF96 plates (Agilent, 102416-100) and allowed to adhere overnight. Cells were then treated with 25 or 50 nM TR-107 for 24 hours. On the day of Seahorse XF analysis, growth medium was replaced with XF base medium (Agilent, 103575-100) supplemented with appropriate concentrations of TR-107. After measurement of basal OCR/ECAR, 1 µM Oligomycin, 1 µM FCCP, 1 µM Rotenone/Antimycin A (Agilent, 103015-100) were added at indicated timepoints. OCR/ECAR were measured every 6.5 minutes for 73 minutes.

Mitochondrial DNA (mtDNA) Copy Number Analysis

Mitochondrial DNA copy number was determined as previously described[22]. Briefly, genomic DNA was isolated from tissue lysate with DNeasy Blood & Tissue kit (Qiagen, 69504). mtDNA copy number was determined by quantitative PCR with Human mitochondrial to nuclear DNA ratio kit (Takara Bio USA, 7246).

Pharmacokinetic Analysis

The compounds were evaluated for pharmacokinetic properties in ICR mice (Sino-British SIPPR/BK Lab Animal Ltd, Shanghai, China) by Shanghai Medicilon, Inc. The compounds were administered either intravenously (tail vein) or orally (oral gavage) in vehicle (5% DMSO, 10% Solutol [Kolliphor HS 15, Sigma Aldrich, 42966] in sterile DPBS, 85% water) to three male mice per study arm.

Blood was taken via the orbital venous plexus (0.03 mL/timepoint) at 0.083, 0.25, 0.5, 1, 2, 4, 8 and 24 hours, unless otherwise noted. Samples were placed in tubes containing heparin sodium and stored on ice until centrifuged. Blood samples were centrifuged at 6800 x g for 6 minutes at 2-8°C within 1 hour following sample collection and stored at -80°C. Proteins from plasma sample aliquots (20 µL) were precipitated by the addition of MeOH (400 µL) containing an internal standard (tolbutamide,100 ng/mL), vortexed for 1 minute, and centrifuged at 18,000g for 7 minutes. Supernatant (200 µL) was transferred to 96 well plates for analysis.

Analysis of samples was conducted as follows. An aliquot of supernatant (1 µL) was analyzed for parent compound by LC-MS/MS using a Luna Omega C18 column (2.1 x 50 mm, 1.6 µm; Phenomenex, 00B-4747-B0) with 0.1% formic acid/water and 0.1% formic acid/acetonitrile gradient system, and a TQ6500+ triple quad mass spectrometer (positive ionization mode). In the case of TR-107, the parent compound and internal standard (IS) were detected with electrospray ionization in positive mode (ESI+) using multiple-reaction monitoring (MRM) of mass transition pairs at m/z of 391.2/247.2 (TR- 107) and 271.1/172.0 (IS, tolbutamide) amu. The calibration curve was obtained by spiking known concentrations (2 to 2000 ng/mL) of TR-107 into blank mouse plasma. The PK parameters including Area Under the Curve (AUC(0-infinity)) elimination half-life (t1/2), maximal plasma concentration (Cmax), and oral bioavailability (F%) were analyzed by non- compartmental methods.

Protein Binding Studies to Plasma Proteins

Protein binding studies were performed by Eurofins Panlabs, Inc. This assay utilizes equilibrium dialysis in a microplate format, as previously described[132]. Briefly, this analysis is used to determine the bound and unbound fraction of the drug and calculate the percentage of the test compound binding to murine plasma proteins.

Mouse Xenograft Studies

Mice

Female athymic nude mice (Crl:NU(Ncr)-Foxn1nu, Charles River) were eight weeks old with a body weight (BW) range of 19.0 to 27.0 grams on Day 1 of the study. Animals were fed ad libitum water (reverse osmosis, 1ppm Cl) and NIH 31 Modified and Irradiated Lab Diet® consisting of 18.0% crude protein, 5.0% crude fat, and 5.0% crude fiber. Mice were housed on irradiated Enrich-o'cobs™ Laboratory

Animal Bedding in static microisolators on a 14-hour light cycle at 20-22°C and 40-60% humidity. Charles River Discovery Services North Carolina (CR Discovery Services) specifically complies with the recommendations of the Guide for Care and Use of Laboratory Animals with respect to restraint, husbandry, surgical procedures, feed and fluid regulation, and veterinary care. Animal care and use program at CR Discovery Services is accredited by the Association for Assessment and Accreditation of Laboratory Animal Care International.

Tumor Cell Culture

MDA-MB-231 human breast adenocarcinoma cells were grown to mid-log phase in RPMI-1640 supplemented with 10% FBS, 2 mM glutamine, 100 units/mL sodium penicillin G, 25 µg/mL gentamicin, 100 µg/mL streptomycin sulfate, 0.075% sodium bicarbonate, 10 mM HEPES, and 1 mM sodium pyruvate. Cells were cultures in 37°C and 5% CO2.

In Vivo Implantation and Tumor Measurement

MDA-MB-231 cells were harvested during exponential growth and resuspended in cold, sterile DPBS. Each animal received an orthotopic injection of 5 x 10^6 cells (0.05 mL volume) into the mammary fat pad. Tumor growth was monitored as the average tumor size approached target range of 60-100 mm^3. Tumors were measured in two dimensions via caliper and volume was calculated using the following formula:

$$Tumor\ Volume = \frac{w^2\ x\ l}{2}$$

Where w =width and l= length (mm) of the tumor. Tumor weight was estimated based on the assumption that 1 mg = 1 mm^3. Fourteen days later (Day 1), animals were sorted into groups (n=10 per group) with a mean tumor volume of 70-73 mm^3.

Treatment

Mice began dosing on Day 1 as summarized in Table S3.1. Compounds were administered orally (p.o.) in a dosing volume of 10 mL/kg. Twice daily doses (B.I.D) were administered at least 6 hours apart.

Endpoint and Tumor Growth Delay (TGD) Analysis

Tumors were measured using calipers biweekly and animals were euthanized upon reaching tumor volume >1500 mm3 or on the final study day (Day 36), whichever came first. Time to endpoint

(TTE) for analysis was calculated for animals that exited the study due to tumor volume using the following equation:

$$TTE = \frac{log_{10}(endpoint\ volume) - b}{m}$$

Where TTE is expressed in days, endpoint volume is expressed in mm^3, b is the y- intercept, and m is the slope of the line obtained by linear regression of a log- transformed tumor growth data set. This dataset consisted of the first observation that exceeded 1500 mm^3 and the preceding three consecutive measurements. Animals that did not reach the tumor volume threshold were assigned a TTE value of 36 days (equivalent to study end). In instanced where this equation yields a TTE day preceding the day prior to reaching endpoint or exceeded the day of reaching endpoint, a linear interpolation was performed to approximate TTE. Animals documented as having died of non-treatment-related causes due to accident or unknown etiology were excluded from TTE calculations and all further analysis. Animals documented having died due to treatment-related deaths or non-treatment-related due to metastasis were assigned a TTE value equivalent to day of death. Treatment outcome was evaluated from tumor growth delay (TGD) defined as the increase in the median TTE. In the treatment group compared to the control group.

Sampling

On Day 36, all animals in all groups were sampled. Tumors were excised, divided into two parts, and weighed. Part 1 was preserved in 5 mL fixative solution (4% formaldehyde, 2% glutaraldehyde in 0.1M cacodylate buffer) and stored at 4°C. Part 2 was trimmed to be less than 0.5 cm in at least one dimension, submerged in 5 volumes of RNAlater solution, and stored at -20°C.

Statistical Analysis

Statistical analysis for viability, mitochondrial respiration, ClpP activity assays, and animal studies was performed using Prism 9 (GraphPad, San Diego, CA, USA). Analysis of pharmacokinetic data was performed using FDA certified pharmacokinetic program Phoenix WinNonlin 7.0 (Pharsight, Mountain View, CA, USA). In the mouse xenograft study, study groups experiencing toxicity beyond acceptable limits (>20% group mean BW loss or >10% treatment-related deaths) or having fewer than five evaluable observations were not included in statistical analysis. Survival was analyzed by Kaplan- Meier method and logrank (Mantel-Cox) test was used to determine significance between overall survival experiences based on TTE values.

Statistical Analysis

Statistical analysis for viability, mitochondrial respiration, ClpP activity assays, and animal studies was performed using Prism 9 (GraphPad, San Diego, CA, USA). Analysis of pharmacokinetic data was performed using FDA certified pharmacokinetic program Phoenix WinNonlin 7.0 (Pharsight, Mountain View, CA, USA). In the mouse xenograft study, study groups experiencing toxicity beyond acceptable limits (>20% group mean BW loss or >10% treatment-related deaths) or having fewer than five evaluable observations were not included in statistical analysis. Survival was analyzed by Kaplan- Meier method and logrank (Mantel-Cox) test was used to determine significance between overall survival experiences based on TTE values.

3.5 Figures and Tables

A

Comp'd (A)	n	X	Y	W	Z	V
ONC201	1	N	H	Me	H	H
ONC206	1	N	H	H	F	F
ONC212/ TR-31	1	N	H	H	H	CF_3
TR-27	1	N	CCH	H	H	Cl
TR-65	1	N	CN	H	H	Cl
TR-98	2	N	CN	H	H	CF_3
TR-106	2*	N	CN	H	H	Cl
TR-109	1	CH	CN	H	H	CF_3
TR-122	1	CH	CN	H	H	Cl

Comp'd (B)	R	V
TR-57	Me	Cl
TR-79	$(CH_2)_3NH_2$	CF_3
TR-80	$(CH_2)_4NH_2$	CF_3

Comp'd (C)	R
TR-97	Me
TR-107	H

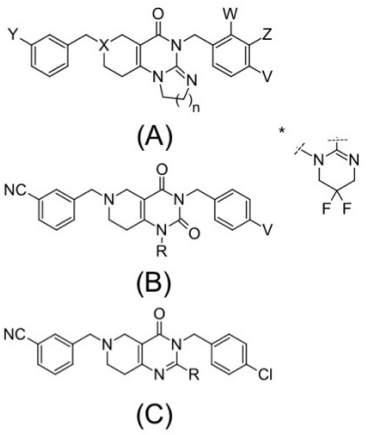

B

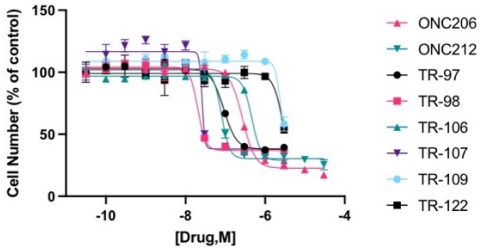

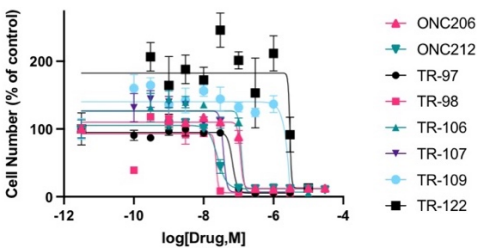

C

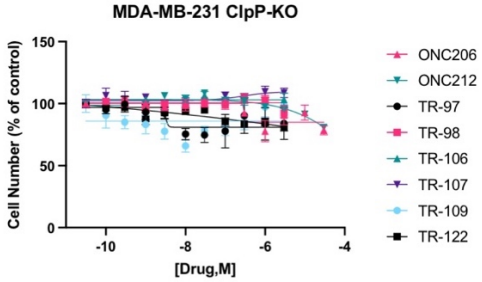

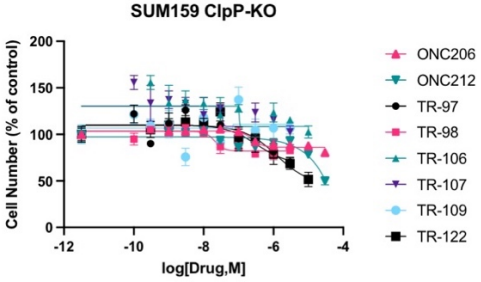

D

Comp'd	IC50 (nM)	
	MDA-MB-231	SUM159
ONC201	1700	1700*
ONC206	260	180
ONC212	80	27
TR-97	104	53
TR-98	21	24
TR-106	430	120
TR-107	23	12
TR-109	2200	4600
TR-122	2600	3500

E

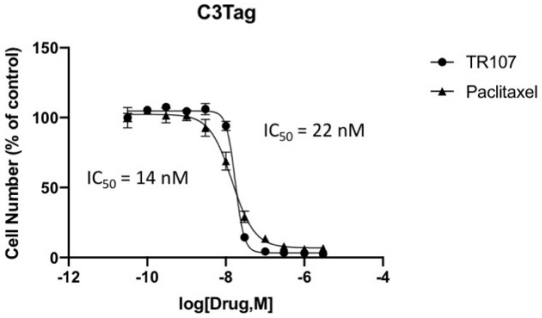

Figure 3.1. New TR compound analogs potently inhibit breast cancer cell growth in a ClpP-dependent manner. A) Comparison of novel TR compound chemical structures to ONC201 and analogs. Cell viability assays of (B) Wildtype (WT) and (C) ClpP knockout (ClpP-KO) MDA-MB-231 and SUM159 cells. Cells were treated with indicated drug concentrations for 72 hours and imaged following addition of Hoechst stain as described in Materials and Methods. Values represent mean ± SEM normalized to DMSO control, representative of N=3. D) IC_{50} values in WT cells for compounds represented in panel B. Values represent mean IC_{50} value (nM), N=3. *ONC201 IC_{50} in MDA-MB-231 cells obtained from data shown in Figure 4D, and IC_{50} of ONC201 in SUM159 cells was previously published[28]. E) Cell viability assay of C3Tag cells following TR-107 and paclitaxel treatment. Cells were treated with drug concentrations as indicated for 72 hours and imaged following Hoechst stain addition. Representative of N=2. Average IC_{50} values indicated to the left and right of the graph for paclitaxel and TR-107, respectively.

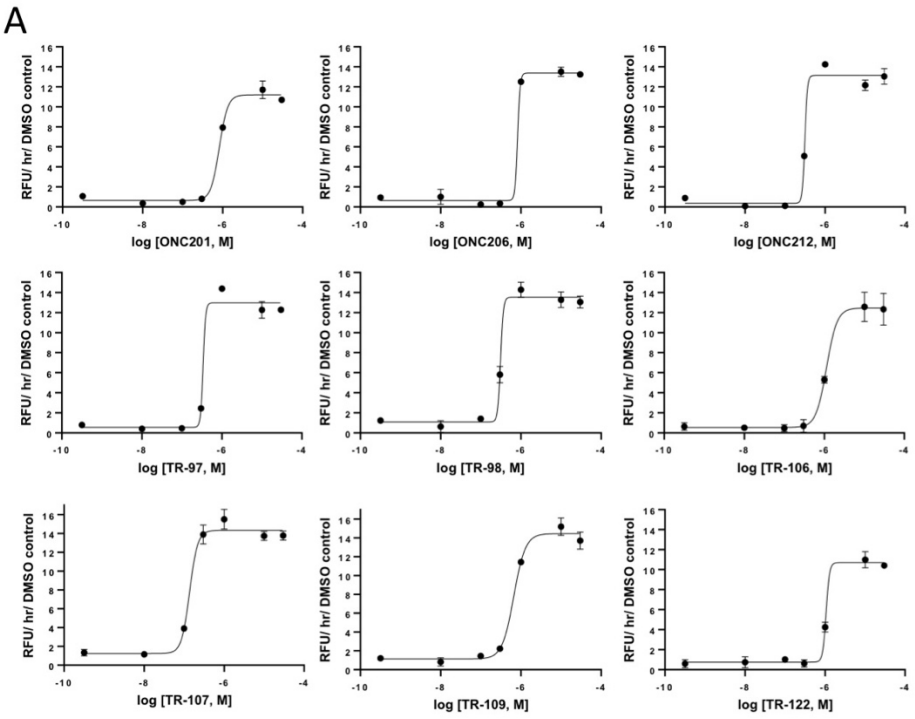

Compound	EC_{50} (nM)
ONC201	820
ONC206	830
ONC212	310
TR-97	340
TR-98	310
TR-106	1100
TR-107	140
TR-109	670
TR-122	1100

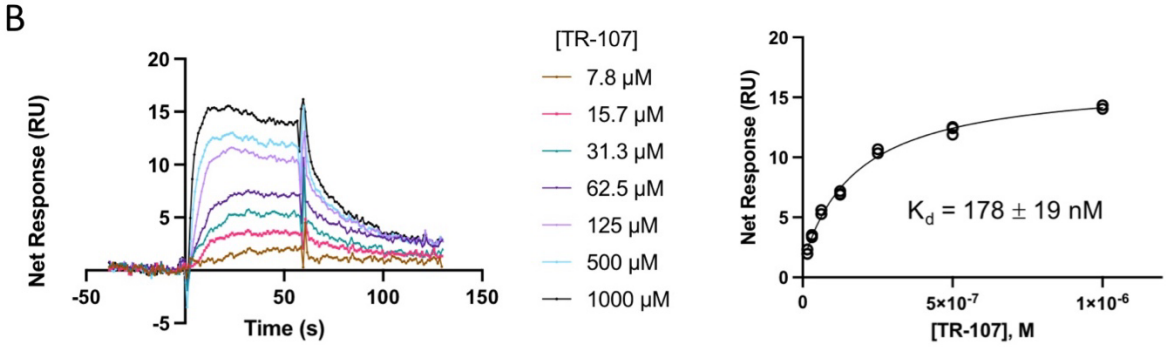

Figure 3.2. New TR compounds are potent activators of mitochondrial ClpP. A) *In vitro* ClpP activity assays were performed as described in Materials and Methods using fluorescent casein-FITC. Increase in fluorescent intensity relative to DMSO controls is shown; values represent mean ± SEM for technical replicates. EC_{50} values are presented in the table to the right. B) Left panel- surface plasmon resonance (SPR) sensorgrams for TR-107 binding to recombinant human ClpP coupled on the chip. Right panel- binding curves are shown as response units (RU) vs. ligand concentration at steady state and fitted to a one-site Langmuir binding model. The apparent K_d value obtained from the fit is shown.

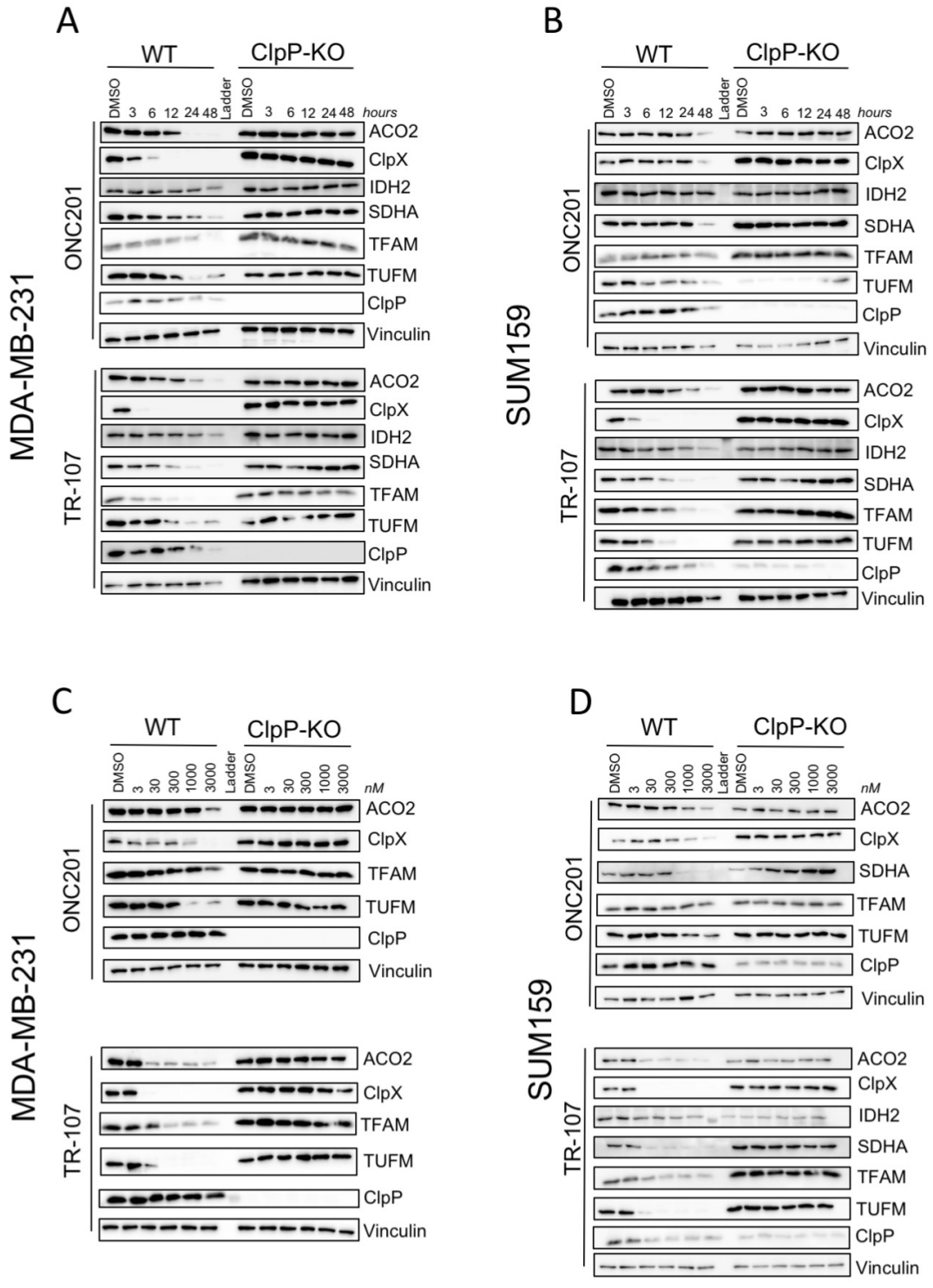

Figure 3.3. TR-107 induces loss of mitochondrial proteins in TNBC cells in a ClpP-dependent manner. Triple-negative breast cancer cells MDA-MB-231 (A, C) and SUM159 (B, D) were treated with 10 μM ONC201 or 100 nM TR-107 for indicated time points (A, B) or indicated doses (C, D) of ONC201 and TR-107 for 24 hours and immunoblot was performed for various mitochondrial proteins. Representative of N=3.

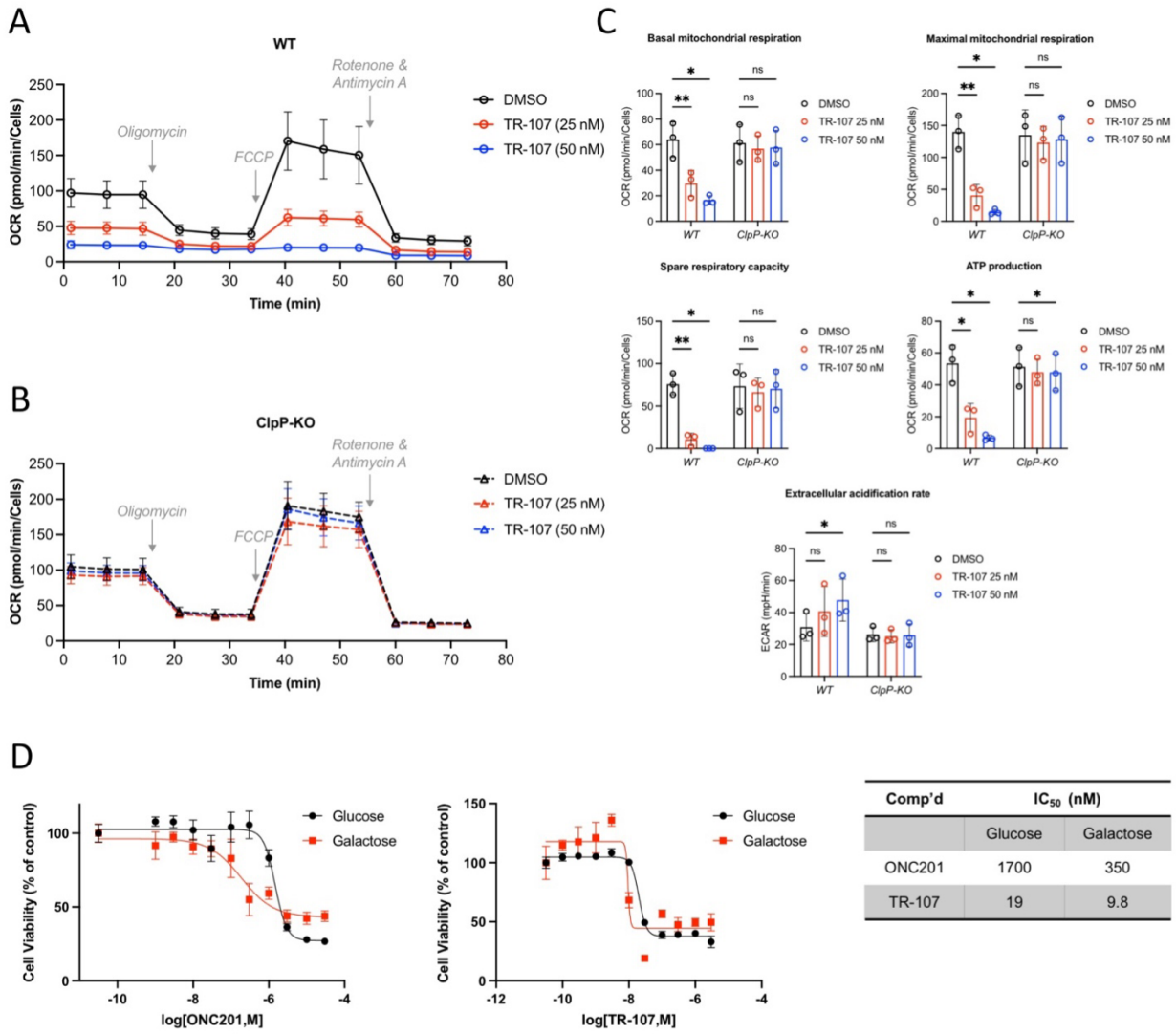

Comp'd	IC_{50} (nM)	
	Glucose	Galactose
ONC201	1700	350
TR-107	19	9.8

Figure 3.4 TR-107 reduces mitochondrial metabolic functions in MDA-MB-231 cells. Oxygen consumption rate (OCR) of MDA-MB-231 cells treated with DMSO or TR-107 at indicated concentrations for 24 hours was measured by Seahorse XK Analyzer as described in Materials and Methods. Traces of oxygen consumption data following TR-107 treatment in (A) WT and (B) ClpP-KO MDA-MB-231 cells, representative of N=3 experiments. Indicated compounds were added at concentrations described in Materials and Methods. C) Bar charts of data shown in (A) and (B), values represent mean ± SEM, N=3. P-value < 0.05 (*), 0.001 (**). D) Cell viability assays (Hoechst stain, 72 hours) of MDA-MB-231 cells treated with ONC201 (left) or TR-107 (right) at indicated concentrations in media containing either glucose (black) or galactose (red). Values represent mean ± SEM, N=3. Average IC_{50} values are presented in table (right).

Table 3.1 Pharmacokinetic analysis of select compounds in mice. Each arm of pharmacokinetic studies were performed as described in Materials and Methods. Blood collection for ONC201 at 25 mg/kg (oral) was 0.083-4 hours. The TR compounds were administered intravenously ("i.v.") (2.0 mg/kg) or by oral gavage ("oral") (10 mg/kg) in vehicle, described in Materials and Methods. *A 2.5X increase in oral gavage dose gave a 46X increase in exposure (AUC). Three male ICR mice were utilized per study arm.

Comp'd	Admin (mg/kg)	$T_{1/2}$ (hr)	C_{max} (ng/mL) [μM]	AUC (0-∞; h*ng/mL)	F%
ONC201	2.0, i.v.	0.26	122 [0.31]	50.7	N/A
	10, oral	0.31	8.99 [0.023]	3.13 (1X)	1.2
	25, oral	---	195 [0.50]	145 (46X)*	N/A
TR-27	2.0, i.v.	1.06	154 [0.35]	155	N/A
	10, oral	1.16	127 [0.29]	255	33
ONC212/TR-31	2.0, i.v.	1.68	950 [2.2]	638	N/A
	10, oral	1.49	282 [0.64]	449	14
TR-65	2.0, i.v.	0.73	636 [1.5]	351	N/A
	10, oral	0.95	294 [0.67]	584	33
TR-57	2.0, i.v.	1.52	1240 [3.0]	886	N/A
	10, oral	1.40	1710 [4.1]	2710	61
TR-107	10, oral	0.90	1440 [3.7]	2360	N/A

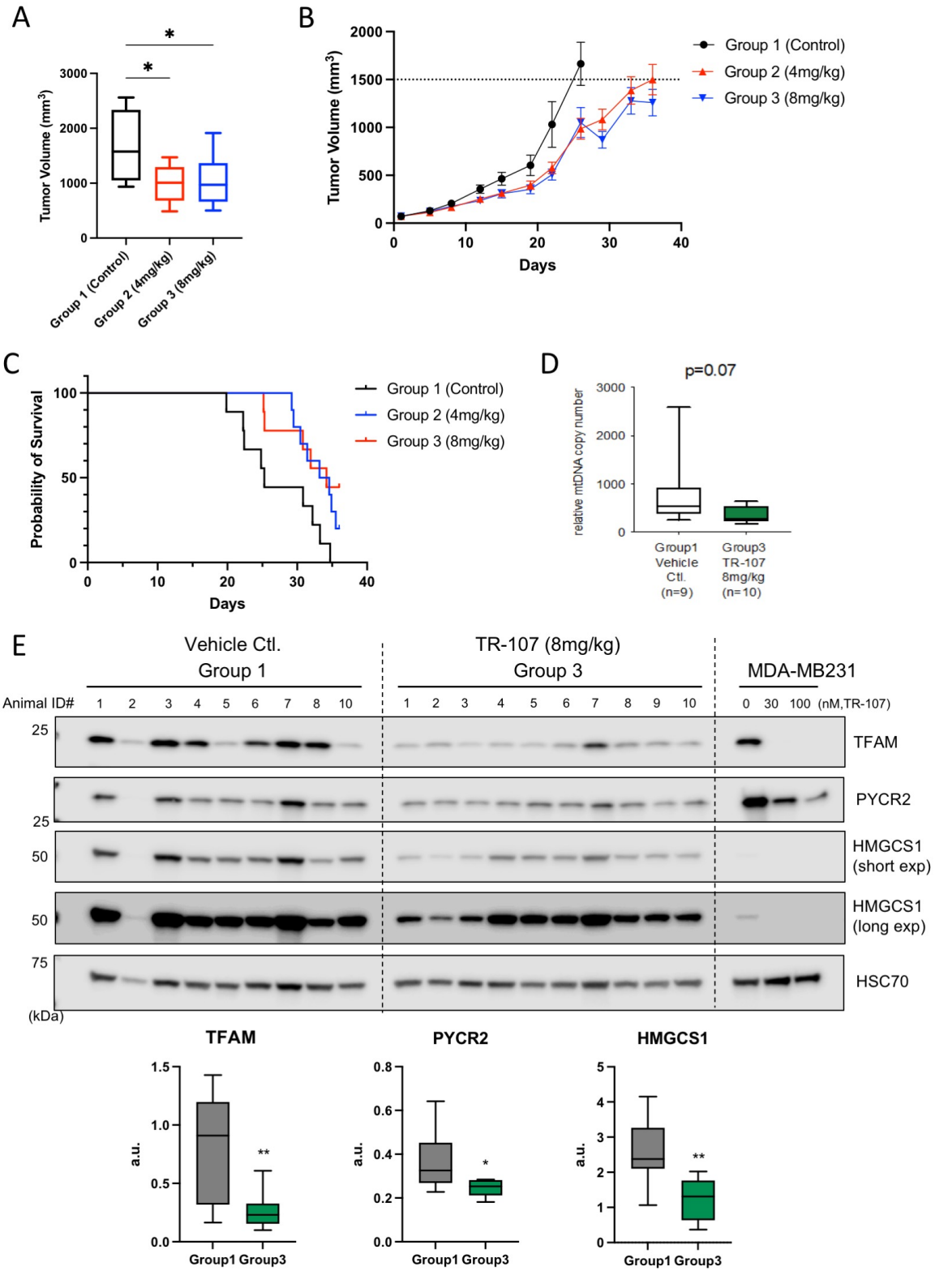
A
Tumor Volume (mm³)
3000
2000
1000
0
*
*
Group 1 (Control)
Group 2 (4mg/kg)
Group 3 (8mg/kg)
B
Tumor Volume (mm³)
2000
1500
1000
500
0
0
10
20
30
40
Days
Group 1 (Control)
Group 2 (4mg/kg)
Group 3 (8mg/kg)
C
Probability of Survival
100
50
0
0
10
20
30
40
Days
Group 1 (Control)
Group 2 (4mg/kg)
Group 3 (8mg/kg)
D
p=0.07
relative mtDNA copy number
3000
2000
1000
0
Group1
Vehicle
Ctl.
(n=9)
Group3
TR-107
8mg/kg
(n=10)
E
Vehicle Ctl.
Group 1
TR-107 (8mg/kg)
Group 3
MDA-MB231
Animal ID#
1 2 3 4 5 6 7 8 10
1 2 3 4 5 6 7 8 9 10
0 30 100 (nM,TR-107)
25
TFAM
25
PYCR2
50
HMGCS1
(short exp)
50
HMGCS1
(long exp)
75
HSC70
(kDa)
TFAM
PYCR2
HMGCS1
a.u.
1.5
1.0
0.5
0.0
**
Group1 Group3
a.u.
0.8
0.6
0.4
0.2
0.0
*
Group1 Group3
a.u.
5
4
3
2
1
0
**
Group1 Group3

Figure 3.5. TR-107 prevents tumor growth in MDA-MB-231 xenograft model. A) Box-and-whisker plot of tumor volume (mm^3) of MDA-MB-231 xenografts following TR-107 treatment at indicated concentrations at Day 26 (Table S3.1). N=8 (Group 1) and 10 (Groups 2, 3). B) Average tumor volume following TR-107 administration as described in Methods. The tumor volume threshold (1500 mm^3) is indicated by dashed line. N=10 per group. Values represent mean ± SEM. C) Kaplan-Meier graph of mouse survival following TR-107 administration as described in Methods and Table S3.1. Long-rank (Mantel-Cox) p-value of 0.0163. Individual mice were recorded as leaving the study following death, tumor volume exceeding threshold (1500 mm^3), or end of study period. D) Box-and-whisker plot of relative mitochondrial DNA (mtDNA) copy number present in mouse xenograft lysate following conclusion of mouse study. N=9 (Group 1) and N=10 (Group 3). E) Immunoblot (top) from tumor lysates of mouse xenografts following administration of vehicle control or 8 mg/kg TR-107. Each animal ID represented an individual mouse. Two images are shown for HMGCS1 representing a short exposure ("short exp") and long exposure ("long exp"). Quantification of these blots is shown in the box-and-whisker plot (bottom) with indicated p-values (<0.05 (*) and 0.01 (**)).

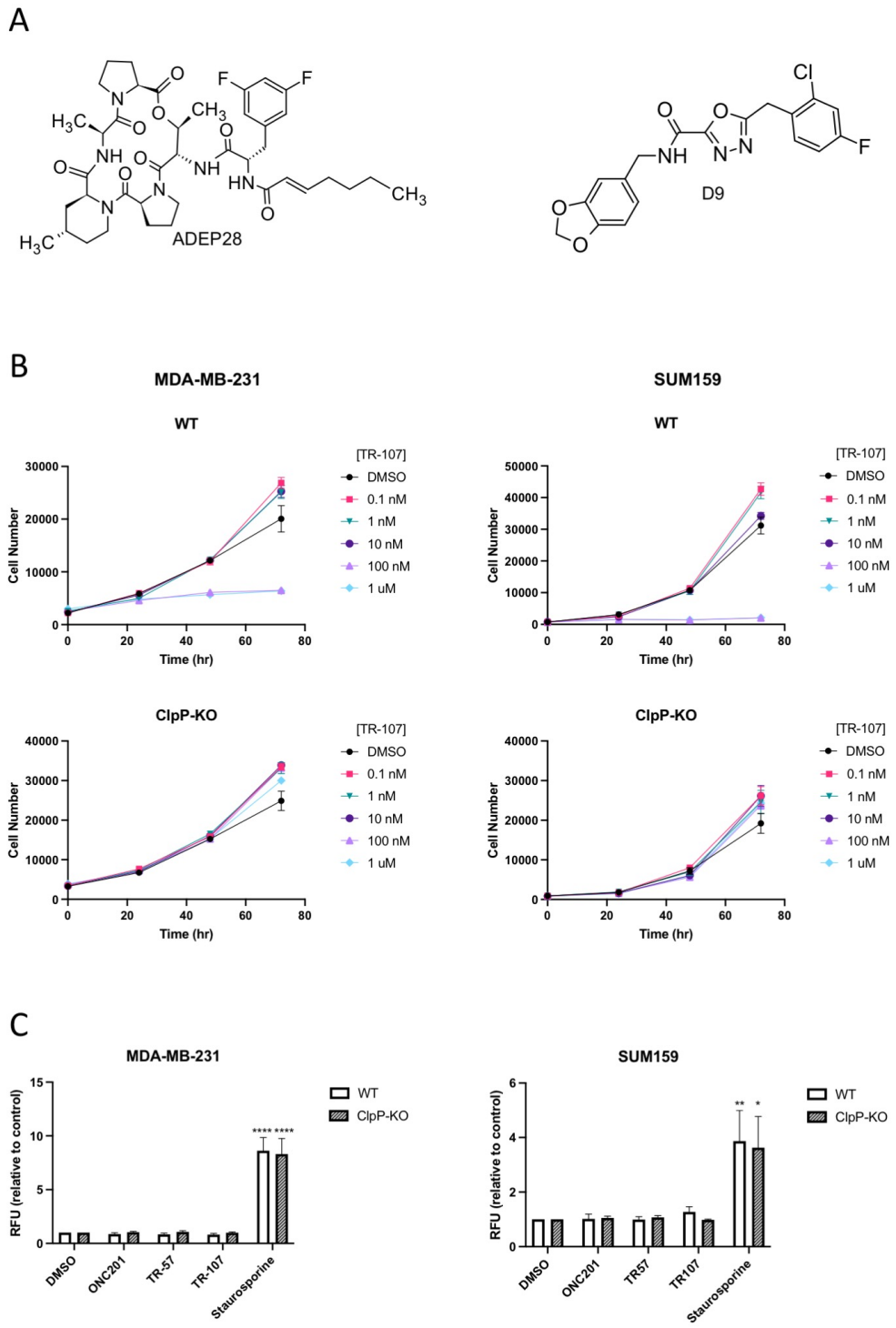

Figure S3.1 TR compounds do not induce cell death in breast cancer cell lines. A) Chemical structures of ClpP activators ADEP28 and D9. B) Total cell count assay in SUM159 and MDA-MB-231 cells (WT and ClpP-KO). Cells were treated with indicated drug concentrations for 0, 24, 48, and 72 hours and counted using Hoechst stain. Values represent mean cell count ± SEM, Representative of N=2. C) *In vitro* caspase-3/7 activity assay in SUM159 and MDA-MB-231 cells (WT and ClpP-KO). Cells were treated with 10 μM ONC201, 150 nM TR-57, 100 nM TR-107 or 100 nM staurosporine for 24 hours and caspase activity was measured via fluorometric caspase activity assay. Values represent mean fluorescence value ± SEM, N=3, p-value < 0.05 (*), 0.01(**), 0.0001 (****)

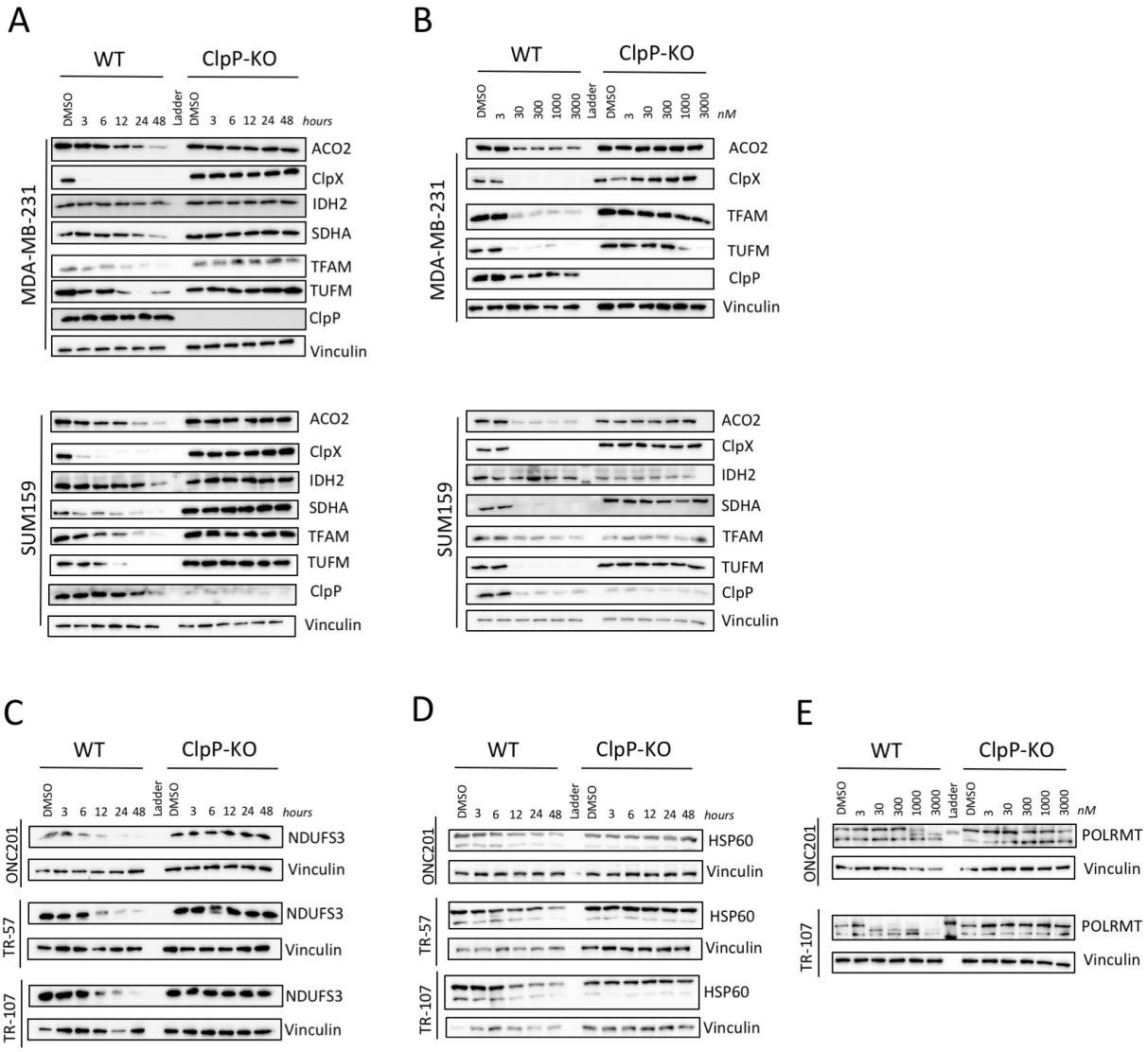

Figure S3.2. ONC201, TR-107 and TR-57 induce loss of mitochondrial proteins in TNBC cells in a ClpP-dependent manner. MDA-MB-231 and SUM159 cells were treated with 150 nM TR-57, for indicated timepoints (A) or with indicated doses for 24 hours (B) and immunoblot was performed for mitochondrial metabolic proteins. MDA-MB-231 cells were treated with 10 μM ONC201, 150 nM TR-57, or 100 nM TR-107 for indicated timepoints and immunoblotted for (C) NDUFS3 and (D) HSP60. (E) MDA-MB-231 cells treated with indicated concentrations of ONC201 or TR-107 for 24 hours were immunoblotted for POLRMT. N=3 (A, B) and N=2 (C-E).

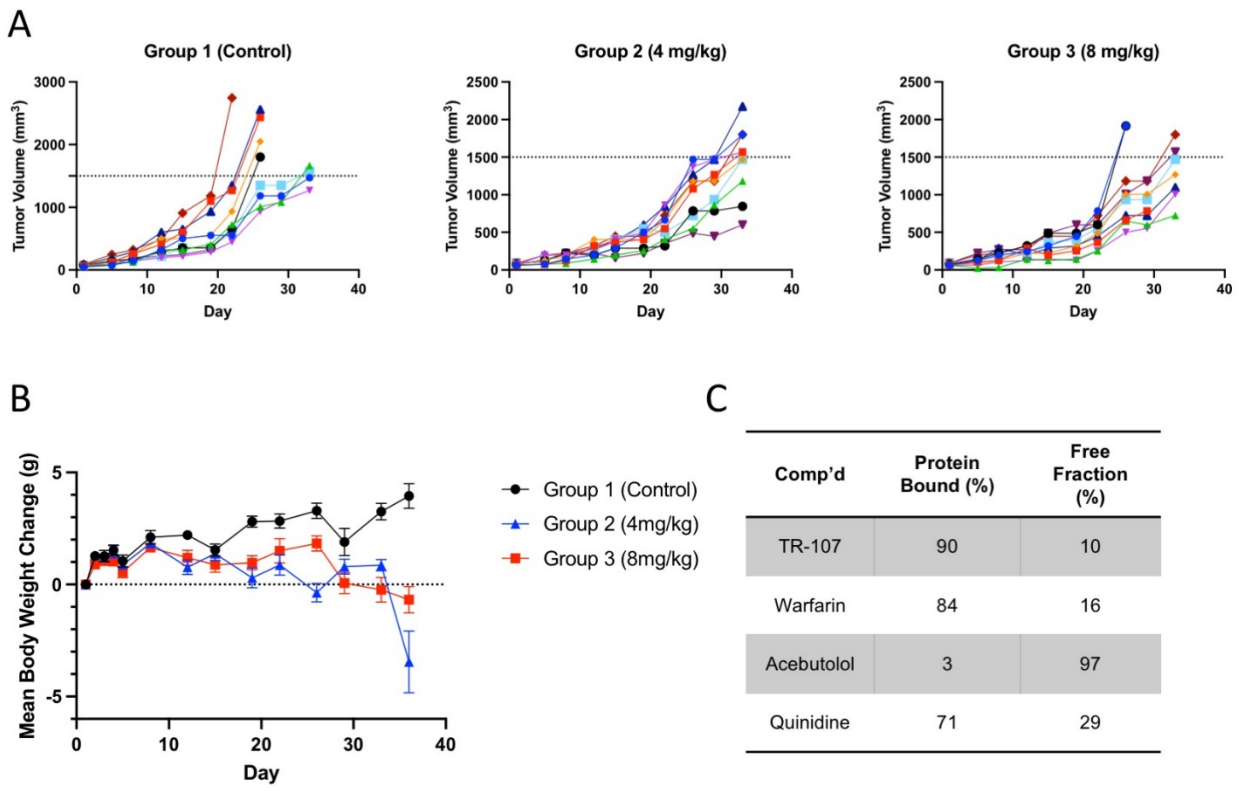

C

Comp'd	Protein Bound (%)	Free Fraction (%)
TR-107	90	10
Warfarin	84	16
Acebutolol	3	97
Quinidine	71	29

Figure S3.3. TR-107 inhibits tumor growth in MDA-MB-231 mouse xenograft model. A) Graphs of individual tumor volume measurements at indicated time points. Each color represents a single mouse participating in the study, N=10 per group. B) Average change in body weight compared to initial measurement of mice receiving vehicle (Group 1) or TR-107 treatment (Group 2 (4 mg/kg) or Group 3 (8 mg/kg)) at indicated time points. Values represent average ± SEM. N=10 per group. C) Murine plasma protein binding profile of TR-107 and control compounds (Warfarin, acebutolol, and quinidine). Values represent mean of N=2 replicates.

Table S3.1. TR-107 dosing and treatment protocol for murine MDA-MB-231 xenograft study. All compounds were dissolved in vehicle as described in Methods and were administered orally (P.O.) to 10 mice per group on schedules indicated.

Group	N	Comp'd	Dose	Route	Schedule	Dosing volume scale (mL/kg)
1	10	Vehicle	N/A	P.O.	B.I.D on Days 2, 5, 9, 12, 16, 19, 23, 26 B.I.D x 1 first day dose on Day 30 then B.I.D on Day 33	10
2	10	TR-107	4 mg/kg	P.O.	B.I.D on Days 2-4, 9-11, 16-18, 23-35 B.I.D x 4 first day 1 dose (start Day 30)	10
3	10	TR-107	8 mg/kg	P.O.	B.I.D on Days 2, 5, 9, 12, 16, 19, 23, 26. B.I.D x 1 first day 1 dose on Day 30 then B.I.D on Day 33	10

CHAPTER 4: MULTI-OMICS ANALYSIS OF CLPP ACTIVATION IN TRIPLE-NEGATIVE BREAST CANCER CELLS[3]

4.1 Introduction

Metabolic reprogramming was first characterized in cancer cells in the 1920s following the identification of increased glycolytic dependence under aerobic conditions[45,46,49]. Known as the Warburg effect, aerobic glycolysis has been confirmed in many rapidly proliferating cell types, but is widely debated as cancer cells often retain functional mitochondria and exhibit sensitivity to mitochondria-targeting compounds[49,133–135]. It has been proposed that the observed upregulation in glycolysis serves to increase adenosine triphosphate (ATP) as well as production of glycolytic intermediates required for anabolic processes, including the tricarboxylic acid (TCA) cycle, amino acid, nucleotide, and lipid biosynthesis[49,54,136]. Cancer dependencies on other metabolic processes have been identified, including glutaminolysis, serine biosynthesis, and nicotinamide adenosine dinucleotide (NAD^+), and this hypothesis continues to be investigated[54]. The identification of metabolic pathways as vulnerabilities in cancer cells has led to the development of numerous metabolism-specific anticancer approaches (approved or in trials) which target mitochondrial metabolic pathways, including oxidative phosphorylation (OXPHOS) (e.g., metformin), TCA cycle (e.g., CPI-613), and glutaminolysis (e.g., CB-839)[51,54].

ONC201 was initially discovered in a TRAIL induction screen[60] and while showing anticancer efficacy in multiple cancer models, its mechanism of action was largely undefined when it entered into Phase I clinical trials[14,16,59]. Greer et al. were the first to demonstrate specific effects of ONC201 on mitochondrial function [22]. Recently, ONC201 and its structural analogs (the TR compounds) were identified as highly specific activators of the mitochondrial protease ClpP[28,29,137]. ClpP forms a complex with ClpX, an ATP-dependent unfoldase that facilitates proteins insertion into the

[3]This chapter has previously appeared as an article in *Front. Pharmacol.* The original citation is as follows: Fennell EMJ, Aponte-Collazo LJ, Pathmasiri W, Rushing BR, Barker NK, Partridge MC, Li YY, White CA, Greer YE, Herring LE, Lipkowitz S, Sumner SCJ, Iwanowicz EJ, Graves LM. Multi-omics Analyses Reveal ClpP Activators Disrupt Essential Mitochondrial Pathways in Triple-Negative Breast Cancer Cells. *Front. Pharmacol.* 2023; 14. doi: 10.3389/fphar.2023.1136317

tetradecameric core of ClpP where they are subsequently degraded[31,33,76]. The proteolytic activity of ClpP not only serves to maintain protein homeostasis within the mitochondria, but is known to induce the mitochondrial unfolded protein response (UPR^{mt}) and integrated stress response (ISR), leading to further transcriptional regulation of metabolic and mitochondrial quality control-related genes[21,42,43,138,139]. In mammalian cells, activating transcription factor 4 (ATF4) has been identified as the key regulator of ISR[67] , and we and others have shown ClpP-dependent induction of ATF4 in TNBC cells following ClpP activation[137].

Activation of ClpP in multiple cancer cell models leads to nonspecific degradation of mitochondrial proteins, including OXPHOS subunits[29,140,141]. We have shown the more potent activators of ClpP (TR compounds) result in depletion of mtDNA *in vivo*, as well as a ClpP-dependent loss of oxygen consumption rate (OCR) and protein-level expression of many mitochondrial metabolic, transcriptional, and homeostatic proteins in triple-negative breast cancer (TNBC) cells[137]. Further investigation into the mechanism of the TR compounds revealed a ClpP-dependent dysregulation of metabolic pathways including one-carbon metabolism, proline biosynthesis, and the mevalonate pathways in TNBC cells, leading to inhibition of breast cancer stem cell function[142].

The paradigm of the UPR^{mt} involves increased mito-nuclear signaling, protein-level changes, and metabolic remodeling[21,42,43,138]. Consistent with this, multiple studies have reported protein- and transcript-level perturbations following ONC201 or TR compound treatment in multiple cancer models[18,19,22,28,29,137,141,142]. The dysregulation of mitochondrial metabolic activity, protein level, and transcriptomic profiles in a wide variety of cancer cell models indicates the need to investigate the full scope of perturbations occurring in cancer cells following ClpP activation. Multi-omics data analysis approaches are a valuable tool for interrogating pathways altered by drug exposures, genetic variation, and disease states[55,58]. Utilization of a multi-omics approach to analyze the proteomic, transcriptomic, and metabolomic landscapes of TNBC cells treated with ONC201 or TR-57 provides the opportunity to achieve a broad understanding of cellular processes altered by ClpP activation.

The objective of this study was to complete a multi-omics profile of TNBC cells following pharmacological ClpP activation. We performed individual analyses of proteomic, transcriptomic, and metabolomic data, as well as multi-omics data analysis using MetaCore pathway analysis software. The data presented herein demonstrates a comprehensive analysis of proteomic, transcriptomic, and metabolomic perturbations in wildtype (WT) and ClpP knockout (ClpP-KO) TNBC cells. Our multi-omics analysis identified significant alterations in mitochondrial metabolic processes, including TCA cycle, (S)-citrulline metabolism, amino acid metabolism, ATF4 induction, and heme biosynthesis.

4.2 Results

Multi-omic Analyses Reveal Loss of Mitochondria-specific Functions Following ClpP Activation in TNBC Cells

To gain a better understanding of the biological consequences of ClpP activation in cancer cells, we compared the effects of 2 well characterized ClpP activators in a model of TNBC. Wildtype SUM159 (WT) and SUM159 ClpP-knockout (ClpP-KO) cells were treated with 10 μM ONC201 or 150 nM TR-57 (~10 fold higher than the respective IC_{50} value previously determined for each compound[28]) for 24 hours. Following extraction, LC-MS analysis and protein/metabolite identification were performed to obtain the proteomics and metabolomics datasets as described in Methods. In parallel, RNAseq was performed on mRNA isolated from treated cells to obtain the transcriptomics data (Fig. 4.1). From these studies, approximately 8000 proteins and 7700 transcripts were quantified in each condition. Approximately 4100 metabolites were measured, 3218 which were matched to specific metabolites using an in-house library or public databases, and 588 were utilized for metabolomics analysis (ontology levels OL1, OL2a/2b, and PDa; see Materials and Methods and Supplemental Data 6). Additionally, phosphoproteomics analysis was performed on these samples, which yielded ~17,000 phosphopeptides (Fig. S4.1).

Proteomics

Analysis of the total proteomics revealed significant differences between WT and ClpP-KO SUM159 cells treated with either ONC201 or TR-57 (Fig. 4.2A). Of the ~8000 proteins quantified, many proteins were significantly downregulated (Log_2(fold change) ≤ -0.5 and p-value ≤0.05) in ONC201 and TR-57 treated cells compared to DMSO control (572 and 686 proteins for ONC201 and TR-57 treated

cells, respectively). In comparison, only 113 and 191 (ONC201 and TR-57, respectively) proteins were found to be significantly upregulated (Log_2(fold change) ≥0.5 and p-value ≤0.05). Overall ClpP activation with ONC201 or TR-57 influenced protein changes in a highly similar manner, with 55 upregulated and 380 downregulated proteins in common (Fig. 4.2B). By contrast, very few proteins were significantly affected by either ONC201 or TR-57 treatment in ClpP-KO cells, suggesting the proteome changes observed in WT cells upon treatment are a direct result of ClpP activation. ONC201 treated ClpP-KO cells showed only 19 significantly upregulated and 0 significantly downregulated proteins, whereas TR-57 treated ClpP-KO cells showed only 1 significantly perturbed protein in either direction (Fig. 4.2A).

Gene ontological (GO) analysis of this data indicated a significant downregulation in mitochondrial proteins as expected for activation of a mitochondrial matrix protease (Fig. S4.2A). In addition to proteins involved in mitochondrial translation, GO analysis of significantly downregulated proteins revealed enrichment in the oxidative phosphorylation pathway, consistent with previous data that ONC201 and TR compounds reduce OXPHOS in TNBC and other cells[22,29,137,142]. Proteins significantly downregulated by ONC201 and TR-57 treatment included ATPase Inhibitor (ATPIF1), mitochondrial 39S ribosomal protein L12 (MRPL12), and mitochondrial elongation factor Tu (TUFM) (Fig. S4.2B). GO analysis of the upregulated proteins demonstrated increases in mainly nuclear, cytosolic, and membrane proteins following ClpP activation, including the proteins Niban 1 (NIBAN1), peroxisome proliferator-activated receptor delta (PPAR-δ), growth/differentiation factor 15 (GDF15) and others (Fig. S4.2A,B).

Analysis of the phosphoproteomics dataset identified changes in protein phosphorylation and kinase activity (Fig. S4.1A). From our dataset of ~17,000 phosphopeptides, we identified >800 significantly upregulated and >1000 significantly downregulated phosphopeptides across both ONC201 and TR-57 treatments in WT SUM159 cells. Between both treatments, 245 upregulated and 477 downregulated phosphopeptides were observed (Fig. S4.1B). Conversely, only 54 significantly upregulated phosphopeptides and 109 significantly downregulated phosphopeptides were found in ClpP-KO SUM159 cells across both treatments.

Using RoKAI[143] to identify patterns of kinase activity from our phosphoproteomics data, we found evidence for activation of multiple kinases in WT SUM159 cells treated with either ONC201 or TR-57 (Fig. S4.1C), including ATM, ATR, AMPK, CK2, MAPKAPK2 and others. Similarly, RoKAI predicted the

kinases CDK2, CDK4, and AurB to be inactivated under these same conditions. Many of these predictions were determined to be ClpP-dependent, as ClpP-KO cells treated with ONC201 or TR-57 showed few predicted changes in kinase activity following treatment (Fig. S4.1C).

Further, Multiplexed kinase inhibitor beads (MIBs)[144] were utilized to profile the effects of ClpP activation on kinase expression in WT SUM159 cells following 30 minutes, 3 hours, and 24 hours of treatment with ONC201 or TR-57. We observed a high degree of similarity between ONC201 and TR-57 treatments (Fig. S4.1D). Consistent with RoKAI analysis, we observed a decline in CDK2, CDK4, and AurB.

Transcriptomics

RNAseq was performed on mRNA isolated from both WT and ClpP-KO cells following a 24-hour treatment with either 0.1% DMSO, 10 μM ONC201, or 150 nM TR-57. Volcano plots of the processed data showed significant changes in the WT cells following ONC201 and TR-57 treatment (Fig. 4.2C). Specifically, >700 and >1000 transcripts were significantly altered in ONC201 or TR-57 treated WT cells, respectively. Of these, 501 upregulated transcripts were identical between both treatments, whereas 492 downregulated transcripts were common (Fig. 4.2D). Again, ClpP-KO cells showed greatly reduced statistically significant changes, with <220 upregulated and <130 downregulated transcripts following 24-hour treatment. To investigate short-term effects of ClpP on the transcriptome, we performed transcriptomic analysis following 1 hour of ONC201 or TR-57 treatment in WT and ClpP-KO SUM159 cells (Fig. S4.3). In these early timepoints, we observed significant upregulation of 80 and 115 genes in WT cells treated with ONC201 and TR-57 respectively, as well as significant downregulation of 174 and 200 genes in these same samples. ClpP-KO SUM159 showed significant changes in 83 upregulated and 94 downregulated genes following ONC201 treatment, and 115 upregulated and 113 downregulated genes in TR-57 treated cells. Significant overlap of changes occurring in WT cells treated with both drugs was seen; however, significant overlap was not observed between WT and ClpP-KO treated cells (Fig. S4.3B,C). GO analysis of 1 hour transcript changes reveals significant downregulation of cytosolic transcripts in both ONC201 and TR-57 treated WT cells. Additionally, significant upregulation of cytosolic and nucleoplasmic transcripts was observed in ONC201 and TR-57 treated WT cells, respectively (Fig. S4.3D). Comparison of the 1 hour and 24 hour treatments with either ONC201 or TR-57 in WT cells did not reveal significant overlap of transcriptional changes (data not shown). Further investigation into

transcriptomic changes following ClpP activation with additional timepoints is necessary to better characterize the temporal regulation of transcription following ClpP activation in TNBC cells.

GO analysis of the significantly up- and downregulated transcripts from WT cells revealed that many these transcripts are nuclear or cytosolic. In contrast to our proteomics results, the most significantly downregulated transcripts were those encoding proteins localized to the cytoplasm, cell membrane, nucleus and other non-mitochondrial organelles (Fig. S4.2C, D). Additionally, these same subcellular localizations were significantly enriched in the analysis of upregulated transcripts (Fig. S4.2C), including transcripts for FLRT1, SKIL, SLC25A6, SLC6A9, and ASNS (Fig. S4.2D). Transcriptomic results also showed significant downregulation of some nuclear-encoded transcripts for mitochondrial proteins; however, this was not observed to the same extent as the proteomics data (Fig. S4.2A, C).

Metabolomics

Individual analysis of the metabolomics data (specifically, ontology levels OL1, OL2a/b, PDa; see Materials and Methods) showed significant ClpP-dependent downregulation of specific metabolites related to mitochondrial function (Fig. 4.2E). Metabolomics data from WT cells showed a high degree of overlap between ONC201 and TR-57 treatment conditions, with 30 upregulated metabolites and 46 downregulated metabolites consistent across conditions (Fig. 4.2F). We observed decreases in ascorbic acid, propionylcarnitine, and ureidosuccinic acid (Fig. S4.2E), metabolites which are involved in redox balance, acylcarnitine metabolism, and aspartic acid catabolism, respectively. Our metabolomics analysis also showed a significant upregulation in α-ketoglutarate and 2-hydroxyglutaric acid, two key metabolites linked to TCA cycle dysfunction and epigenetics regulation[54,145]. Significant changes in multiple di- and tripeptides was also observed.

Multi-omics Comparative Analysis Reveals Significantly Altered Mitochondrial Metabolism in TNBC Cells

To further evaluate the effects of ClpP activation on TNBC cells, MetaCore pathway analysis software was used to perform multi-omics analysis of all the data from ONC201 and TR-57 treated WT and ClpP-KO SUM159 cells. Each cell line and treatment group were analyzed in comparison to their respective DMSO control, and observations meeting significance criteria from all three datasets (proteomics, transcriptomics, and metabolomics) were used for each analysis when available. From this analysis, the top 50 significantly altered endogenous metabolic networks (EMNs) were identified by

MetaCore software, with 42 of these 50 EMNs occurring in both ONC201 and TR-57 treated WT SUM159 cells (Fig. 4.3). From this analysis we detected significant perturbations in pathways involving amino acid metabolism and transport, TCA cycle, glycosphingolipid, citrulline, and sucrose metabolism (Table 4.1). To determine ClpP-dependence of these EMN perturbations, we performed the same MetaCore analysis for ClpP-KO cells treated with ONC201 or TR-57. This yielded no significant EMNs for ONC201 treated ClpP-KO SUM159 cells. Additionally, proteomics observations meeting the significance criteria for TR-57 treatment did not occur in ClpP-KO SUM159 cells. For these reasons, MetaCore analysis of ClpP-KO SUM159 cells was performed using only transcriptomic and metabolomic datasets (Fig. S4.4, Table S4.1).

Within these pathways, multiple proteins, transcripts, and metabolites were identified as significantly up- or downregulated in WT cells through MetaCore EMN analysis (Fig. 4.3). Analysis of these pathway changes showed that significant perturbations in all three datasets contributed to their enrichment (Fig. 4.4). Within the TCA cycle, proteomic downregulation was observed for citrate synthase (CS), isocitrate dehydrogenase 2 (IDH2), α-ketoglutarate dehydrogenase (αKGDH), succinyl-CoA synthetase (CSC), succinate dehydrogenase A (SDHA), fumarate hydratase (FH), and malate dehydrogenase (MDH) (Fig. 4.4A), consistent with previous observations by immunoblot[137] and BioID[29]. Significant proteomic downregulation of aconitase (ACO2) was observed in both ONC201 and TR-57 treated WT SUM159 cells (Fig. 4.4A). Additionally, transcriptomic downregulation was observed for many of these TCA cycle enzymes, including significant downregulation of CS in TR-57 treated cells and αKGDH and SDHA in ONC201 treated cells (Fig. 4.4A). Suggesting potential compensation towards glycolysis, β-enolase (ENO3) showed significant proteomic upregulation following both ONC201 and TR-57 treatment. Similarly, phosphoenolpyruvate carboxykinase (PEPCK) showed significant transcriptomic upregulation following both treatments. Metabolites including citrate, succinate, and 3-phosphoglycerate were significantly decreased following both ONC201 and TR-57 treatment in WT cells while α-ketoglutarate was significantly upregulated. Glucogenic amino acids tryptophan and glutamic acid were both significantly upregulated while serine was significantly downregulated. The ketogenic amino acid leucine was significantly upregulated (Fig. 4.4A). While also identified as a significant EMN for TR-57

treated ClpP-KO SUM159 cells, this was on the basis of one transcript and one metabolite being present in the data (Fig. S4.4).

Pyrimidine Metabolism

Our data analysis identified that the *de novo* pyrimidine synthesis and scavenging pathway, a cytoplasmic and mitochondrial metabolic pathway, was significantly downregulated (Fig. 4.4B). We observed the trend of proteomic downregulation amongst most enzymes involved in this pathway and significant transcriptomic downregulation of cytidine deaminase (CDA). Substrates and metabolites of *de novo* pyrimidine biosynthesis, including aspartic acid, ureidosuccinic acid, and dihydroorotate, were downregulated as well as uridine and cytidine.

Citrulline Pathway

The (S)-citrulline pathway/urea cycle, another mitochondrial and cytosolic pathway, showed many significant changes following ONC201 or TR-57 treatment (Fig. 4.4C). A consistent protein-level downregulation was observed with delta-1-pyrroline-5-carboxylate synthase (P5CS) and ornithine decarboxylase (ODC) following TR-57 and ONC201 treatment, respectively. P5CS and ODC are part of the glutamine catabolic pathway leading to citrulline biosynthesis. Moreover, pyrroline-5-carboxylate reductase (PYCR2), part of the proline biosynthesis pathway was strongly downregulated consistent with a previous report in TNBC cells[142]. Mitochondrial arginase 2 (ARG2) was significantly increased at the proteomic level following both compound treatments. In comparison, upregulation of PYCR2 and argininosuccinate synthetase (ASS1) was observed at the transcriptomic level, whereas significant transcriptomic downregulation was also observed with guanidinoacetate N-methyltransferase (GAMT) and P5CS following ONC201 treatment. Glutamic acid and homocitrulline were both significantly upregulated in the metabolomic data following compound treatment, while argininosuccinic acid (ARS) was significantly decreased. S-adenosylmethionine, the methyl-donor in the reaction catalyzed by GAMT, was also significantly upregulated following both compound treatments. The S-citrulline pathway was also identified as significant in the EMN analysis of ClpP-KO SUM159 cells treated with TR-57. However, similar to the TCA cycle, this was due to the presence of one metabolite and three transcripts (Fig. S4.4).

ClpP Activation Induces ATF4 Expression and Affects ATF4-dependent Gene Expression

MetaCore pathway analysis revealed significant changes in amino acid metabolism following pharmacological ClpP activation (Fig. 4.3B, Table 4.1). EMN analysis showed significant perturbations in proteins and transcripts including ASNS, SHMT2, GPT2, and phosphoserine aminotransferase (PSAT1), genes whose expression have been previously reported to be ATF4-dependent[67,146,147]. Further investigation of the proteomic and transcriptomic data revealed that many ATF4-dependent genes were significanwtly upregulated at both the transcript- and protein-level following activation of ClpP with ONC201 or TR-57 (Fig. 4.5A). Consistent with these data, the induction of ATF4 and ASNS was validated at the protein level by immunoblotting (Fig. 4.5B). ASNS protein expression was induced in WT SUM159 but not ClpP-KO SUM159 cells following 24-hour treatment with either 10 μM ONC201 or 150 nM TR-57. Additionally, increases in ASNS were not observed in WT SUM159 cells treated with an ATF4 siRNA prior to ONC201 or TR-57 incubation, indicating that expression of these proteins was ATF4-dependent (Fig. 4.5B). ATF4 regulates a number of processes, and further investigation into potential additional ATF4 substrates[146] identified multiple significantly upregulated enzymes involved in metabolic processes (e.g., PEPCK2), autophagy (e.g., p62), and redox homeostasis (e.g., HMOX) (Fig. 4.5C).

MetaCore Pathway Analysis Identifies Multiple Amino Acid Metabolic Pathways Affected by ONC201 or TR-57

MetaCore pathway analysis identified amino acid metabolism, including serine metabolism, as significantly affected by ONC201 and TR-57 treatment (Table 4.1). Significant upregulation of PSAT1 (Fig. 4.5A,C) through ATF4 indicates a potential upregulation of the serine biosynthetic pathway (Fig. S4.5A). We observed significant upregulation of phosphoglycerate dehydrogenase (PHGDH), and PSAT1 at both the proteomic and transcriptomic level and phosphoserine phosphatase (PSPH) at the proteomic level. Additionally, we observed significant loss of 3-phosphoglycerate and serine following ONC201 and TR-57 treatment. Recently, Pacold et al. identified a novel PHGDH inhibitor, NCT-503[148], and demonstrated its ability to inhibit cell growth in TNBC cells highly expressing PHGDH, but not in TNBC cells expressing low levels of PHGDH. Because ONC201 and TR-57 induce PHGDH expression in SUM159 cells, we investigated whether NCT-503 would further sensitize SUM159 cells to TR-57 or vice versa. Despite using relatively high levels of NCT-503 (up to 50 μM), SUM159 cells were not inherently

sensitive to NCT-503 (Fig. S4.5B). Additionally, treatment of SUM159 cells with 150 nM TR-57 did not alter the IC_{50} of cells to NCT-503, nor did 10 μM NCT-503 affect the IC_{50} of cells to TR-57 (Fig. S4.5B).

ONC201 and TR-57 Affect the Heme Biosynthetic Pathway in TNBC Cells

MetaCore pathway analysis also revealed significant changes in glycine pathways and cellular transport following ClpP activation. Glycine and succinyl-CoA are substrates required for heme biosynthesis through the rate-limiting enzyme ALAS1. Our proteomics data revealed that ALAS1, PPO, and FECH, three key enzymes required for heme biosynthesis, were downregulated following ONC201 and TR-57 treatment. By contrast, the transcript levels of ALAS1, PPO, and FECH, were not significantly changed following ONC201 or TR-57 treatment, suggesting that loss of these proteins is due to degradation caused by ClpP activation (Fig. 4.6A). Immunoblot analysis validated ONC201 and TR-57 mediated ALAS1 decline in WT, but not in ClpP KO SUM159 cells (Fig. 4.6B), consistent with previous reports of ClpP degrading ALAS1[41,149,150]. The downregulation of ALAS1 occurred as early as 30 minutes of treatment with TR-57 in WT, but not knockout SUM159 cells (Fig. 4.6D).

Since LonP, another mitochondrial matrix protease, has also been reported to degrade ALAS1[149–151], we investigated whether the loss of ALAS1 was due to ClpP or LonP activation. To accomplish this, bortezomib (10 nM) was used to inhibit both LonP and the proteasome, whereas epoxomicin (1 μM) was used as an inhibitor of only the proteasome[152–154]. Neither of these co-treatments with ONC201 or TR-57 prevented the loss of ALAS1 (Fig. 4.6B). LonP siRNA was also used to examine whether LonP was responsible for the observed loss of ALAS1 in WT SUM159 cells (Fig. 4.6C). Transient knockdown of LonP did not prevent the degradation of ALAS1 in WT SUM159 cells following treatment, indicating that the effect of ONC201 or TR-57 on ALAS1 was due to activation of ClpP.

Because our data identified components of the heme metabolic pathway as being significantly down-regulated by ONC201 and TR-57 treatment at the protein level, we next investigated whether inhibition of heme biosynthesis was required for growth arrest in response to these compounds. To accomplish this, we supplemented the cell media with hemin, a cell-permeable form of heme and examined the effects on cell growth inhibition following ONC201 or TR-57 treatment. Cell proliferation assays (72-hour) did not show restoration of cell growth following hemin supplementation (Fig. S4.6A). However, to further determine if hemin supplementation over an extended exposure would prevent

growth inhibition, we used long-term hemin exposure in crystal violet assays (Fig. S4.6B, S4.7). These results demonstrated that extended hemin supplementation did not counteract cell growth inhibition following ONC201 or TR-57 treatment in either WT SUM159 or MDA-MB-231 cells.

4.3 Discussion

The mechanism of action of ONC201 has been proposed as dopamine receptor antagonism[14,15,17], atypical activation of the ISR[14,18,19], and more recently, ClpP agonism[28,29]. We and others have shown that ONC201 and the related TR compounds affect mitochondrial metabolic function (e.g., OXPHOS, TCA cycle) and mitochondrial protein levels in cancer models[22,29,137,141,142]. The current study utilized a comprehensive multi-omics approach to identify protein, transcript, and metabolite-level changes to further elucidate the specific mechanism of action of these compounds and identify potential cancer cell vulnerabilities resulting from ClpP activation.

We identified many protein, transcript, and metabolite perturbations occurring in TNBC cells following a brief (24-hour) exposure to ONC201 or TR-57. These perturbations were determined to be largely ClpP dependent as most were not observed in ClpP-KO cells (Fig. 4.2). We previously showed ONC201 and TR compound treatment result in similar phenotypic responses in TNBC cells[137,142] and comparisons of the responses to these structurally distinct ClpP activators in WT SUM159 cells demonstrated highly similar responses to these compounds. Thus, our data further illustrates the high degree of specificity of these compounds for ClpP and confirm that this is the major target protein for these molecules in cancer cells.

GO analysis of significantly downregulated proteins revealed multiple mitochondrial proteins, including mitochondrial matrix and inner membrane proteins, in both treatments. Mitochondrial translation and mitochondrial protein transport were identified as significantly downregulated at the proteomic level (Fig. S4.2A). Significant decreases in nuclear-encoded mitochondrial transcripts were also identified (Fig. S4.2C), however, the number of identified transcripts does not fully account for the overall observed decline in mitochondrial proteins, supporting the loss of mitochondrial protein as due to direct proteolysis. In agreement with activation of the ISR or UPR^{mt}, upregulated proteins and transcripts showed a strong enrichment for nuclear and cytosolic components, as well as non-mitochondrial organelles (e.g.,

endoplasmic reticulum and Golgi apparatus) and membrane components, as a likely compensatory response to this stress.

Multi-omics analysis using MetaCore pathway analysis identified multiple metabolic networks that were significantly altered by ClpP activation in WT SUM159 cells, including amino acid biosynthesis and the (S)-citrulline pathway (Table 4.1, Fig. 4.3, 4.4). We also found that the TCA cycle was significantly downregulated at both the proteomic and transcriptomic level following ClpP activation. Additionally, we observed significant downregulation of TCA cycle intermediates citrate and succinate, and upregulation of α-ketoglutarate (Fig. 4.4A). Loss of succinate dehydrogenase (SDH), isocitrate dehydrogenase (IDH2), and ACO2 were previously reported following treatment with ONC201 or TR compounds[29,137]. The TCA cycle serves as a source for both anabolic metabolism intermediates as well as NADH and TR-57 has been reported to reduce NAD^+ and NADH in a ClpP-dependent manner and induce redox imbalance in TNBC cells[142]. Decreased flux through the TCA cycle, as well as loss of SDH (complex II of the electron transport chain), could explain the observed loss of OXPHOS following ClpP activation[22,137,141].

The citrulline pathway, including the urea cycle, was identified as a significantly perturbed pathway from our multi-omics analysis (Fig. 4.4C). We observed downregulation of arginosuccinate synthase 1 (ASS1) on a proteomic level, which is proposed to preserve aspartate levels in cancer cells for use in biosynthetic pathways. This proteomic decline was accompanied by a significant transcriptomic upregulation of ASS1 in WT cells following both ONC201 and TR-57 treatment. We also observed significant proteomic upregulation of arginase (ARG2) following ClpP activation. Additionally, we observed a significant decrease in both aspartate and argininosuccinate (Fig. 4.4C), which may be due to the significant upregulation of ASNS (Fig. 4.5), which depletes aspartate through conversion to asparagine. Loss of arginine synthesis was reported to suppress transcription of genes including those involved in OXPHOS, glycolysis, and nucleotide biosynthesis, and alterations in mitochondrial morphology[155–157], potentially explaining some phenotypes previously observed following ClpP activation[22,137,142].

Aspartate is also required for *de novo* pyrimidine biosynthesis, and further analysis of *de novo* and scavenging pathways of pyrimidine biosynthesis showed significant downregulation of metabolites including aspartate, dihydroorotate, uridine, and cytosine. We observed a proteomic downregulation of

CAD protein, a trifunctional enzyme facilitating the conversion of carbamoyl-phosphate to dihydroorotate. Interestingly, the key mitochondrial enzyme (DHODH) and 4th enzyme in the pyrimidine biosynthetic pathway, was not reduced in our proteomics analysis. Inhibition of *de novo* nucleotide biosynthesis has been widely investigated as an anticancer therapy and as a metabolic vulnerability to be exploited in co-treatment development[50,51]. As pyrimidine nucleotides are required for continued cell proliferation, the observed downregulation of pyrimidine biosynthetic metabolites and enzymes could play a critical role in the mechanism by which ClpP activation leads to cell growth inhibition.

Dependence on serine biosynthesis was previously identified as a metabolic vulnerability in cancer models, including breast cancer[51]. We identified significantly decreased serine levels with significant proteomic and transcriptomic upregulation of the serine biosynthetic pathway in cells treated with ONC201 or TR-57 (Table 4.1, Fig. S4.5A). This is indicative of cells potentially upregulating this pathway to synthesize more serine for utilization by other pathways (e.g., tetrahydrofolate cycle, glycine synthesis, glutathione synthesis). Inhibition of PHGDH was reported to inhibit cell growth in cells highly expressing PHGDH[148]. We hypothesized that if dependence on serine biosynthesis is a metabolic vulnerability in cells treated with ClpP activators, that a combination treatment with NCT-503, a novel PHGDH inhibitor[148], would sensitize cells to ClpP activators. We did not observe sensitization of WT SUM159 cells to TR-57, nor did TR-57 co-treatment sensitize cells to NCT-503. However, despite induction of PHGDH following TR-57 treatment, SUM159 may not express PHGDH to the extent required for cells to be sensitive to NCT-503 treatment alone[148]. Importantly, while our metabolomics data provided a snapshot of the metabolome following 24-hour treatment with ClpP agonists it cannot not reflect the actual flux through the serine biosynthetic pathway or the use of serine in other metabolic pathways, or the uptake of serine from cell growth media. Future studies involving more detailed analysis of metabolic flux using stable isotope approaches, could be applied to investigate differences in pathway flux.

Consistent with perturbations in amino acid biosynthesis, analysis of significantly upregulated proteins and transcripts identified many ATF4-dependent genes, including ASNS, GDF15, and PSAT1 (Fig. 4.5). ATF4 has been widely shown to be induced by ClpP activation[18,28,61,158]. ATF4, a key regulator of the cellular response to the ISR/UPR^{mt}, is known to regulate transcription of genes involved in amino acid uptake and biosynthesis, metabolic enzymes, and redox homeostasis[67,146]. We identified

upregulation of ASNS following ClpP activation in both proteomic and transcriptomic data, and this was confirmed by immunoblotting (Fig. 4.5). Additionally, we showed that the upregulation of ASNS was prevented in ATF4-knockdown SUM159 cells treated with ONC201 and TR-57. The observed activation of ATF4 and ATF4-dependent genes may explain metabolic perturbations observed following ClpP activation, including upregulation in the serine biosynthetic pathway and loss of cellular aspartate pools.

ALAS1, the rate limiting step of heme biosynthesis, has previously been identified as a ClpP substrate[41,149,159] and loss of heme biosynthesis has been implicated as a metabolic vulnerability in acute myeloid leukemia[160]. Our data clearly showed significant and rapid downregulation of ALAS1 in response to ClpP activators. Because LonP has also been reported to degrade ALAS1[149,151], we additionally utilized bortezomib co-treatment and LonP siRNA to determine the role of LonP in ALAS1 stability following treatment with ONC201 or TR-57 (Fig. 4.6). We found ALAS1 was stabilized in ClpP-KO SUM159 cells, but not in either bortezomib-treated or LonP knockdown SUM159 cells, suggesting that loss of ALAS1 is due to ClpP activation in these experiments. We attempted to investigate whether loss of the heme biosynthetic pathway was essential for ClpP activation-mediated cell growth inhibition. However, supplementation with hemin, a cell permeable form of heme, did not restore cell growth in treated WT SUM159 cells, suggesting loss of the heme biosynthetic pathway may be one of many consequences of ClpP activation that leads to reduced cell growth. Inability to sensitize or desensitize cells to ONC201 or TR-57 treatment could be due to ClpP activation broadly affecting a number of metabolic pathways in cancer cells. Therefore, interrupting or restoring single metabolic pathways may not be sufficient to increase or decrease sensitivity to ClpP activators.

In summary, this study has identified significant proteomic, transcriptomic, and metabolomic perturbations occurring following ClpP activation by two chemically distinct ClpP agonists. We have shown that the vast majority of these changes are ClpP-dependent, including induction of ATF4-dependent genes and protein-level loss of the heme biosynthetic pathway. Applying multi-omics analysis identified 42 significantly perturbed pathways following treatment with ONC201 or TR-57, including amino acid biosynthesis, TCA cycle, and the citrulline pathway. The identification of the broad effects of ClpP activation on cancer cell metabolism provides critical insight into the mechanism by which

pharmacological activation of ClpP inhibits cancer cell growth and suggest a response that is both multi-nodal and dependent on the dysregulation of multiple pathways.

4.4 Materials and Methods

Cell Culture

The human triple-negative breast cancer (TNBC) cell line SUM159 was cultured in Dulbecco's modified Eagle's medium: Nutrient Mixture F-12 (DMEM/F-12, Gibco, 11330-032) supplemented with 5% fetal bovine serum (VWR-Seradigm, 97068-085), 1% antibiotic/antimycotic (ThermoFisher Scientific, 15240062), 5 µg/mL insulin (Gibco, 12585014), and 1 µg/mL hydrocortisone. CRISPRi was used to generate CLPP-knockout SUM159 cells as previously described[137]. WT MDA-MB-231 cells were cultured in RPMI 1640 media (Gibco, 11875-093) supplemented with 10% FBS and 1% antibiotic/antimycotic. Cells were incubated at 5% CO_2 and 37°C and periodically tested for mycoplasma.

Cell Viability

Total Cell Counting

WT and ClpP-KO SUM159 cells were seeded at 1000 cells/well in a 96-well plate (Perkin Elmer, 6005050) and allowed to adhere overnight. Media was replaced by 100 µL of media supplemented with drugs at concentrations indicated in figures and figure legends. 0.1% DMSO treatment was used a negative control. Following treatment, media was aspirated and replaced with 100 µL Dulbecco's phosphate buffered saline (DBPS, Gibco, 14190-144) with 1µg/mL Hoechst stain (ThermoFischer Scientific, H3570) and allowed to incubate at 37°C for 30 minutes. Cell number was quantified using Celigo Imaging Cytometer (Nexcelom).

Crystal Violet Assays

Crystal violet assays were performed by plating WT or ClpP-KO SUM159 or WT MDA-MB-231 cells (1000 cells/well) in a 6-well plate (Corning) and allowing them to adhere overnight. Media was aspirated and replaced by 2 mL of media containing desired compound treatments. Media was replaced with growth media containing the same drug treatments every 48 hours until one well was 100% confluent. Once confluent, cells were stained (0.5% crystal violet, 20% methanol) for 10 minutes at RT, rinsed 3 times and allowed to dry overnight.

RNAi

All siRNA stocks were purchased through Horizon Discovery at 2 nmol/siRNA and resuspended in 100 uL 1X siRNA reconstitution buffer (Horizon Discovery) to create a 20 μM stock. Dharmafect I was diluted 1:266 in OptiMEM media and separated into the appropriate number of 250 μL aliquots. Individual siRNAs were added to OptiMEM:Dharmafect aliquots for a final concentration of 125 nM, incubated at RT for 30 minutes, and then added to a 6-well plate. SUM159 cells were washed with DPBS and trypsinized and 37°C for 5 minutes. Cells were resuspended to a final concentration of 1 x 10^5 cells/mL in 1:1 DMEM:F-12 supplemented with 5% FBS, 5 μg/mL insulin, and 1 μg/mL hydrocortisone. Cells were added to each well (1.0 mL/well) containing siRNA and incubated for 24 hours. Cells were then treated with 10 μM ONC201 or 150 nM TR-57 for the timepoints indicated in the figure legends and harvested as described above.

Proteomics

Sample Preparation

For whole cell and phosphoproteomics, SUM159 (WT and ClpP-KO) cells were plated in a 10 cm^2 dish (Corning) and allowed to adhere overnight. Cells were then treated with 0.1% DMSO, 10 μM ONC201, or 150 nM TR-57 for 24 hours. Cells were washed with 3 x 5 mL ice-cold Dulbecco's Phosphate Buffered Saline (DPBS, Gibco, 14190-144) and lysed in 8M urea buffer [8M urea, 50 mM Tris (pH 7.4), 2.5 mM Na_3VO4, 1 mM NaF, 1X protease inhibitor cocktail, 1X phosphatase inhibitor cocktail 2, 1X phosphatase inhibitor cocktail 3]. Lysates were clarified by centrifugation and protein concentration quantified by Bradford Assay (BioRad). Protein lysates (400 μg) were reduced with 5 mM DTT at 56ºC for 30 minutes, then alkylated with 15 mM iodoacetamide at RT in the dark for 45 minutes. Protein was precipitated using 4-times the volume of cold acetone and stored overnight at -20ºC. The next day, samples were centrifuged at 15,000 x g for 15 minutes at 4ºC, then the protein pellets were reconstituted in 1M urea. Samples were digested with LysC (Wako) for 2 hours and trypsin (Promega) overnight at 37ºC at a 1:50 enzyme:protein ratio. The resulting peptide samples were acidified, desalted using Thermo desalting spin columns, then the eluates were dried via vacuum centrifugation. Peptide concentration was determined using Pierce Quantitative Fluorometric Peptide Assay.

Samples were split into two TMTpro 16plex sets based on drug treatment (ONC201 or TR-57). In TMT set 1, the samples included: SUM159 WT cell line with 3 DMSO controls (n=3) and ONC201 treated samples (n=4), and SUM159 ClpP KO cell line with 3 DMSO controls (n=3) and ONC201 treated samples (n=4), along with two pooled samples to assess technical variability. TMT set 2 included the same experimental design except with TR57 treatment instead of ONC201. A total of sixteen samples per set, which were labeled with TMTpro 16plex (Thermo Fisher); a sample key can be found in the PRIDE submission (PXD038990). 125 µg of each sample was reconstituted with 50 mM HEPES pH 8.5, then individually labeled with 250 µg of TMTpro reagent for 1 hour at room temperature. Prior to quenching, the labeling efficiency was evaluated by LC-MS/MS analysis of a pooled sample consisting of 1ul of each sample. After confirming >98% efficiency, samples were quenched with 50% hydroxylamine to a final concentration of 0.4%. Labeled peptide samples for each set were combined 1:1, desalted using Thermo desalting spin column, and dried via vacuum centrifugation. The dried TMT-labeled samples (two TMT sets total) were fractionated using high pH reversed phase HPLC[161]. Briefly, the samples were offline fractionated over a 90 minute run, into 96 fractions by high pH reverse-phase HPLC (Agilent 1260) using an Agilent Zorbax 300 Extend-C18 column (3.5-µm, 4.6 × 250 mm) with mobile phase A containing 4.5 mM ammonium formate (pH 10) in 2% (vol/vol) LC-MS grade acetonitrile, and mobile phase B containing 4.5 mM ammonium formate (pH 10) in 90% (vol/vol) LC-MS grade acetonitrile. The 96 resulting fractions were then concatenated in a non-continuous manner into 24 fractions and 5% of each were aliquoted, dried down via vacuum centrifugation and stored at -80ºC until further analysis.

The remaining 95% of each fraction was further concatenated into 3 fractions and dried down via vacuum centrifugation. For each fraction, phosphopeptides were enriched with a two-step method, where High Select Fe-NTA kit (Thermo) was first used, and from that enrichment step the flow-through and eluates were collected. Then, with the flow-through of each fraction, the High Select TiO_2 kit (Thermo) was used to further enrich for phosphopeptides. Manufacturer protocols were followed for both enrichments. Fe-NTA and TiO_2 eluates were dried down via vacuum centrifugation and stored at -80ºC until further analysis.

For kinome profiling, WT SUM159 cells were plated on 15 cm^2 dishes (Corning) and allowed to adhere overnight. Cells were treated with 0.1% DMSO, 10 µM ONC201, or 150 nM TR-57 for 30 minutes,

3 hours, or 24 hours. Samples were then prepared as previously described[162]. Briefly, cells were washed 3 x 5 mL with ice-cold DPBS and lysed [50 mM HEPES (pH 7.5), 150 mM NaCl, 0.5% Triton X-100, 1.0 mM EDTA, 1.0 mM EGTA, 10 mM NaF, 2.5 mM $NaVO_4$, Complete protease inhibitor cocktail (Roche), complete phosphatase inhibitor cocktail 2 and 3 (Roche)]. Samples were sonicated, clarified by centrifugation (14,000*g*, 10 minutes), and filtered with 0.2 µm surfactant-free cellulose acetate membrane filters. Protein concentration was determined by Bradford assay and salt concentration adjusted to 1M NaCl. Poly-prep chromatography columns (BioRad) were prepped with MIBs resin and equilibrated with high-salt wash buffer [50 mM HEPES (pH 7.5), 150 mM NaCl, 0.5% Triton X-100, 1.0 mM EDTA, 1.0 mM EGTA] via gravity flow. Lysates were then passed over equilibrated columns, then columns were washed with high-salt buffer followed by low-salt buffer [50 mM HEPES (pH 7.5), 1.0 mM NaCl, 0.5% Triton X-100, 1.0 mM EDTA, 1.0 mM EGTA] then SDS wash buffer [50 mM HEPES (pH 7.5), 1.0 mM NaCl, 0.5% Triton X-100, 1.0 mM EDTA, 1.0 mM EGTA, 0.1% SDS]. Proteins were eluted from the column via boiling in elution buffer [100 mM tris-HCl (pH 6.8), 0.5% SDS, 1% β-mercaptoethanol]. Eluates were then reduced, alkylated, and concentrated, followed by extraction with chloroform-methanol precipitation and digested overnight with sequencing grade porcine trypsin (Promega). Peptides were then extracted with 3 washes of ethyl acetate and desalted using Pierce C-18 spin columns (Thermo Fisher Scientific).

Data Acquisition and Processing

Two sets of 24 fractions for the proteome analysis and two sets of 6 fractions (FeNTA and TiO_2 eluates) for the phosphoproteome analysis were analyzed by LC/MS/MS using an Easy nLC 1200 coupled to an Orbitrap Fusion Lumos Tribrid mass spectrometer (Thermo Scientific). Samples were injected onto an Easy Spray PepMap C18 column (75 µm id × 25 cm, 2 µm particle size) (Thermo Scientific) and separated over either a 120-minute method for the proteome fractions or a 150-minute method for the phosphoproteome fractions. For the proteome fractions, the gradient for separation consisted of 5–40% mobile phase B at a 250 nl/min flow rate, where mobile phase A was 0.1% formic acid in water and mobile phase B consisted of 0.1% formic acid in 80% ACN.

For the proteome fractions, the Lumos was operated in SPS-MS3 mode[163] with a 3s cycle time. Resolution for the precursor scan (m/z 400–1500) was set to 120,000 with a AGC target set to standard and a maximum injection time of 50 ms. MS2 scans consisted of CID normalized collision energy (NCE)

32; AGC target set to standard; maximum injection time of 50 ms; isolation window of 0.7 Da. Following MS2 acquisition, MS3 spectra were collected in SPS mode (10 scans per outcome); HCD set to 55; resolution set to 50,000; scan range set to 100-500; AGC target set to 200% with a 100 ms maximum inject time. Dynamic exclusion was set to 30 seconds.

For the phosphoproteome fractions, the Lumos was operated in MS2 mode[164,165] with a 3s cycle time. Resolution for the precursor scan (m/z 400–1500) was set to 60,000 with a AGC target set to standard and a maximum injection time of 50 ms. For MS2 scans, HCD was set to 35; AGC target set to 200%; maximum injection time of 120 ms; isolation window of 0.7 Da; resolution set to 50,000. Dynamic exclusion was set to 30 seconds. Peptides isolated from MIB enrichment were analyzed by LC-MS/MS using a Thermo Fisher Q Exactive HF mass spectrometer. Peptides were analyzed as described below.

Identification and Annotation

For proteome and phosphoproteome data, all raw files were processed using Proteome Discoverer version 2.5. 'TMTpro 16plex' was used as the quantitation method, and the two TMTpro 16plex datasets (Set 1: ONC201; Set 2: TR-57) were analyzed separately. Peak lists were searched against a reviewed Uniprot human database (downloaded Feb 2020 containing 20,350 sequences), appended with a common contaminants database (from MaxQuant, containing 245 sequences), using Sequest HT within Proteome Discoverer. Data were searched with up to two missed trypsin cleavage sites and fixed modifications were set to TMTpro peptide N-terminus and Lys, and carbamidomethyl Cys. Dynamic modifications were set to N-terminal protein acetyl and oxidation Met. Percolator node was used to calculate peptide false discovery rates (FDR).

For phosphoproteome data, additional dynamic modification was set to phosphorylation Ser, Thr, Tyr. TMT quantitation was set to MS2, precursor mass tolerance was set to 10 ppm and fragment mass tolerance was set to 0.02 Da. Peptide FDR was set to 1%. The ptmRS node was used to localize phosphorylation sites within peptides. Reporter abundance based on intensity and co-isolation threshold was set to 50. Normalization was enabled ('use all peptides').

For proteome data, quantitation was set to MS3, precursor mass tolerance was set to 20 ppm and fragment mass tolerance was set to 0.5 Da. Peptide FDR was set to 1%. Reporter abundance based

on intensity, SPS mass matches threshold set to 50, and razor and unique peptides were used for quantitation. Normalization was enabled ('use all peptides').

For kinome data, raw data was processed using MaxQuant software for identification of label-free quantification (LFQ). Peptides were aligned to proteins using the UniProt human database using global normalization. Kinases were identified and Argonaut was used for further analysis, removing proteins with <1 unique+razor peptide and >50% missing values, and calculating Log_2(fold change) of LFQs compared to DMSO controls. Data was visualized using GraphPad.

Transcriptomics

Sample Preparation

SUM159 (WT and ClpP-KO) cells were plated and treated as described for Proteomics. Cells were washed 3 x 5 mL ice-cold DPBS and RNA was extracted using a Qiagen RNeasy Kit (74104) following manufacturer's directions. RNA samples were sent to Novogene Co. for RNAseq analysis.

Identification and Annotation

Raw reads for each sample were obtained as FASTQ files from Novogene Co. and was indexed and quantified in alignment-based mode through Salmon using reference transcriptome [Transcript Sequences v. 27] from GENCODE. Resulting quantification files were imported to R and DESeq2 was used to normalize samples and analyze differential expression. Significance cutoffs including a base mean exceeding 50 and p value equal to or exceeding 0.5 were applied to the dataset.

Metabolomics

Sample Preparation

SUM159 (WT and ClpP-KO) cells were plated as described for proteomics analysis. Cells were washed 3 x 5 mL ice-cold DPBS and metabolites were extracted as previously described[166,167]. Briefly, 1 mL -20°C acetonitrile and 750 µL ice cold H_2O were added to washed plates and cells were mechanically scraped and transferred to 15 mL conical tubes and stored at -80°C until extraction was performed. To extract metabolites, ~five 2mm zirconia beads were added to each 15 mL conical followed by 500 µL chloroform (-20°C) and samples were vortexed 3 x 30 seconds. Samples were then centrifuged in a 4°C swing-bucket centrifuge (3,700*g*, 60 minutes). The aqueous layer was then transferred to a 2 mL Lo-Bind tube and the organic layer to a glass vial. Remaining samples were transferred to a 1.5 mL Lo-Bind tube

and 15 mL conicals were washed with 300 µL 2:1 chloroform:methanol solution (-20°C) and transferred to corresponding 1.5 mL Lo-Bind tube and centrifuged at 4°C (15,000*g*, 20 minutes). Aqueous and organic layers were transferred to corresponding 2 mL Lo-Bind tube and glass vial for each sample and frozen at -80°C.

Aqueous fractions of cell extracts were dried by speed vac and reconstituted using 200 µL of reconstitution solution (95:5 water:methanol), and 150 µL of the reconstituted extract was transferred to new tubes. An aliquot of 20 µL was taken from each extract and combined to make a total study pool (SP). All samples and the SP were centrifuged at 4 °C and 16,000 x g for 10 minutes, and the supernatants were transferred to LC-MS vials. An injection volume of 5 µL was used for LC-MS analysis.

Data Acquisition and Processing

Metabolomics data were acquired on a Vanquish UHPLC system coupled to a Q Exactive™ HF-X Hybrid Quadrupole-Orbitrap Mass Spectrometer (Thermo Fisher Scientific, San Jose, CA). Metabolites were separated via an HSS T3 C18 column (2.1 × 100 mm, 1.7 µm, Waters Corporation) at 50 °C with binary mobile phase of water (A) and methanol (B), each containing 0.1% formic acid (v/v). The UHPLC linear gradient started from 2% B, and increased to 100% B in 16 min, then held for 4 min, with the flow rate at 400 µL/min. The untargeted data was acquired from 70 to 1050 m/z using the data-dependent acquisition mode. Method blanks and SP injections were placed after every 6 samples (n=3 each). Progenesis QI (version 2.1, Waters Corporation) was used for peak picking, alignment, and normalization. Background signals were filtered out by removing peaks with a fold change less than 3 in the total SP vs the blank injections. Samples were then normalized in Progenesis QI using the “normalize to all” feature[168]. Coefficient of variation (CV) values were calculated across the total SP replicates for each peak and those with CV >30% were removed. Filtered, normalized data was exported and multivariate analysis was performed using SIMCA 16.

Identification and Annotation

Metabolites were identified in Progenesis QI using an in-house physical standards library of >2400 reference standards. All reference standards were analyzed under the same instrument conditions used to analyze the study samples. Peaks were matched to metabolites in the in-house library by exact mass (MS), fragmentation pattern (MS/MS), and retention time (rt). An ontology system was provided for

each peak match to indicate the evidence basis for each identification. A peak was considered to have a match by rt if the peak eluted within 0.5 min compared to the reference standard, an MS match was defined as <5 ppm error compared to the theoretical mass based on the metabolite chemical formula, and an MS/MS match was defined as a similarity score >30% to a reference standard (calculated using MS/MS match algorithms in Progenesis QI). Peaks were also annotated to additional metabolites by matching signals to public mass spectral databases (NIST, METLIN, HMDB). OL1 refers to an in-house metabolite match by rt, MS, and MS/MS; OL2a refers to an in-house match by rt and MS only; OL2b refers to an in-house match by MS and MS/MS only; PDa refers to a public database match by MS and experimental MS/MS, PDb refers to a public database match by MS and theoretical MS/MS, PDc refers to a public database match by MS and isotope similarity (>90%); PDd refers to a public database match by MS only.

Immunoblotting

SUM159 cells (WT and ClpP-KO) were plated (1 x 10^5 cells/well) on a 6-well plate (Corning, 3516) and incubated with compounds at concentrations as indicated in figure legends. Following treatment, cells were rinsed 3x with 2 mL of ice-cold DPBS and lysed using RIPA buffer (20 mM Tris [pH 7.4], 137 mM NaCl, 10% glycerol, 1% Nonidet P-40, 0.5% deoxycholate, 2 mM EDTA) supplemented with 10 mM NaF, 2 mM Na_3VO_4, 0.0125 μM calyculin A, and complete protease inhibitor cocktail (Roche Diagnostics, 11873580001). Lysates were clarified and immunoblotted as previously described. Membranes were incubated with primary antibodies [ATF4 (Cell Signaling Technologies, 11815), ASNS (Cell Signaling Technologies, 20843), ALAS1 (Abcam, ab154860), LonP (Cell Signaling Technologies, 28020), ClpP (Cell Signaling Technologies, 14181), Vinculin (Santa Cruz Biotechnology sc-73614)] diluted 1:1000 in 1% fish gelatin (Sigma Aldrich, G7041)/TBST overnight at 4°C, then washed 3 x 5 minutes in TBST and incubated at room temperature in the appropriate secondary antibody (1:10,000 in 5% milk/TBST) for 1 hour. Membranes were then washed 3 x 5 minutes in TBST and incubated in ECL reagent (BioRad, 170-5061) and imaged using Chemidoc MP (BioRad). Acquired images were processed using ImageLab software (BioRad).

Statistics and Software

ImageLab (BioRad) was used to process immunoblot images. Prism 9 (GraphPad) was used to generate bar charts. BioVenn[169] was used to generate Venn diagrams and VolcanoseR[170] was used to generate volcano plots. Proteome Discoverer was used to perform statistical analysis on proteomics and phosphoproteomics data. Protein and phosphopeptide p-values for each pairwise comparison was calculated using Student's t-test, and p-value <0.05 was considered significant. Log_2(Fold Change) was calculated for each pairwise comparison using the normalized TMT intensities averaged across 3 replicates. Salmon and DESeq were used to process transcriptomics data. P-values for each pairwise comparison was calculated using Student's t-test, and p-value <0.05 was considered significant. P-values were not adjusted for multiple comparisons for use in volcano plots due to the exploratory, rather than confirmatory, nature of this study[171]. Adjusted p-values are shown for proteomic and transcriptomic data in Figure 5, 6, and S2. Log_2(Fold Change) was calculated for each pairwise comparison using normalized counts averaged across 3 replicates ProgenesisQI was used to process UPLC-MS metabolomics data and SIMCA (Sartorious) was used to calculate variable importance to projection (VIP) scores. Log_2(Fold Changes) of means (proteins, transcripts) or medians (metabolomics) and their respective $-log_{10}$(p-value) were determined for significant proteins, transcripts, and metabolites using Excel (Microsoft). Proteomic and transcriptomic observations meeting the fold change and significance threshold (Log_2(Fold Change)$\geq|0.5|$ and $-log_{10}$(p-value) ≤ -1.3) and metabolomic observations meeting the fold change threshold, significance threshold, or SIMCA VIP score ≥ 0.95 were used for multi-omics analysis. These thresholds were chosen to due frequent use in -omics studies. MetaCore pathway analysis software (Clarivate Analytics) was used for multi-omics data analysis. DAVID[172] (v. 2021) was used for gene ontology analysis. Specifically, data was analyzed using GO terms for biological processes (GOTERM_BP_DIRECT), cellular components (GOTERM_CC_DIRECT), molecular functions (GOTERM_MF_DIRECT), and KEGG pathways. Data collected from DAVID is available in Supplemental Data files. BioRender was utilized to generate all schematics and pathways.

Data Availability

Proteomics data is available on the Proteomics Identification Database (PRIDE, https://www.ebi.ac.uk/pride/; Project ID: PXD038990). Transcriptomics data is available at the NCBI's

Gene Expression Omnibus (GEO, https://www.ncbi.nlm.nih.gov/geo/; Series accession number: GSE221327). Metabolomics data is available at the NIH Common Fund's National Metabolomics Data Repository (NMDR) website (Metabolomics Workbench, https://www.metabolomicsworkbench.org; Project ID: PR001550; DOI: http://dx.doi.org/10.21228/M8BM6G).

4.5 Figures and Tables

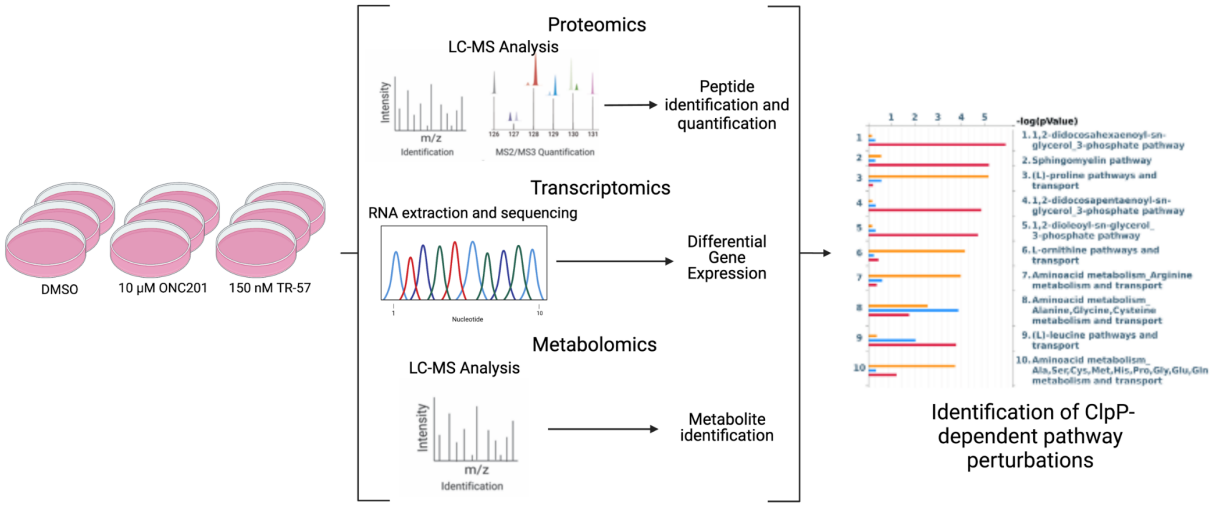

Figure 4.1. Schematic of multi-omic data collection and analysis of triple-negative breast cancer cells. SUM159 cells were treated with 10 μM ONC201 or 150 nM TR-57 and samples were collected and prepared for transcriptomics, metabolomics, and proteomics analyses using appropriate methods. Datasets were then analyzed individually using standard methods and as a combined multi-omics dataset using MetaCore.

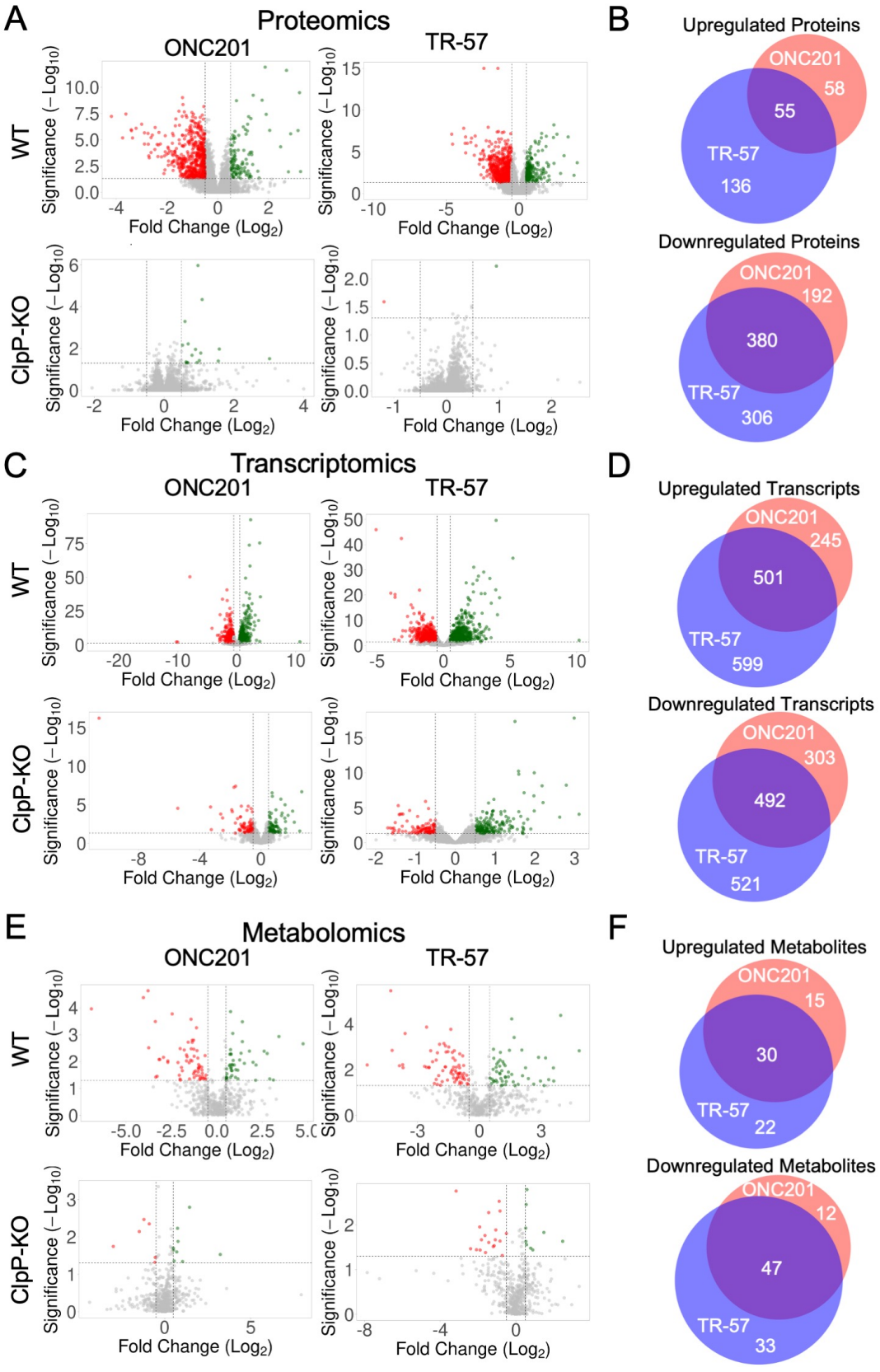
A
Proteomics
ONC201
TR-57
WT
ClpP-KO
Significance (−Log10)
Fold Change (Log2)
B
Upregulated Proteins
ONC201
58
55
TR-57
136
Downregulated Proteins
ONC201
192
380
TR-57
306
C
Transcriptomics
ONC201
TR-57
WT
ClpP-KO
Significance (−Log10)
Fold Change (Log2)
D
Upregulated Transcripts
ONC201
245
501
TR-57
599
Downregulated Transcripts
ONC201
303
492
TR-57
521
E
Metabolomics
ONC201
TR-57
WT
ClpP-KO
Significance (−Log10)
Fold Change (Log2)
F
Upregulated Metabolites
ONC201
15
30
TR-57
22
Downregulated Metabolites
ONC201
12
47
TR-57
33

Figure 4.2. Analysis of omics data reveals significant and similar ClpP-dependent effects of ONC201 and TR-57 on triple-negative breast cancer cells. Wildtype (WT) and ClpP knockout (ClpP-KO) SUM159 cells were treated with 10 μM ONC201 or 150 nM TR-57 for 24 hours and analyzed for proteomic (A, B), transcriptomic (C, D), and metabolomic (E, F) perturbations. Volcano plots of each dataset are shown in A, C, and E. Axes are Log_2(Fold Change) and -Log_{10}(unadjusted p-value). Vertical dashed lines indicate fold change threshold (Log_2(FC) >|0.5|) and horizontal dashed lines indicate significance threshold (-Log_{10}(p-value) >1.3), N=3. Venn diagrams of significantly perturbed proteins (B), transcripts (D), and metabolites (F) were generated from small molecules meeting the fold change and significance thresholds previously mentioned. Red: ONC201; blue: TR-57; purple: Both drug treatments.

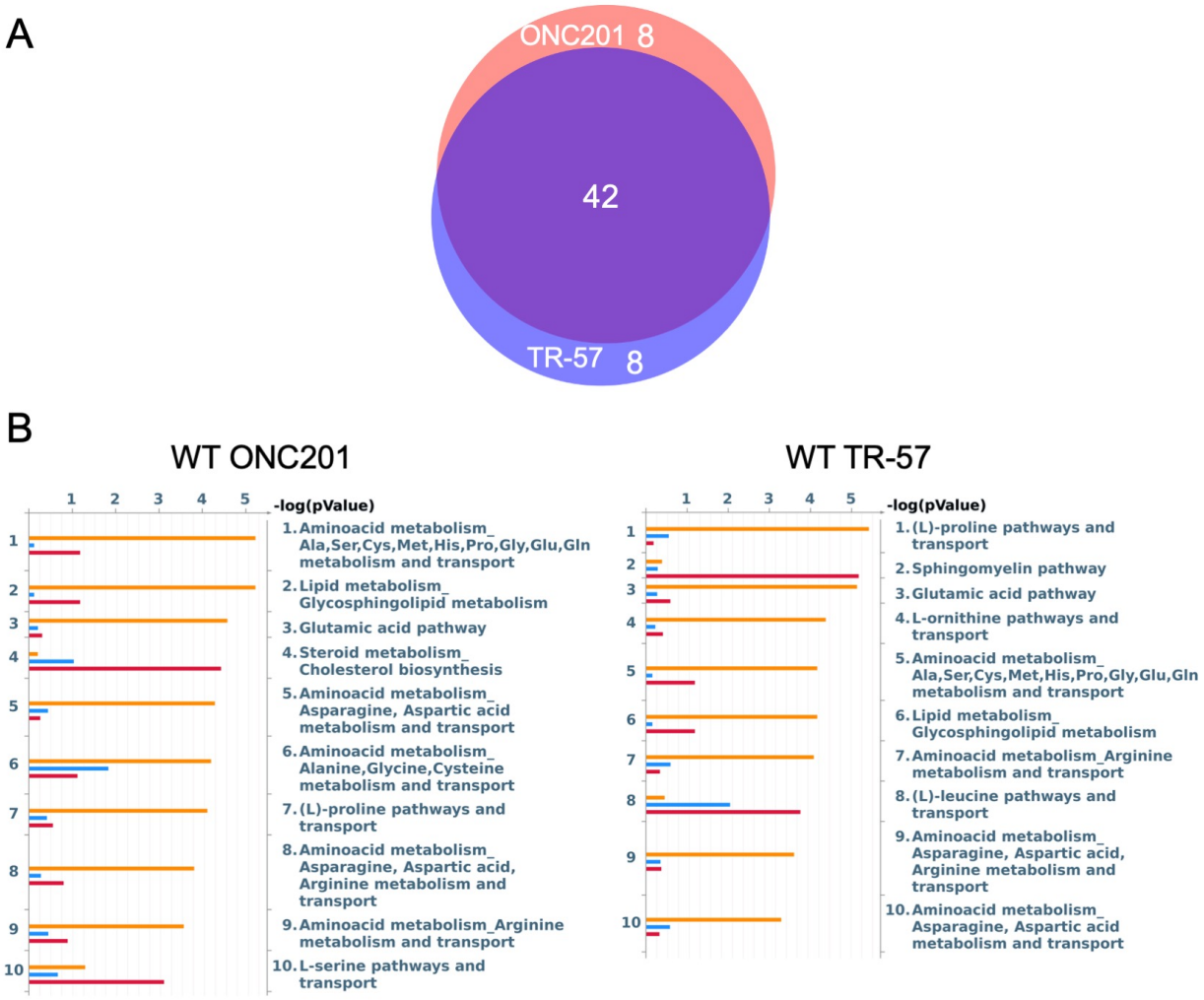

Figure 4.3. MetaCore analysis reveals multiple pathways affected at the proteomic, transcriptomic, and metabolomic level with potential for further investigation in triple-negative breast cancer cells. A) Venn diagram of group classification. Values represent number of pathways found in each group using data from Figures 1-3. B) MetaCore Endogenous Metabolic Network analysis from proteomic (blue), metabolomic (orange), and transcriptomic (red) datasets for Wildtype (WT) SUM159 cells treated with 10 uM ONC201 or 150 nM TR-57.

Table 4.1. ClpP activation perturbs many metabolic pathways across proteomic, transcriptomic, and metabolomic landscapes in triple-negative breast cancer cells. Representative top endogenous metabolic networks (EMN) identified using MetaCore for each group, as outlined in Figure 4.3. Number of hits (perturbed EMN members) and p-value are listed for each dataset in the order they appear in the group name.

Group	Metabolic Networks	Hits	P value
ONC201	*1-acyl-glycerol, 3-phosphocholine pathway*	6/88	1.08×10^{-1}
	Glycine pathway	10/90	1.14×10^{-1}
	1-oleoyl-sn-glycerol-3-phosphocholine pathway	8/121	3.56×10^{-1}
TR-57	*Sphingomyelin pathway*	17/97	6.77×10^{-6}
	Carbohydrate metabolism, Glycolysis, Glucogenesis, and glucose transport	7/134	4.00×10^{-1}
	D-glucuronic acid pathway	10/77	9.53×10^{-3}
ONC201 and TR-57	*Amino acid metabolism: Ala, Ser, Cys, Met, His, Pro, Gly, Glu, Gln metabolism and transport*	26, 24/190	5.92×10^{-6}, 7.14×10^{-5}
	Glutamic acid pathway	14, 16/103	2.72×10^{-5}, 7.47×10^{-6}
	Tyrosine pathway	11, 14/90	2.69×10^{-3}, 7.57×10^{-4}
	Lipid Metabolism, Glycosphingolipid metabolism	26, 24/190	5.92×10^{-6}, 7.14×10^{-5}
	Amino acid metabolism: Asn, Asp metabolism and transport	15, 14/112	5.33×10^{-5}, 5.58×10^{-4}
	Amino acid metabolism: Ala, Gly, Cys metabolism and transport	22, 23/115	6.56×10^{-5}, 6.66×10^{-4}
	Steroid metabolism, Cholesterol biosynthesis	17, 14/88	3.84×10^{-5}, 1.05×10^{-3}
	Vitamin, mediator, and cofactor metabolism: CoA biosynthesis and transport	12, 7/81	3.77×10^{-2}, 1.59×10^{-1}
	Sucrose pathway	9, 11/90	2.92×10^{-1}, 1.44×10^{-2}
	(L)-leucine pathways and transport	13, 17/85	1.96×10^{-2}, 1.87×10^{-4}
	(L)-proline pathways and transport	17, 16/118	8.04×10^{-5}, 3.75×10^{-6}
	(S)-citrulline pathway	12, 10/75	9.65×10^{-3}, 5.04×10^{-2}
	Carbohydrate metabolism: TCA and tricarboxylic acid transport	15, 13/101	9.38×10^{-4}, 1.50×10^{-3}

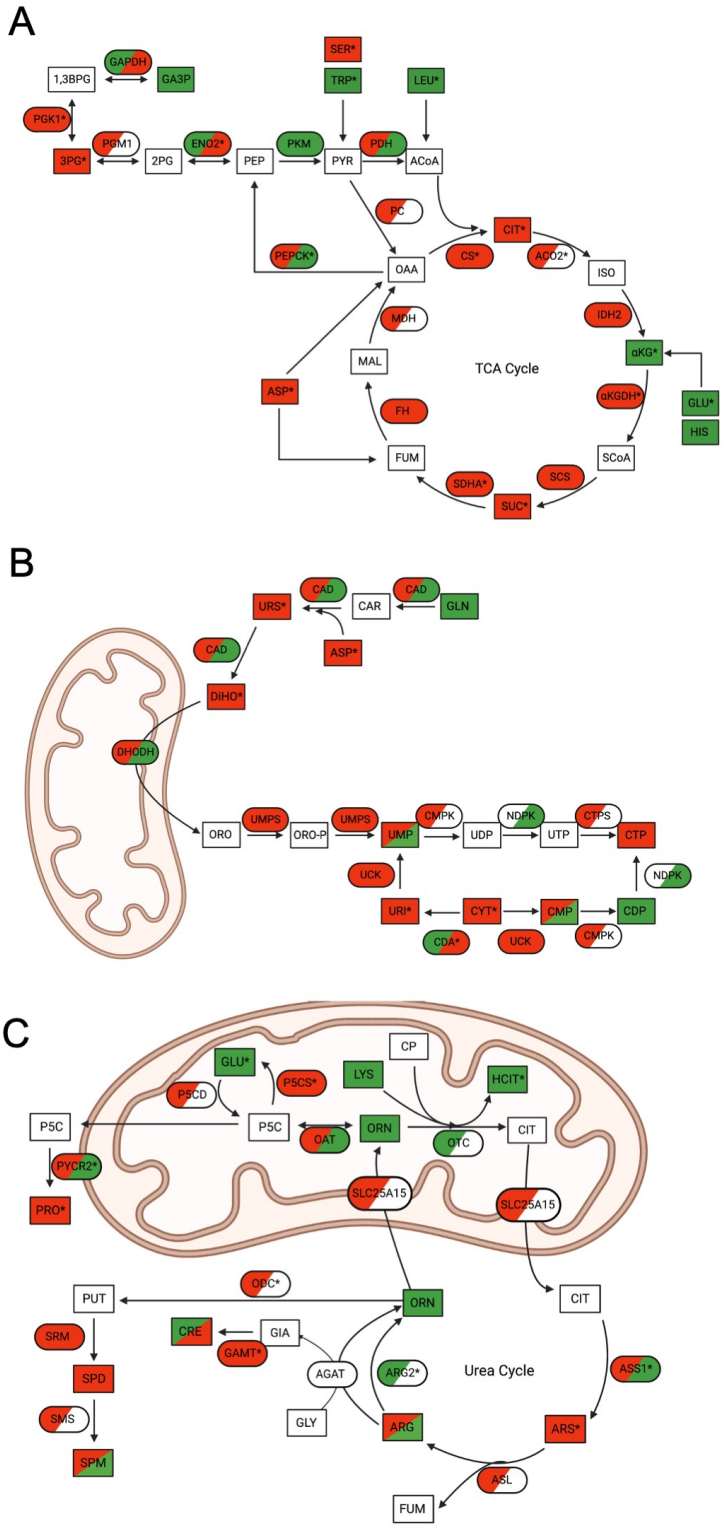
A
1,3BPG
GAPDH
GA3P
PGK1*
3PG*
PGM1
2PG
ENO2*
PEP
PKM
PYR
SER*
TRP*
LEU*
PDH
ACoA
PC
PEPCK*
OAA
CIT*
CS*
ACO2*
ISO
IDH2
αKG*
αKGDH*
GLU*
HIS
SCoA
SCS
SUC*
SDHA*
FUM
FH
MAL
MDH
ASP*
TCA Cycle
B
URS*
CAD
CAR
CAD
GLN
ASP*
CAD
DiHO*
DHODH
ORO
UMPS
ORO-P
UMPS
UMP
CMPK
UDP
NDPK
UTP
CTPS
CTP
UCK
URI*
CYT*
CMP
CDP
NDPK
CDA*
UCK
CMPK
C
GLU*
P5CD
P5CS*
P5C
LYS
CP
HCIT*
P5C
OAT
ORN
OTC
CIT
PYCR2*
PRO*
SLC25A15
SLC25A15
ODC*
PUT
ORN
CIT
SRM
SPD
SMS
SPM
CRE
GIA
GAMT*
AGAT
GLY
ARG2*
ARG
Urea Cycle
ASS1*
ARS*
ASL
FUM

Figure 4.4. Multi-omics analysis reveals significant mitochondrial metabolic pathway perturbations following ONC201 or TR-57 treatment in SUM159 cells. In all schematics, rectangles represent metabolites and ovals represent enzymes. Directionality of change is indicated by color (downregulation (red), upregulation (green), not detected (white)) and * denotes significant change in at least one dataset. Dual-colored enzymes represent those with different directional changes in proteomics (left side) and transcriptomics (right side) while dual-colored metabolites indicate different directional changes in ONC201 treatment (left side) and TR-57 treatment (right side). A) Schematic of the tricarboxylic acid (TCA) cycle. CIT: *citrate*; ISO: *isocitrate*; αKG: *α-ketoglutarate*; GLU; *glutamic acid*; HIS: *histidine*; SCoA: *succinyl-CoA*; SUC: *succinate*; FUM: *fumarate*; MAL: *malate*: OAA: *oxaloacetate*; ASP: *aspartic acid*; ACoA: *acetyl-CoA*; PYR: *pyruvate*; PEP: *phosphoenolpyruvate*: TRP: *tryptophan*; SER: *serine*; LEU: *leucine*; 2PG: *2-phosphoglycerate*; 3PG: *3-phosphoglycerate*; 1,3BPG: *1,3-bisphopshoglycerate*; GA3P: *glyceraldehyde-3-phosphate*; ACO2: *aconitase 2*; IDH2: *isocitrate dehydrogenase 2*; αKGDH: *α-ketoglutarate dehydrogenase*; SCS: *succinyl-CoA synthetase*; SDHA: *succinate dehydrogenase A*; FH: *fumarase*: MDH: *malate dehydrogenase*; PC: *pyruvate carboxylase*; PEPCK: *phosphoenolpyruvate carboxykinase*; PDH: *pyruvate dehydrogenase*; PKM: *pyruvate kinase*; ENO2: *enolase 2*; PGM1: *phosphoglycerate mutase 1*; PGK1: *phosphoglycerate kinase 1;* GAPDH: *glyceraldehyde phosphate dehydrogenase*. B) Schematic of *de novo* and scavenging pathways of pyrimidine synthesis. GLN: *glutamine*; ASP: *aspartic acid*; URS: *ureidosuccinic acid*; DiHO: *dihydroorotate*; ORO: *orotate*; ORO-P: *phospho-orotate*; UMP: *uridine 5'-monophosphate*; UDP: *uridine 5'-diphosphate*; UTP: *uridine 5'-triphosphate*; CMP: *cytidine 5'-monophosphate*; CDP: *cytidine 5'-diphosphate*; CTP: *cytidine 5'-triphosphate*; URI: *uridine*; CYT: *cytidine*; CAD: *carbamoyl-phosphate synthetase 2, aspartate trasncarbamylase, and dihydroorotase*; DHODH: *dihydroorotate dehydrogenase*; UMPS: *uridine 5'-monophosphate synthase*; CMPK: *UMP-CMP kinase*; NDPK: *nucleoside diphosphate kinase*; CTPS: *CTP synthase*; UCK: *uridine-cytidine kinase*; CDA: *cytidine deaminase*. C) Schematic of urea cycle and citrulline pathway. CIT: *citrulline*; ARS: *argininosuccinate*; FUM: *fumarate*; ARG: *arginine*; ORN: *ornithine*; CP: *carbamoyl phosphate*; LYS: *lysine*; HCIT: *homocitrulline*; GLY: *glycine*; GIA: *guanidinoacetate*; CRE: *creatine*; PUT: *putrescine*; SPD: *spermidine*; SPM: *spermine*; P5C: *1-pyrroline-5-carboxylic acid*; PRO: *proline*; GLU: *glutamic acid*; OTC: *ornithine transcarbamylase*; SLC25A15: *mitochondrial ornithine transporter 1*; ASS1: *argininosuccinate synthase*; ASL: *argininosuccinate lyase*; ARG2: *arginase-2*; ODC: *ornithine decarboxylase*; SRM: *spermidine synthase*; SMS: *spermine synthase*; AGAT: *glycine amidinotransferase*; GAMT: *guanidinoacetate N-methyltransferase*; OAT: *ornithine aminotransferase*: P5CS: *1-pyrroline-5-carboxylic acid synthase*; P5CD: *1-pyrroline-5-carboxylic acid dehydrogenase*; PYCR2: *Pyrroline-5-carboxylate reductase 2*.

A

Gene Name	Encoded Protein	Log_2 Fold Change (ONC201, TR-57)		P value (ONC201, TR-57)	
		Transcriptomic	Proteomic	Transcriptomic	Proteomic
ASNS	Asparagine synthetase [glutamine-hydrolyzing]	2.44, 2.83	1.75, 1.85	3.71×10^{-23}, 1.87×10^{-18}	2.71×10^{-6}, 4.99×10^{-4}
GDF15	Growth/differentiation factor 15	2.94, 2.45	3.17, 2.39	3.09×10^{-15}, 1.16×10^{-4}	1.94×10^{-4}, 1.92×10^{-5}
GPT2	Alanine aminotransferase 2	2.21, 2.37	1.18, 1.14	1.50×10^{-4}, 1.44×10^{-4}	8.48×10^{-5}, 2.40×10^{-4}
LARP6	La-related protein 6	1.46, 1.26	1.12, 1.32	3.25×10^{-12}, 1.65×10^{-4}	3.12×10^{-4}, 1.21×10^{-3}
NQO1	NAD(P)H dehydrogenase [quinone] 1	0.91, 1.06	0.51, 0.66	6.51×10^{-14}, 9.76×10^{-5}	7.74×10^{-1}, 1.33×10^{-2}
PSAT1	Phosphoserine aminotransferase	1.23, 1.75	1.4, 1.53	4.79×10^{-2}, 2.9×10^{-3}	1.44×10^{-6}, 1.03×10^{-4}
RBCK1	RanBP-type and C3HC4-type zinc finger-containing protein 1	1.17, 0.89	0.52, 0.59	4.97×10^{-27}, 4.40×10^{-2}	5.44×10^{-3}, 9.67×10^{-3}
RNF41	E3 ubiquitin-protein ligase NRDP1	0.47, 1.00	0.38, 0.46	2.34×10^{-2}, 4.35×10^{-6}	6.47×10^{-3}, 4.81×10^{-2}
TRIB3	Tribbles homolog 3	2.58, 2.55	2.88, 2.36	2.73×10^{-28}, 4.67×10^{-5}	2.97×10^{-4}, 9.91×10^{-5}
TRIM25	E3 ubiquitin/ISG15 ligase TRIM25	1.42, 1.91	0.38, 0.35	4.88×10^{-5}, 2.48×10^{-4}	2.37×10^{-2}, 1.21×10^{-3}
WARS1	Tryptophan--tRNA ligase, cytoplasmic	1.33, 1.70	0.69, 0.74	1.21×10^{-21}, 1.59×10^{-22}	6.06×10^{-4}, 1.62×10^{-3}

B

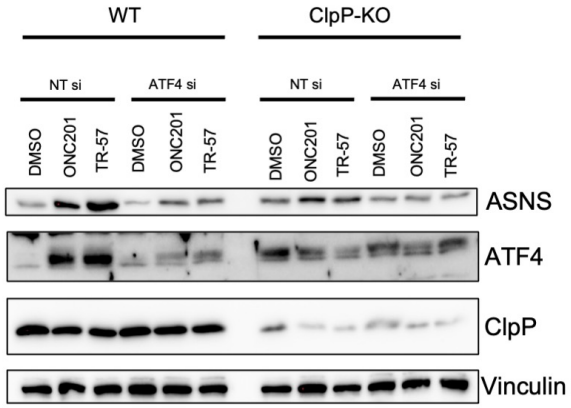

C

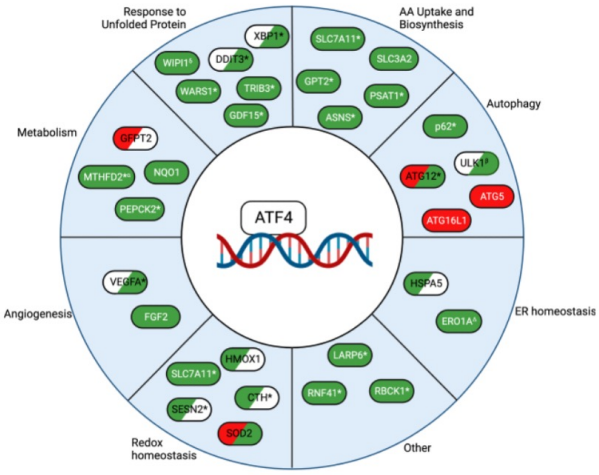

Figure 4.5. Pharmacological ClpP activation leads to ATF4 induction and induction of ATF4 target genes in TNBC cells. A) Table of selected ATF4-dependent genes/proteins and their measured Log_2(Fold Change) and p-value from proteomics and transcriptomics data from WT SUM159 cells treated with 10 μM ONC201 and 150 nM TR-57 for 24 hours. B) Immunoblot of SUM159 cells treated with 0.1% DMSO, 10 μM ONC201, or 150 nM TR-57 for 24 hours. Cells were either treated with a non-targeting siRNA or an ATF4 siRNA. Representative of N=2. C) Schematic of ATF4 target genes and their involvement in diverse cellular processes. Green: transcripts and protein were upregulated in WT SUM159s treated with either ONC201 or TR-57. Red: transcripts and protein were downregulated in WT SUM159s treated with either ONC201 or TR-57. White: not detected in our datasets. Items in two colors indicate direction of change in proteomics (left) and transcriptomics (right). *At least one dataset is significant (p value <0.05); $^{\alpha}$TR-57 treated SUM159 cells showed decreased proteomic values; $^{\beta}$TR-57 treated SUM159 cells showed decreased transcriptomic values; $^{\Delta}$TR-57 treated SUM159 cells showed decreased proteomic and transcriptomic values; $^{\delta}$ Not detected in TR-57 treated SUM159 cells (proteomics).

A

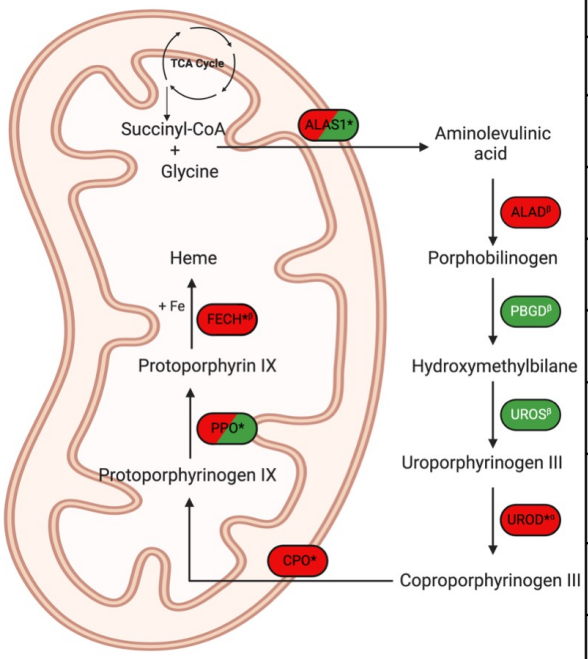

Gene Name	Encoded Protein	Log_2 Fold Change (ONC201, TR-57)		P value (ONC201, TR-57)	
		Transcriptomic	Proteomic	Transcriptomic	Proteomic
ALAS1	5-aminolevulinate synthase	0.2, 0.09	-0.51, -1.18	2.96×10^{-1}, 8.23×10^{-1}	1.08×10^{-1}, 3.24×10^{-2}
ALAD	Delta-aminolevulinic acid dehydratase	-0.17, 0.28	-0.36, -0.21	8.69×10^{-1}, 7.04×10^{-1}	7.32×10^{-1}, 7.68×10^{-1}
PBGD	Porphobilinogen deaminase	-0.31, 0.17	0.1, 0.3	6.00×10^{-1}, 7.82×10^{-1}	5.37×10^{-1}, 3.42×10^{-1}
UROS	Uroporphyrinogen III synthase	-0.06, 0.1	0.13, 0.21	9.01×10^{-1}, 8.37×10^{-1}	1, 6.49×10^{-1}
UROD	Uroporphyrinogen decarboxylase	-0.37, -0.72	-0.15, 0.02	2.56×10^{-1}, 4.34×10^{-2}	1, 1
CPO	Oxygen-dependent coproporphyrinogen III oxidase	-0.27, -1.59	-0.34, -0.45	7.56×10^{-1}, 3.93×10^{-3}	6.07×10^{-1}, 7.74×10^{-1}
PPO	Protoporphyrinogen oxidase	0.58, 0.47	-0.64, -1.3	1.53×10^{-1}, 2.48×10^{-1}	2.56×10^{-1}, 8.05×10^{-2}
FECH	Ferrochelatase, mitochondrial	-0.28, 0.43	-1.17, -1.8	5.7×10^{-1}, 4.93×10^{-1}	5.26×10^{-2}, 5.69×10^{-3}

B

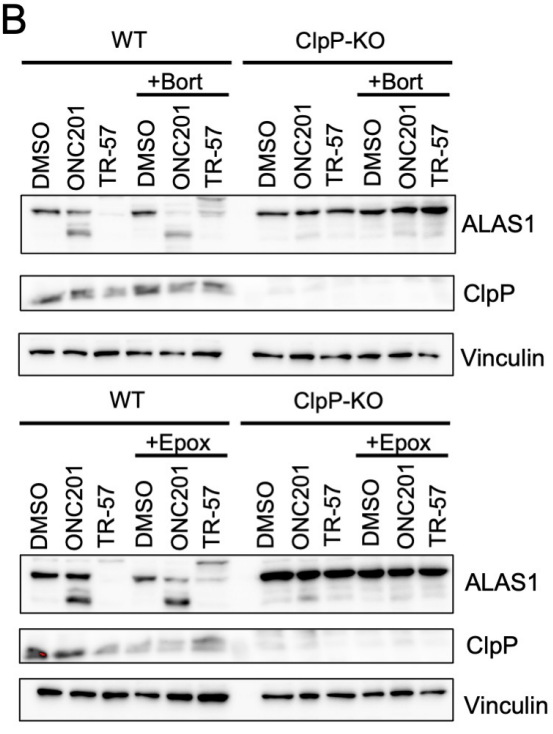

C

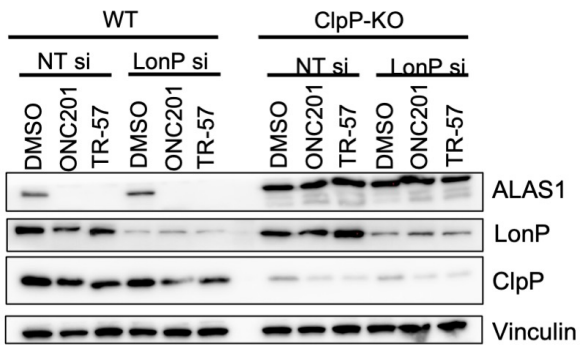

D

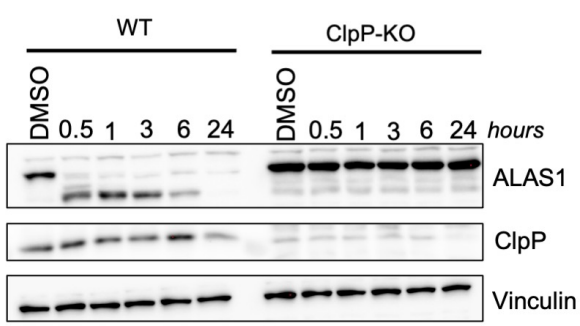

Figure 4.6 ClpP activation induces loss of major components of the heme biosynthetic pathway in TNBC cells. A) Schematic of heme biosynthetic pathway (left). Directionality of change is indicated by color (downregulation (red), upregulation (green), not detected (white)). * indicates significant in at least one dataset, conflicting $^{\alpha}$proteomic, $^{\beta}$transcriptomic, or $^{\Delta}$both datasets for one treatment. $^{\delta}$Not detected in TR-57 proteomics dataset. Dual-colored enzymes represent those with different directional changes in proteomics (left side) and transcriptomics (right side) while dual-colored metabolites indicate different directional changes in ONC201 treatment (left side) and TR-57 treatment (right side). ALAS1: 5'-*aminolevulinate synthase 1*; ALAD: *aminolevulinate dehydratase*; PBGD: *porphobilinogen deaminase*; UROS: *uroporphyrinogen III synthase*; UROD: *uroporphyrinogen decarboxylase*; CPO: *coproporphyrinogen oxidase*; PPO: *protoporphyrinogen oxidase*; FECH: *ferrochelatase*. WT and ClpP-KO SUM159 cells were immunoblotted for ALAS1 following 24 hours of 10 μM ONC201 or 150 nM TR-57 fin the presence or absence of B) 10 nM bortezomib (Bort) or 1 μM epoxomicin (Epox) or C) LonP siRNA knockdown (LonP si). Cells were reverse transfected with either non-targeting or LonP1-targeting siRNA for 48 hours before ClpP activator treatment. D) Time-dependent immunoblot of 150 nM TR-57 treatment in WT and ClpP-KO SUM159 cells. All blots are representative of N=2.

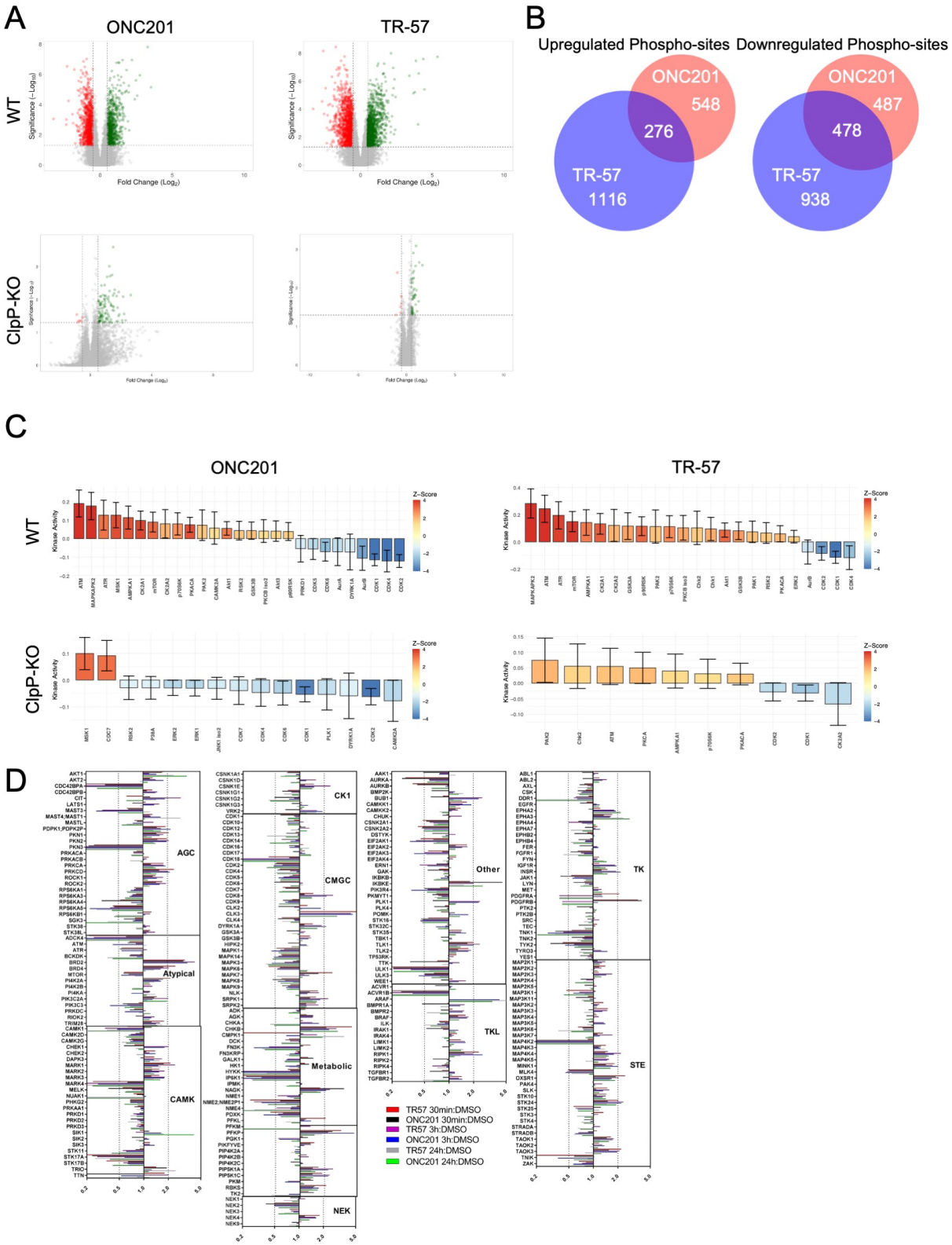
A
ONC201
TR-57
WT
ClpP-KO
Significance (−Log10)
Fold Change (Log2)
B
Upregulated Phospho-sites
Downregulated Phospho-sites
ONC201
548
276
TR-57
1116
ONC201
487
478
TR-57
938
C
ONC201
TR-57
WT
ClpP-KO
Kinase Activity
Z-Score
D
AGC
Atypical
CAMK
CK1
CMGC
Metabolic
NEK
Other
TKL
TK
STE
TR57 30min:DMSO
ONC201 30min:DMSO
TR57 3h:DMSO
ONC201 3h:DMSO
TR57 24h:DMSO
ONC201 24h:DMSO

Figure S4.1. Pharmacological ClpP activation induces significant changes in the phosphoproteome of SUM159 cells. A) Volcano plots of phosphoproteomic data of SUM159 (WT and ClpP-KO) treated with 10 μM ONC201 or 150 nM TR-57 for 24 hours. Volcano plots show log_2(Fold Change) (x-axis) and $-log_{10}$(p-value) (y-axis) for each collected datapoint. Dashed lines indicate fold change threshold (log_2(Fold Change)>|0.5|) and significance threshold ($-log_{10}$(p-value)>1.3). Phospho-site changes meeting fold change and significance thresholds were used to generate Venn diagrams (B) and used in (C) RoKAI analysis for predicted changes in kinase activity. D) Multiplex inhibitor beads (MIBs) were utilized to identify changes in kinase expression following ONC201 or TR-57 treatment at 30 minutes, 3 hours, and 24 hours. N=1.

A

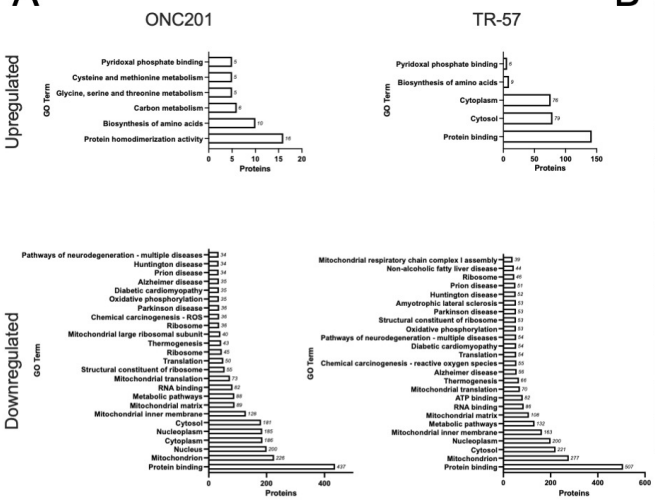

B

Protein Name (Accession)	Subcellular Localization	Log_2 (Fold Change) ONC201, TR-57	P-value ONC201, TR-57
ATPIF1 (Q9UII2)	Mitochondria	-2.32, -4.62	2.5×10^{-4}, 5.8×10^{-5}
MRPL12 (P52815)	Mitochondria	-2.72, -4.56	9.5×10^{-3}, 2.9×10^{-4}
BOLA3 (Q53S33)	Mitochondria	-3.22, -3.8	1.4×10^{-4}, 3×10^{-5}
TUFM (P49411)	Mitochondria	-2.36, -3.7	1.0×10^{-2}, 2.6×10^{-4}
TSFM (P43897)	Mitochondria	-4.19, -3.67	3.0×10^{-5}, 8.9×10^{-5}
FAT3 (Q8TDW7)	Membrane	2.07, 3.77	6.3×10^{-1}, 8×10^{-2}
NIBAN1 (Q9BZQ8)	Cytoplasm, Membrane	2.48, 3.09	2.3×10^{-3}, 2.9×10^{-3}
Profilin-3 (P60673)	Cytoplasm, Nucleus	2.62, 2.85	4.9×10^{-1}, 6.2×10^{-2}
PPAR-δ (Q03181)	Nucleus	2.23, 2.74	7.7×10^{-1}, 3.0×10^{-1}
GDF15 (Q99988)	Secreted	3.17, 2.39	1.9×10^{-4}, 1.9×10^{-5}

C

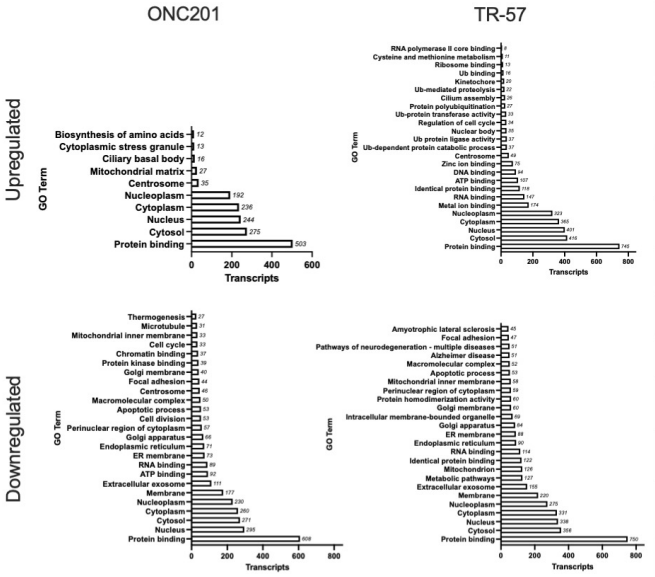

D

Gene Name	Subcellular Localization of encoded protein	Log_2 (Fold Change) ONC201, TR-57	P-value ONC201, TR-57
INSIG1	Endoplasmic reticulum membrane	-2.85, -3.64	1.9×10^{-20}, 4.7×10^{-17}
CPA4	Secreted	-3.01, -3.97	3.5×10^{-6}, 1.4×10^{-18}
CMKLR1	Cell membrane	-2.52, -2.28	3.0×10^{-5}, 8.7×10^{-6}
PTPRC	Cell membrane	-4.22, -3.65	7.8×10^{-11}, 3.9×10^{-18}
DIO2	Cell membrane	-2.22, -5.08	1.6×10^{-5} , 7.3×10^{-43}
FLRT1	Cell membrane	4.00, 3.92	3.1×10^{-33}, 8.2×10^{-20}
SKIL	Cytoplasm, nucleus	3.34, 4.05	5.7×10^{-3}, 1.8×10^{-10}
SLC25A6	Mitochondrial inner membrane	3.12, 3.11	3.9×10^{-20}, 1.9×10^{-18}
SLC6A9	Cell membrane	2.36, 2.74	3.0×10^{-7}, 3.7×10^{-6}
ASNS	Cytosol	2.44, 2.83	3.7×10^{-23}, 1.9×10^{-18}

E

Metabolite	Log_2 (Fold Change) ONC201, TR-57	P-value ONC201, TR-57
α-Ketoglutarate	4.75, 4.84	2.2×10^{-3}, 1.5×10^{-3}
2-hydroxyglutaric acid	3.41, 3.93	1.2×10^{-3}, 4.2×10^{-5}
Thymine	1.93, 2.63	1.3×10^{-1}, 4.3×10^{-2}
S-adenosylmethionine	1.18, 1.25	6.9×10^{-2}, 6.7×10^{-3}
L-Tryptophan	1.16, 1.11	4.5×10^{-2}, 3.2×10^{-2}

Metabolite	Log_2 (Fold Change) ONC201, TR-57	P-value ONC201, TR-57
L-Aspartic acid	-6.9*	1×10^{-4}, 1.1×10^{-4}
Orotic acid	-3.29, -0.23	3.6×10^{-2}, 4.6×10^{-1}
L-Ascorbic acid	-3.14, -5.44	8.4×10^{-3}, 6.2×10^{-3}
Hypoxanthine	-1.8, -0.92	3.7×10^{-3}, 1.4×10^{-2}
Argininosuccinic acid	-3.19*	8.4×10^{-3}, 5.0×10^{-3}

Figure S4.2. Gene ontological analysis reveals significant mitochondrial downregulation at the proteomic and transcriptomic level. Gene ontological analysis of proteomic (A) and transcriptomic (C) data was performed using proteins and transcripts meeting fold change and significance thresholds using DAVID, as described in Methods. The top 25 significant GO terms (or fewer if fewer were identified) are shown. Select significant up- and downregulated proteins and transcripts are shown in (B) and (D), respectively. E) Select significantly up- and downregulated metabolites. *Indicates detection in ONC201 only.

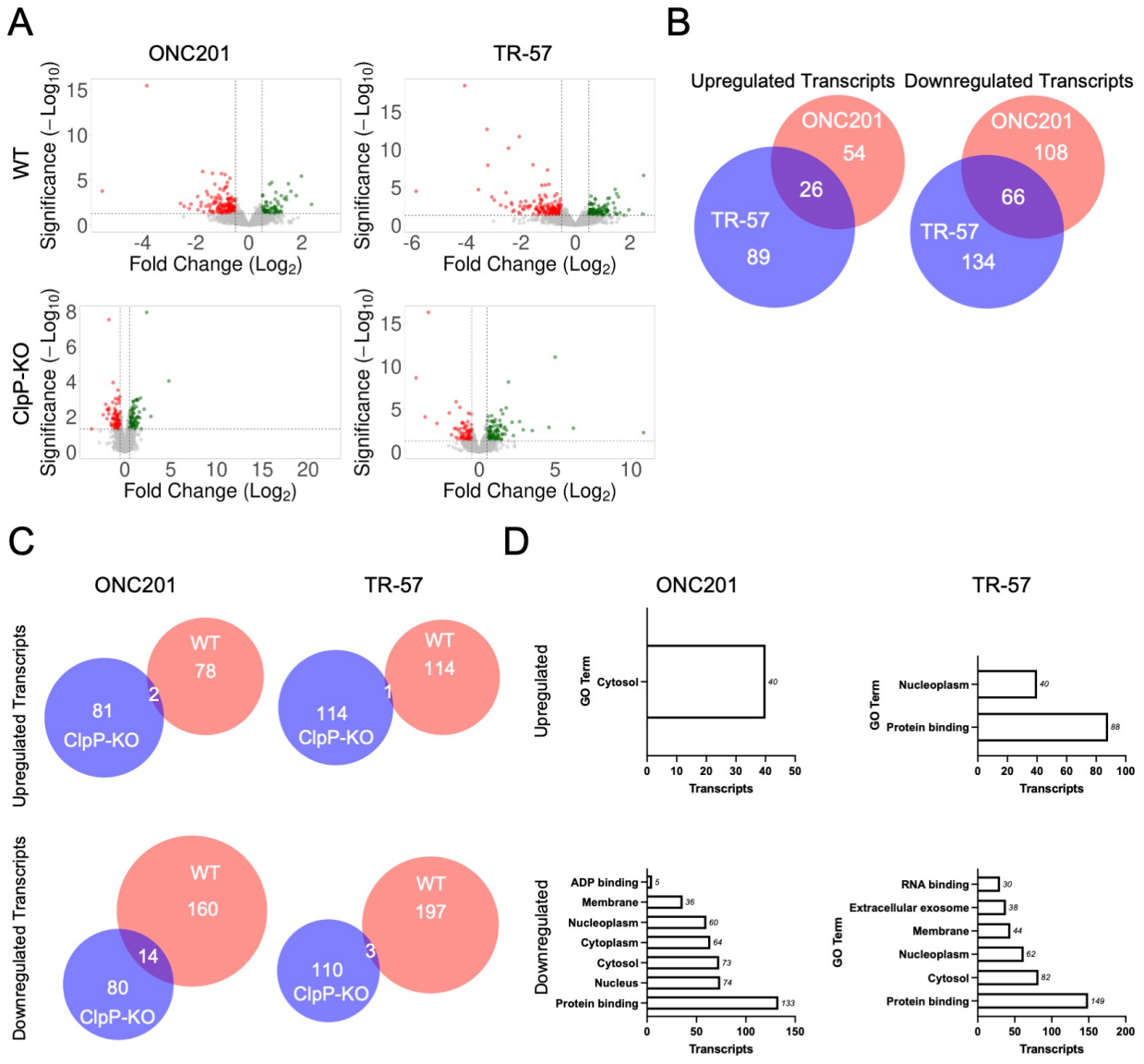

Figure S4.3. Early event transcriptomics reveals significant changes following ONC201 and TR-57 treatment in triple-negative breast cancer cells. SUM159 cells (WT and ClpP-KO) were treated with 0.1% DMSO, 10 μM ONC201, or 150 nM TR-57 for 1 hour. RNAseq was performed as described in methods and Log_2(mean Fold Change) of drug treatment compared to DMSO control was calculated for each detected transcript. Data was used to generate (A) volcano plots. Transcripts meeting significance thresholds (log_2(Fold Change)>|0.5| and -log_{10}(p value)>1.3) were used to generate Venn diagrams comparing (B) WT ONC201 and TR-57 treatments and (C) responses in WT and ClpP-KO cells. (D) Gene ontological analysis of significant transcripts in WT SUM159 cells. N=3.

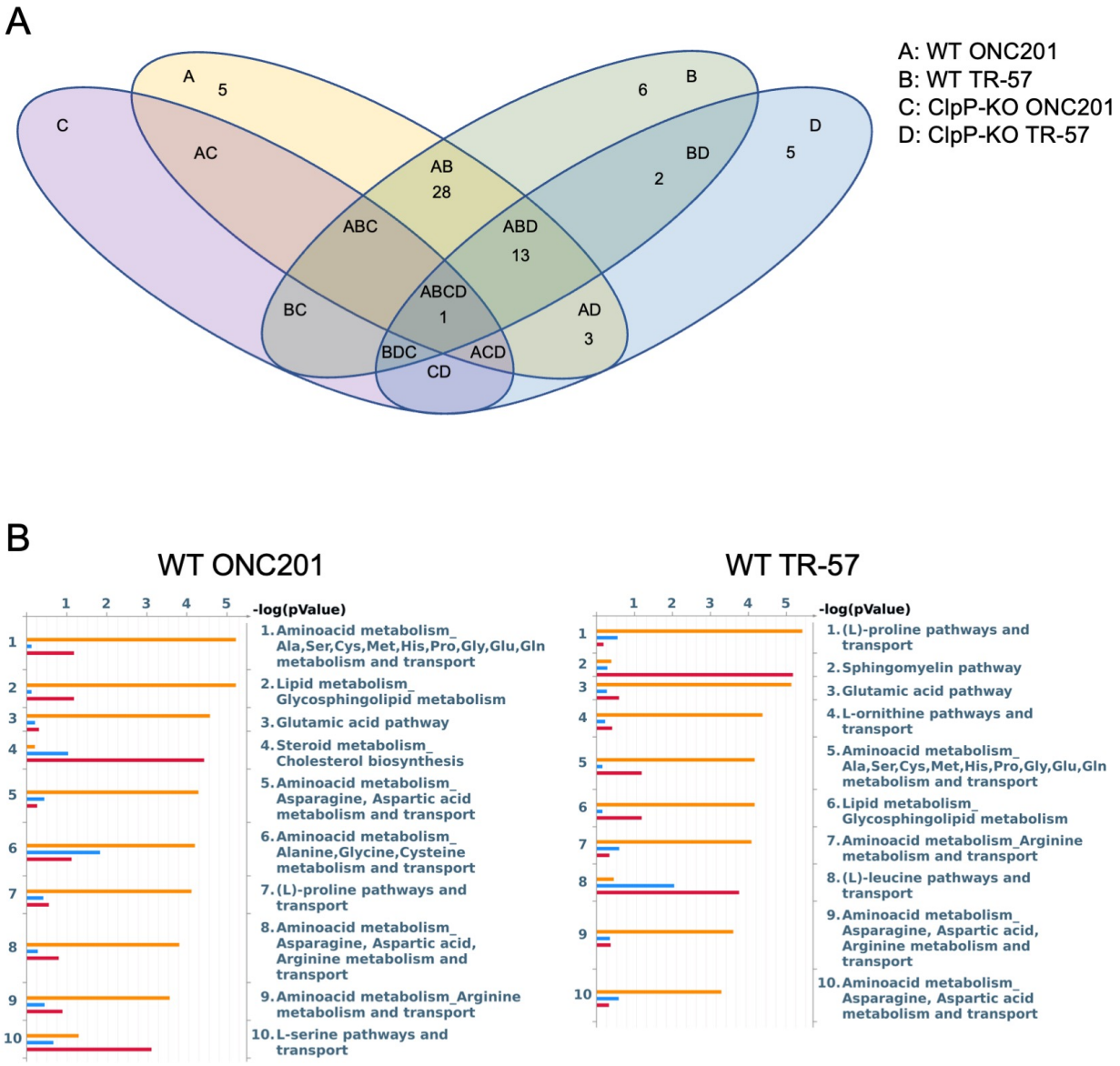

Figure S4.4 MetaCore endogenous metabolic network (EMN) analysis reveals multiple pathways affected in a ClpP-dependent manner at the proteomic, transcriptomic, and metabolomic level A) Venn diagram of group classification. Values represent number of pathways found in each group using data from Figures 2. Groups with no values listed had 0 significant EMNs. B) Top ten EMNs from MetaCore Endogenous Metabolic Network analysis using proteomic (blue), metabolomic (orange), and transcriptomic (red) datasets for WT SUM159 cells treated with 10 μM ONC201 or 150 nM TR-57.

Table S4.1. Triple-negative breast cancer cells show significant pathway perturbations across the proteomic, transcriptomic, and metabolomic level following ClpP activation. Representative list of top endogenous metabolic networks (EMN) identified using MetaCore for each group, as outlined in Figure S4.4. Number of pathway hits (identified EMN members) and p-value are listed for each dataset in the order they appear in the group name. MetaCore output for datasets including proteomics, transcriptomics, and metabolomics for ONC201 treated ClpP-KO SUM159 cells yielded no EMNs due to lack of significant changes. ClpP-KO SUM159 cells treated with TR-57 lacked significant changes in proteomics data. For these reasons, only transcriptomic and metabolomic data were used for EMN analysis for ClpP-KO cells.

Group	Endogenous Metabolic Networks	Hits	P value
A	*1-acyl-glycerol, 3-phosphocholine pathway*	6/88	1.08×10^{-1}
	Glycine pathway	10/90	1.14×10^{-1}
	1-oleoyl-sn-glycerol-3-phosphocholine pathway	8/121	3.56×10^{-1}
B	*Sphingomyelin pathway*	17/97	6.77×10^{-6}
	Carbohydrate metabolism, Glycolysis, Glucogenesis, and glucose transport	7/134	4.00×10^{-1}
	D-glucuronic acid pathway	10/77	9.53×10^{-3}
D	*L-carnitine pathway*	2/90	2.10×10^{-1}
	Vitamin, mediator, and cofactor metabolism: Nitric oxide biosynthesis and transport	6/51	1.50×10^{-3}
	L-lysine pathways and transport	5/107	2.99×10^{-2}
AB	*Amino acid metabolism: Ala, Ser, Cys, Met, His, Pro, Gly, Glu, Gln metabolism and transport*	26, 24/190	5.92×10^{-6}, 7.14×10^{-5}
	Glutamic acid pathway	14, 16/103	2.72×10^{-5}, 7.47×10^{-6}
	Tyrosine pathway	11, 14/90	2.69×10^{-3}, 7.57×10^{-4}
	Lipid Metabolism, Glycosphingolipid metabolism	26, 24/190	5.92×10^{-6}, 7.14×10^{-5}
	Amino acid metabolism: Asn, Asp metabolism and transport	15, 14/112	5.33×10^{-5}, 5.58×10^{-4}
	Amino acid metabolism: Ala, Gly, Cys metabolism and transport	22, 23/115	6.56×10^{-5}, 6.66×10^{-4}
	Steroid metabolism, Cholesterol biosynthesis	17, 14/88	3.84×10^{-5},1.05×10^{-3}
	Vitamin, mediator, and cofactor metabolism: CoA biosynthesis and transport	12, 7/81	3.77×10^{-2}, 1.59×10^{-1}
	Sucrose pathway	9, 11/90	2.92×10^{-1}, 1.44×10^{-2}
	(L)-leucine pathways and transport	13, 17/85	1.96×10^{-2}, 1.87×10^{-4}
ABD	*(L)-proline pathways and transport*	17, 16, 10/118	8.04×10^{-5},3.75×10^{-6},1.59×10^{-5}
	(S)-citrulline pathway	12, 10, 4/75	9.65×10^{-3}, 5.04×10^{-2},8.01×10^{-4}
	Carbohydrate metabolism: TCA and tricarboxylic acid transport	15, 13, 4/101	9.38×10^{-4},1.50×10^{-3}, 7.74×10^{-2}

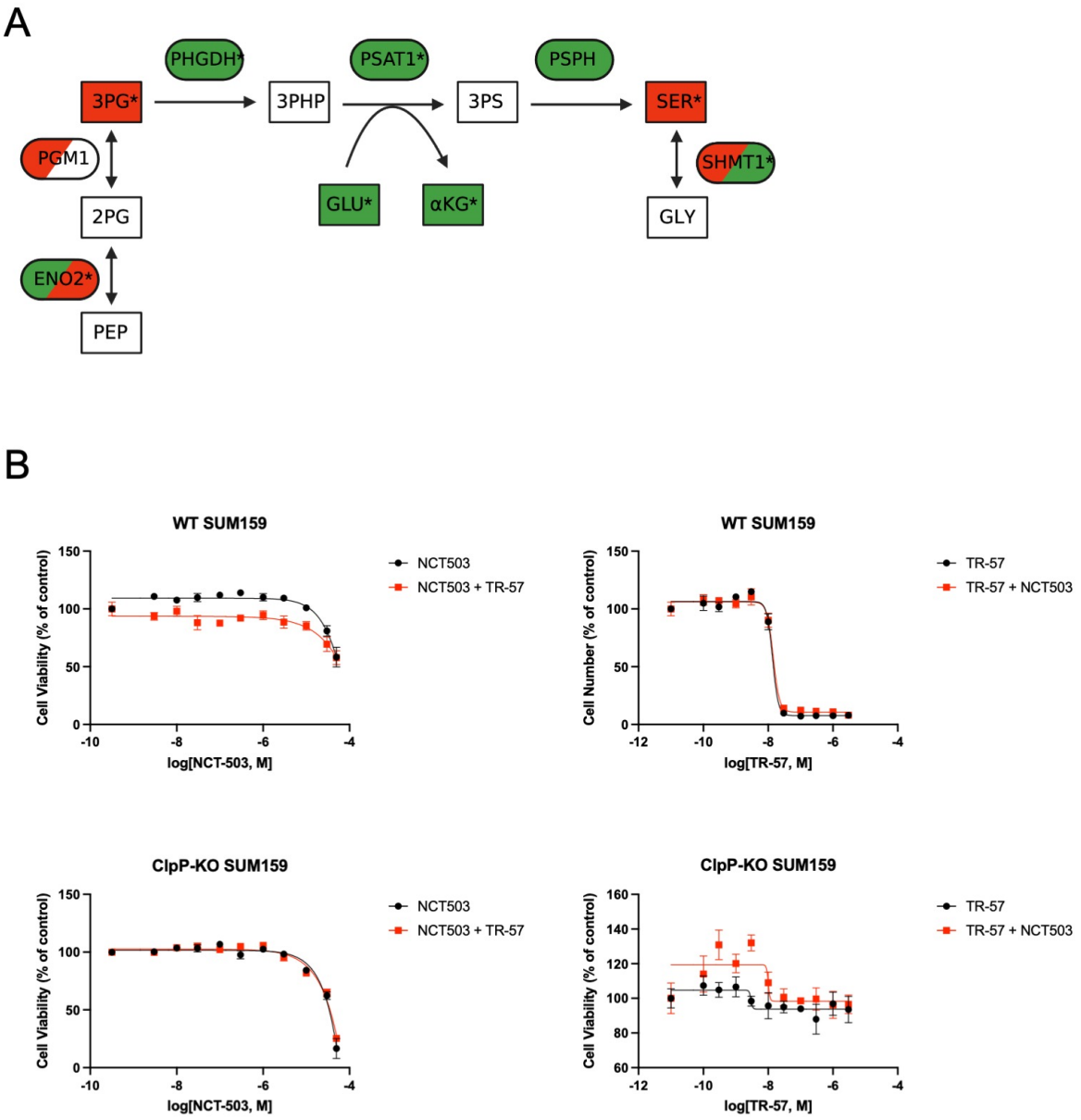

Figure S4.5 ClpP activation perturbs serine biosynthesis but does not synergize with the PHGDH inhibitor NCT503 in SUM159 cells. A) Schematic of serine biosynthesis. Rectangles represent metabolites and ovals represent enzymes. Directionality of change is indicated by color (downregulation (red), upregulation (green), not detected (white)) and * denotes significant change in at least one dataset. Dual-colored enzymes represent those with different directional changes in proteomics (left side) and transcriptomics (right side) while dual-colored metabolites indicate different directional changes in ONC201 treatment (left side) and TR-57 treatment (right side). PEP: phosphoenolpyruvate; 2PG: *2-phosphoglycerate*; 3PG: *3-phosphoglycerate*; 3PHP: *3-phosphohydroxypyruvate*; 3PS: *3-phosphoserine*; SER: *serine*; GLY: *glycine*; GLU: *glutamate*; αKG: *alpha-ketoglutarate*; ENO2: *enolase 2*; PGM1: *phosphoglycerate mutase 1*; PHDGH: *phosphoglycerate dehydrogenase*; PSAT1: *phosphoserine aminotransferase 1*; PSPH: *phosphoserine phosphatase*; SHMT1: *serine hydroxymethyltransferase 1*. B) Hoechst stain viability assays of SUM159 (WT and ClpP-KO) cells treated with indicated concentrations of the PHGDH inhibitor NCT503 in the presence or absence of 150 nM TR-57 (left) or indicated concentrations of TR-57 in the presence or absence of 10 μM NCT503 (right). Values represent mean ± SEM, representative of N=3 (left), N=2 (right).

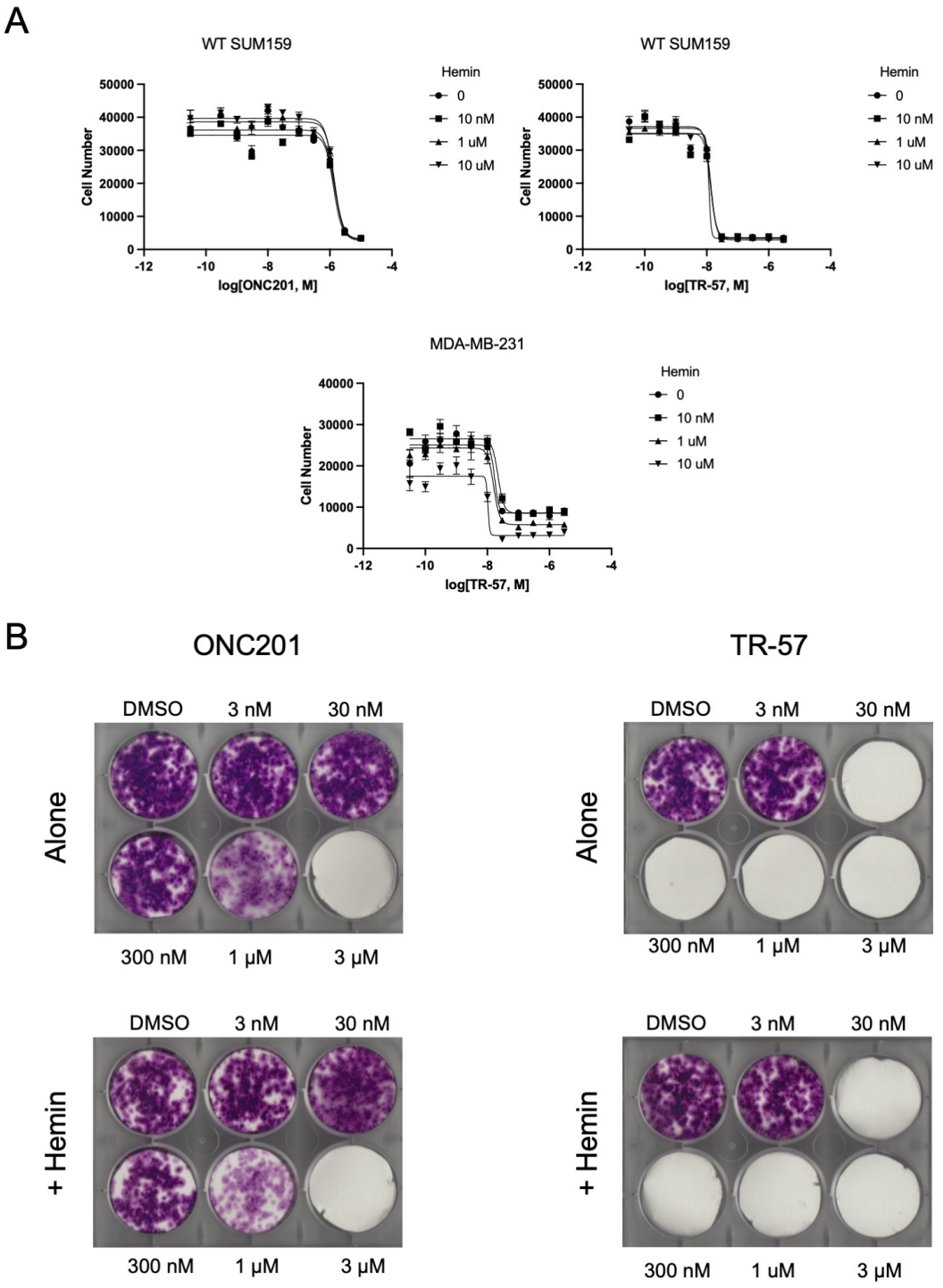

Figure S4.6 Hemin supplementation does not restore cell viability in TNBC cells following ONC201 or TR-57 treatment. A) 72-hour cell viability assays of WT SUM159 and MDA-MB-231 cells following treatment with ONC201 or TR-57 at indicated concentrations, co-treated with 0, 10 nM, 1 µM, or 10 µM hemin supplementation. B) Long-term crystal violet assays of SUM159 cells treated continuously with indicated concentrations of ONC201 or TR-57, with and without 2 µM hemin supplementation. All experiments are representative of N=2.

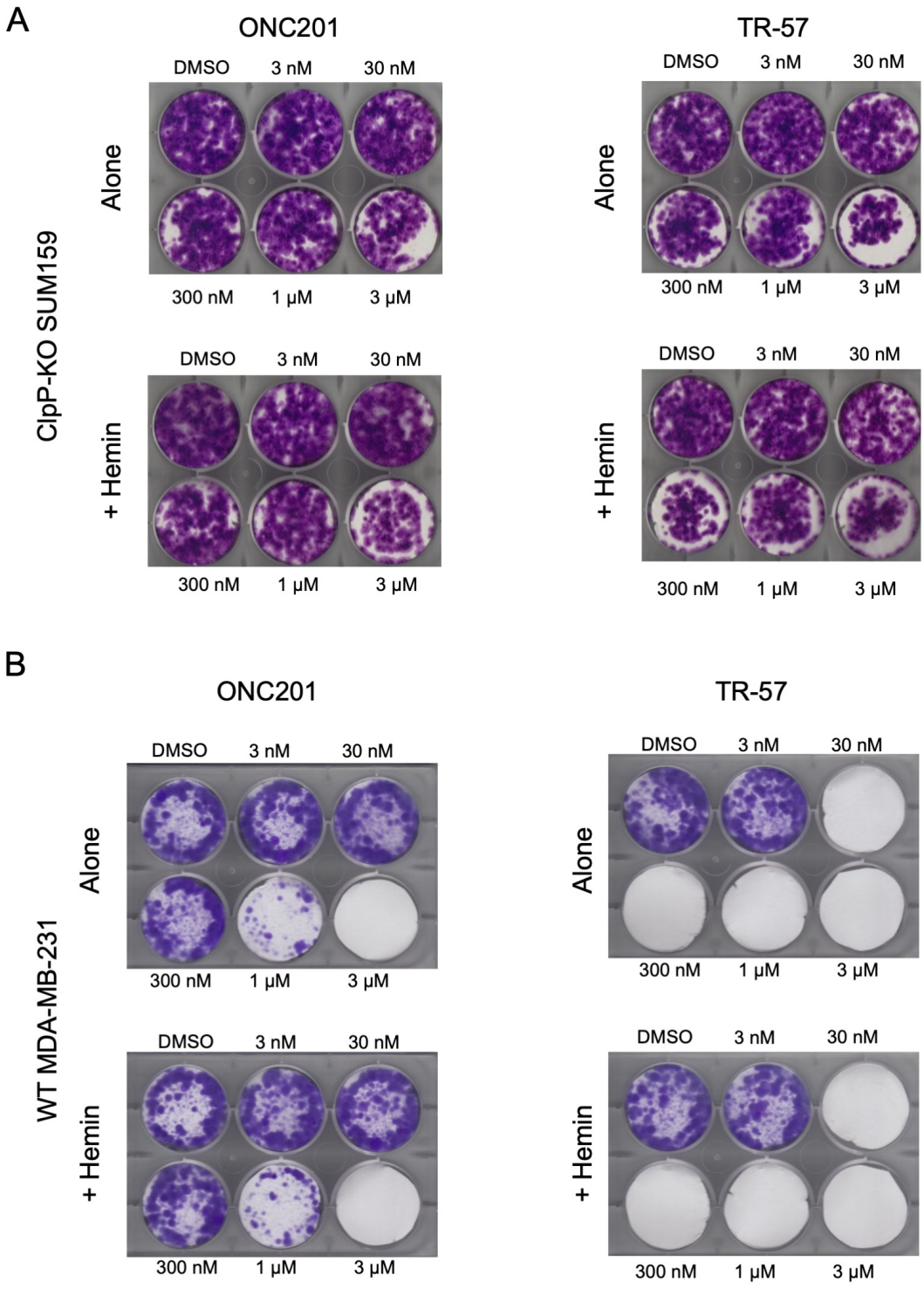

Figure S4.7 Hemin supplementation does not affect cell sensitivity to ClpP activators in ClpP-KO SUM159 cells or WT MDA-MB-231 cells. Long-term crystal violet assays of A) ClpP-KO SUM159 cells and B) WT MDA-MB-231 cells with and without 2 μM hemin supplementation. All experiments representative of N=2.

CHAPTER 5: FINAL DISUCSSION, CONCLUSIONS, AND FUTURE DIRECTIONS

5.1 Final Discussion and Conclusions

In Chapter 1, I provided an overview of the history of the discovery of ONC201 as a TRAIL inducer and the development of the TR compounds. When I joined the Graves Lab, the direct binding partner of ONC201 and the TR compounds had yet to be determined, but I demonstrated that TR compounds more potently inhibited cell growth than ONC201 (Fig. 2.1). As a lab that frequently implements proteomics methods in drug target identification, we performed whole-cell proteomics on SUM159 cells treated with ONC201 and TR-57 and found a drastic decline in mitochondrial proteins, leading us to believe that these drugs somehow affected mitochondrial function. The proteomics method of affinity chromatography utilizing kinase inhibitors bound to beads (Multiplexed Inhibitor Beads (MIBs))[144] to identify changes in kinase expression and/or activity following compound treatment was also utilized for ONC201 and TR-57 at 30 minutes, 3 hours, and 24 hours of treatment (Fig. S4.1D). While the kinase profiles of both compounds are similar, there was no significant pattern identified in these experiments, leading us to believe that ONC201 and TR compounds were not directly inhibiting a specific kinase. To determine the target of ONC201 and the TR compounds, we utilized TR-80 (because of its long linker region) bound to agarose beads in an affinity chromatography experiment, as described in Chapter 2. Cell lysates treated with and without free TR-80 were passed through the TR-80 columns and proteins bound to the columns were analyzed via silver stain and by mass spectrometry (Fig 2.2). Of particular interest in this experiment were proteins that bound to the column in the absence of free TR-80, but not in the presence of free TR-80, indicating that the TR-80 present in the lysate had bound to this protein and prevented its binding to the column. Given the significant downregulation of mitochondrial proteins identified from preliminary proteomics data, it was unsurprising that the protein identified as the target from this experiment was a mitochondrial protein. More surprisingly, this protein was the mitochondrial protease ClpP.

Proteases are involved in many biological processes, but it is estimated that only 5-10% of targets being pursued for drug development are proteases[173] . The majority of compounds showing efficacy against proteases are protease inhibitors (e.g., bortezomib, ACE inhibitors) due to the upregulation of these proteases and their increased activity contributing to disease progression[173–175]. However, utilization of protease activity has gained popularity in designing pro-biologics that require highly active proteases in the target tissues[175] and in development of antibacterial agents[33,34,36,41,105]. Because protease inhibition had previously been successful as an anticancer treatment (e.g., bortezomib)[173], we performed *in vitro* ClpP activity assays expecting to observe declined activity following ONC201 or TR compound treatment. In actuality, we observed that these compounds activate ClpP activity (Fig. 2.3, Fig. 3.2), similar to ClpP activating antibiotics[33,34,103,104]. Further analysis by our lab and others[29,40] demonstrated that ONC201 and TR compounds directly bind to ClpP (Fig. 3.2).

Despite being discovered during a TRAIL induction screen[11,60], ONC201 and its structural analogs (including TR compounds) are now widely accepted as ClpP activators. Our publication on the effects of ONC201 and TR compounds in triple-negative breast cancer (Chapter 2) was the first published study identifying ClpP as the direct binding partner of ONC201 and structural analogs. This study not only identified ClpP as the direct binding partner through affinity chromatography (Fig. 2.2), but also showed that siRNA-mediated knockdown of ClpP prevented the growth inhibitory effects of ONC201 and TR-57 in TNBC cells (Fig. 2.4). Activation of the ISR, specifically ATF4 induction, had previously been reported following ONC201 activation in acute myeloid leukemia (AML), mantle cell lymphoma (MCL) and colon cancer cell models[18,19]. Our study confirmed the induction of the ISR in TNBC cells following both ONC201 and TR-57 treatment and demonstrated that this induction is a ClpP-dependent response (Fig. 2.4, Fig. S2.3).

Shortly after our publication, Ishizawa et al. confirmed ClpP as the direct binding partner of ONC201, identified through a compound screen for ClpP activators[29]. Additionally, they showed that ONC201 binds the hydrophobic pocket between ClpP subunits, opening the axial pore of apo-ClpP and thus activating it in the absence of ClpX. Since, we have published an additional paper demonstrating that TR compounds are more potent ClpP activators and better TNBC cell growth inhibitors than ONC201 and other ONC201 structural analogs (e.g., ONC206) (Chapter 3). Having tested the growth inhibitory

capacity of many TR compounds, we have been able to perform structure-activity relationship (SAR) assessments to determine locations and substitutions in the TR compound scaffold that confer potency. Nanjing Gator Meditech determined lipophilic moiety substitution is preferred at the V- and Z- positions as opposed to the W-position on one benzyl ring[64] (as labeled in Fig. 2.1 and Fig. 3.1). Our studies have shown that substitution of a nitrile reside at the Y-position on the other benzyl ring is preferred (Fig. 2.1). Optimization of both benzyl rings results in compound TR-65, which demonstrated nM IC_{50} values (growth inhibition) and EC_{50} values (ClpP activation) compared to the μM values of ONC201 (Fig. 2.1, Fig. 2.3). The importance of the basic nitrogen located in the 3-piperidine moiety (X-position, Fig. 3.1) is demonstrated by μM IC_{50} values of TR-109 and TR-122, where both compounds have a carbon substituted in place of the basic nitrogen. TR-57 contains a modified acylguanidine moiety (Fig 2.1) and shows improved potency over ONC201. Additional modification resulting in the removal of the R group (Fig. 3.1), resulting in TR-107, yields an equipotent compound, indicating that the multi-ring imipridone structure is not necessary for potent ClpP activation. The understanding of the structure-activity relationships of these compounds is highly valuable for the development of the next generation of ClpP activators.

Following the identification of ClpP as the target of ONC201 and TR compounds, we generated ClpP-KO SUM159 cells using CRISPR-Cas9, and our colleagues in the Lipkowitz Lab at the NCI generated a ClpP-KO MDA-MB-231 cell line. We tested the growth inhibitory effects of TR compounds and other ONC201 scaffold analogs on both ClpP-KO cell lines and found no inhibitory effects, confirming that these compounds act through ClpP activation (Fig. 3.1). After previously observing loss of mitochondrial proteins (Chapter 2, proteomics data (unpublished)), we investigated whether the loss of these proteins is ClpP-dependent, as well as the time- and dose-dependence of protein loss (Fig. 3.3, Fig. S3.2). We found that the loss of these mitochondrial proteins was both time- and dose-dependent, with proteins lost at various timepoints, but doses near the observed IC_{50} was sufficient to result in protein loss in WT cells. Additionally, the loss of these proteins did not occur in ClpP-KO cells, confirming their loss to be ClpP-dependent. Previous studies reported a loss in mitochondrial function as assessed through oxygen consumption rate (OCR) in MDA-MB-231 cells[22]. We assessed the effects of TR-107 on both WT and ClpP-KO MDA-MB-231 cells (Fig. 3.4) and observed a dose-dependent decline in OCR in

WT cells, indicating TR-107 inhibits OXPHOS. In ClpP-KO cells, we did not observe this same decline, demonstrating OXPHOS decline is ClpP-dependent. Additionally, we observed a ClpP-dependent increase in extracellular acidification rate (ECAR), a measurement of glycolytic function. Consistent with an increase in glycolytic function, culturing cells in galactose containing media increased the potency of ONC201 and TR-107.

Due to the abundance of data that ClpP activators are causing loss of both mitochondrial proteins and metabolic function, my dissertation project focused on completing a multi-omic profile of ClpP activation in TNBC cells. This multi-omic analysis was intended to provide increased clarity on (1) the mechanism by which ClpP activation inhibits cell growth and (2) metabolic vulnerabilities (significant, ClpP-dependent perturbations) that could be further exploited for additive or synergistic co-treatments. From this data, we have demonstrated significant ClpP-dependent up- and downregulation at the proteomic, transcriptomic, and metabolomic level (Fig. 4.1). Proteomics data revealed significant, ClpP-dependent downregulation of mitochondrial proteins, including those previously identified (Chapters 2 and 3) as well as mitochondrial OXPHOS, transcription, and translational machinery. Transcriptomic data revealed significant upregulation of many ATF4-dependent genes, confirming previously observed ATF4 induction. Metabolomic data revealed significant, ClpP-dependent perturbations in many mitochondrial metabolites, indicating perturbations in additional mitochondrial metabolic pathways. Additionally, transcriptomics data did not consistently match significant proteomic downregulation, suggesting that the loss of many proteins following ClpP activation are due to degradation by ClpP.

Multi-omic analysis revealed significant changes to mitochondrial metabolic processes. Amino acid metabolism was significantly altered, consistent with the loss of amino acids at the metabolite level, as well as the upregulation of ATF4-dependent genes (e.g., ASNS, PSAT1), and the protein-level changes of many enzymes involved in amino acid synthesis. Multi-omic profiling identified significant, ClpP-dependent downregulation in the tricarboxylic acid (TCA) cycle, further confirming the previously observed loss of OCR (Fig. 3.4). Additional downregulated pathways identified by multi-omic profiling include pathways required for cell proliferation, including pyrimidine synthesis, and (S)-citrulline metabolism (Fig. 4.4). The identification of these pathways not only identifies potential metabolic vulnerabilities, but also demonstrates the multi-nodal activity of ClpP activation.

Anticancer treatments that target a single metabolic pathway in cancer (e.g., trametinib) have frequently found successful combination treatments with drugs that target a different regulatory node in the same pathway (e.g., dabrafenib) or other cellular processes (e.g., nivolumab, paclitaxel)[176,177], resulting in decreased tumor burden and reduced resistance development. Metabolic reprogramming has been known to play a role in cancer biology since the 1920s following the work of Warburg and the Cori's[45,178]. The Warburg effect, or the reliance of cancer cells on glycolysis to generate ATP, has been a common example of metabolic reprogramming in cancer since its identification. Since this discovery, many other metabolic pathways (including those reliant on glycolytic or TCA cycle intermediates) have been shown to be significantly altered in cancer cells, including heme metabolism[179], glutaminolysis[120], serine dependence[51], and (S)-citrulline metabolism[51], nucleotide biosynthesis[51,122]. Identification of which pathways cancer cells rely on for continued proliferation has since aided in identifying potential anticancer compounds[51,89,118,122].

I have often hypothesized many potential synergistic co-treatments for TR compounds in TNBC cells based off the -omics data that we have collected. Drugs targeting enzymes that are lost after ClpP activation have, as expected, had no additive or synergistic effects when combined with TR-57 treatment. I have also tried inhibitors that target enzymes and pathways upregulated following ClpP activation (e.g., autophagy, pAKT, LDH (unpublished data)), as the upregulation of these pathways likely indicates a dependence on these pathways to stay alive following TR-57 treatment. However, these treatments have also failed to demonstrate a synergistic effect when combined with ONC201 or TR-57. Interestingly, we do see a shift in IC_{50} when cells are cultured in galactose containing media (as opposed to glucose containing media), suggesting that an overall inability to generate OXPHOS-related intermediates further exacerbates the effects of ClpP activators (Fig. 3.4). Our collaborators in the Lipkowitz Lab at the National Cancer Institute have also performed compound screens to identify potential synergistic partners with ClpP activators and have largely found that many compounds, particularly those involved in apoptosis regulation, do not synergize with ClpP activators.

From the data gathered from our multi-omic analysis of ONC201 and TR-57, we hypothesized that ClpP activators upregulate the ATF4-dependent enzyme phosphoglycerate dehydrogenase (PHGDH), an enzyme essential for serine biosynthesis from glycolytic intermediates, and a pathway

cancer cells are often dependent on for increased proliferation[51]. L-serine levels were significantly declined following 24-hour ONC201 and TR-57 treatment, leading to the hypothesis that ClpP activation induced serine depletion, which in turn lead to ATF4-dependent upregulation of PHDGH in order to compensate for the loss of L-serine. Co-treatment with the PHGDH enzymatic inhibitor NCT-503 did not lead to significant additive or synergistic effects in SUM159 cells when treated in normal culture conditions. However, it is possible that these culture conditions were not ideal for this experiment, as L-serine is a nonessential amino acid that could be (1) synthesized from other pathways (e.g., from glycine via serine hydroxymethyltransferase (SHMT) or via one carbon metabolism) or (2) taken up from serine provided in cell culture media. Removing serine from cell culture media could potentially provide increased strain on treated cells that are dependent on serine biosynthesis for survival.

In conclusion, the data presented in this dissertation provides ample evidence that ONC201 and TR compounds bind to and activate ClpP, leading to ClpP's multi-nodal effect of perturbation of multiple mitochondrial metabolic pathways at the proteomic, transcriptomic, and metabolomic levels. Observed inhibition in cell growth is likely due to the multi-nodal nature of ClpP activation, due to the subsequent downregulation of many mitochondrial proteins and loss of mitochondrial metabolites requires for the biosynthesis of amino acids and nucleotides. This multi-omic data can be further utilized to identify additional metabolic perturbations whose exploitation may have additive or synergistic effects with TR compounds. Expansion of this multi-omics data to include additional timepoints or isotopic labeling of glucose (metabolomics) would result in the ability to monitor proteomic and transcriptomic changes over time and metabolic flux, leading to further elucidation of the mechanism of action of the TR compounds.

5.2 Future Directions

ClpP activators had previously been investigated as potential antibiotic compounds[33,34,103] and had shown anticancer activity in ClpP-overexpressing AML[37]. ONC201 and TR compounds have since shown anticancer activity in a wide variety of cancer models, including cell lines that do not over express ClpP. Through work with our colleagues at many universities, I know that these compounds are in continued testing in many cancer cell models. In the coming years, I hope the mechanism of action of these compounds is fully elucidated. The role of ClpP has been relatively well characterized in *C. elegans* and is known to play a role in ISR/UPR^{mt} activation[42,43]. Additionally, putative direct substrates of human

ClpP have been recently published[109] and the functions of human ClpP, canonical and following activation by TR compounds continues to be elucidated by the Graves Lab and our colleagues. Our collaborators at the University of Toronto have recently published an exciting paper on identification of novel N-termini generation following ClpP activation[40], which will undoubtedly advance the field's understanding of ClpP substrates. In the future, I envision the identification of direct ClpP substrates effected by pharmacological activation will allow for the identification of peptides released (if any) from mitochondria and whether these contribute to the mito-nuclear crosstalk that occurs following ONC201 and TR-57 treatment evidenced by ATF4/CHOP induction (Chapters 2 and 4). I believe that the proteomic, transcriptomic, and metabolomic data presented in this dissertation can be utilized and expanded upon to further elucidate this mechanism.

The multi-omic profiling presented herein (Chapter 4) to identify metabolic reprogramming and vulnerabilities can be utilized and expanded upon to (1) generate hypotheses regarding potential co-treatments for TR compound treatment and (2) identify additional metabolic vulnerabilities not discussed in this dissertation. This data demonstrated a significant downregulation in amino acid metabolism in treated cells, indicating a potential need to investigate the autophagic flux in these cells and whether drugs targeting autophagy have additive or synergistic effects when combined with TR compounds. Targeting the pentose phosphate pathway (PPP), which is an important source of ribose and NADPH[180], may also be a viable strategy for identifying synergy with ClpP agonism. In collaboration with Stanley Lipkowitz's Lab at NCI, we demonstrated loss of proline biosynthesis following ClpP activation, which relies on NADPH generation from the PPP[142]. This study also found significant downregulation (~50%) of NADPH levels following ClpP activation. Additionally, the PPP is required for nucleotide biosynthesis, which we found to be downregulated following ClpP activation (Chapter 4). We found *de novo* synthesis of pyrimidines, a process connected to mitochondria through dihydroorotate dehydrogenase[50], to be dysregulated following ClpP activation (Chapter 4). We observed the downregulation of multiple metabolites in this pathway, including dihydroorotate and aspartate (Fig. 4.4B). Pyrimidines can also be made through the pyrimidine salvage pathway[181], and inhibition of this pathway may serve as an additional potential co-treatment strategy. Nutritional interventions, or metabolic vulnerabilities that can be exploited by changes in diet or supplements, would be an interesting topic for the field to explore.

Nutritional interventions could be used *in vivo* to exploit metabolic vulnerabilities identified by multi-omic studies, by either (1) adding nutrients that improve response to drug (e.g., galactose (Chapter 3)) or (2) removing nutrients from the diet to improve response.

The loss of mtDNA following ONC201 or TR compound treatment has been observed in our studies (Chapter 3) and by Greer et al. both *in vitro* and *in vivo*. The mechanism by which mtDNA is lost following ClpP activation are not yet known, but may involve the observed loss of TFAM, a mitochondrial transcription factor also involved in mtDNA stability, TUFM, and other mitochondrial nucleoid proteins[182,183]. Additionally, ONC201 and TR compounds result in a significant loss in mitochondrial transcription and translational machinery (e.g., POLRMT, MRPL12) observed in the proteomics data (Chapter 4) and there is a significant observed loss of overall protein synthesis (Chapter 2). Expansion of this research to investigate the role of ClpP in regulation of mitochondrial transcription and translation will help to elucidate (1) ClpP substrates, (2) the mechanism by which these compounds induce mtDNA loss, and (3) whether this mtDNA loss plays a role in the significant observed loss of OXPHOS function.

Loss of TFAM and mtDNA, and the subsequent release of mtDNA into the cytosol, may also be implicated in the activation of the cGAS-STING pathway[184–186], an immune response known to promote *de novo* interferon and cytokine synthesis and initiate an anti-viral response[187]. We have observed that TR compounds induce an immune response in TNBC cells measured by significantly increased mRNA of multiple cytokines, including the IRF3-dependent IL-12. Additionally, we have observed increased IL-10 levels in cell culture media following TR-57 treatment (Aponte-Collazo et al., In Submission). Clinical data of patients with refractory solid tumors demonstrate increased immune cell recruitment to tumor sites[188], and we have preliminary data indicating that treated TNBC cells can recruit natural killer (NK) cells, further supporting the hypothesis that these cells induce an immune response. Additionally, cell surface expression of the ER protein calreticulin has demonstrated to increase cell clearance by macrophages[189,190], and we have observed an increased level of calreticulin on the cell surface of TR-57 treated TNBC cells using cell surface proteomics methods(unpublished). Further investigation into whether these compounds (1) induce mtDNA release into the cytosol and subsequently (2) activate the cGAS-STING pathway and (3) whether this activation is involved in the observed induction of cytokines, as well as (4) the role of calreticulin cell surface expression affects immune recruitment would have a

significant impact on the field's understanding of how these compounds regulate an immune response/immune recruitment to treated cells.

My greatest hope for the TR compounds is to enter clinical trial for difficult to treat cancers based, in part, on the *in vitro* and *in vivo* evidence collected during my graduate career. ONC201 has previously been used in multiple clinical trials, and published data indicates ONC201 is well tolerated with minimal side effects while being administered on a low-frequency schedule[16,59]. Our studies presented in Chapters 2 and 3 of this dissertation have demonstrated that TR compounds act similarly to and more potently than ONC201 *in vitro*. Further, xenograft models of TNBC have shown TR-107 is well tolerated while also reducing tumor burden in mice, suggesting it is a potential candidate for clinical trials of TNBC, and potentially other aggressive cancers, moving forward. I also hope that the identification of metabolic vulnerabilities from data presented in Chapter 4 and any data collected in the future can provide potential therapeutic combination treatments with other anticancer agents or nutritional interventions.

REFERENCES

1. Vital Statistics Reports N. National Vital Statistics Reports Volume 70, Number 8 July 26, 2016 Deaths: Final Data 2019. 2021;70(8).

2. American Cancer Society. *Cancer Facts and Figures 2022*. Atlanta: American Cancer Society; 2022.

3. Waks AG, Winer EP. Breast Cancer Treatment: A Review. *JAMA - J Am Med Assoc*. 2019;321(3):288-300. doi:10.1001/jama.2018.19323

4. American Cancer Society. *Breast Cancer Fact And Figures 2022-2024.* Atlanta: American Cancer Society; 2022.

5. Debela DT, Muzazu SGY, Heraro KD, Ndalama MT, Mesele BW, Haile DC, Kitui SK, Manyazewal T. New approaches and procedures for cancer treatment: Current perspectives. *SAGE Open Med*. 2021;9:1-10. doi:10.1177/20503121211034366

6. Walko CM, Lindley C. Capecitabine: A review. *Clin Ther*. 2005;27(1):23-44. doi:10.1016/j.clinthera.2005.01.005

7. Padma VV. An overview of targeted cancer therapy. *Biomed*. 2015;5(4):1-6. doi:10.7603/s40681-015-0019-4

8. Giang I, Boland EL, Poon GMK. Prodrug applications for targeted cancer therapy. *AAPS J*. 2014;16(5):899-913. doi:10.1208/s12248-014-9638-z

9. Sharma P. Biology and Management of Patients With Triple-Negative Breast Cancer. *Oncologist*. 2016:1050-1062. doi: 10.1634/theoncologist.2016-0067

10. Greer YE, Lipkowitz S. TIC10 / ONC201 : a bend in the road to clinical development. *Oncoscience*. 2015;2(2):2-3. doi:10.18632/oncoscience.133

11. Allen JE, Krigsfeld G, Mayes PA, Patel L, Dicker DT, Patel AS, Dolloff NG, Messaris E, Scata KA, Zhou J, Wu GS, El-Deiry WS. Dual Inactivation of Akt and ERK by TIC10 Signals Foxo3a Nuclear Translocation, TRAIL Gene Induction, and Potent Antitumor Effects. *Sci Transl Med*. 2013;5(171):1-23. doi:10.1126/scitranslmed.3004828.Dual

12. Ashkenazi A, Dixit VM. Death receptors: Signaling and modulation. *Science (80-)*. 1998;281(5381):1305-1308. doi:10.1126/science.281.5381.1305

13. Jacob NT, Lockner JW, Kravchenko V V., Janda KD. Pharmacophore reassignment for induction of the immunosurveillance cytokine TRAIL. *Angew Chemie - Int Ed*. 2014;53(26):6628-6631. doi:10.1002/anie.201402133

14. Allen JE, Kline CLB, Prabhu V V., Wagner J, Ishizawa J, Madhukar N, Lev A, Baumeister M, Zhou L, Lulla A, Stogniew M, Schalop L, Benes C, Kaufman HL, Pottorf RS, Nallaganchu BR, Olson GL, Al-Mulla F, Duvic M et al. Discovery and clinical introduction of first-in-class imipridone ONC201. *Oncotarget*. 2016;7(45). doi:10.18632/oncotarget.11814

15. Arrillaga-Romany I, Chi AS, Allen JE, Oster W, Wen PY, Batchelor TT. A phase 2 study of the first imipridone ONC 201, a selective DRD 2 antagonist for oncology, administered every three weeks in recurrent glioblastoma. *Oncotarget*. 2017;8(45):79298-79304. doi:10.18632/oncotarget.17837

16. Ralff MD, Lulla AR, Wagner J, El-Deiry WS. ONC201: a new treatment option being tested clinically for recurrent glioblastoma. *Transl Cancer Res*. 2017;6(Suppl 7).

doi:10.21037/tcr.2017.10.03.ONC201

17. Kline CLB, Ralff MD, Lulla AR, Wagner JM, Abbosh PH, Dicker DT, Allen JE, El-Deiry WS. Role of Dopamine Receptors in the Anticancer Activity of ONC201. *Neoplasia (United States)*. 2018;20(1):80-91. doi:10.1016/j.neo.2017.10.002

18. Kline CLB, Heuvel APJ Van Den, Allen JE, Prabhu V V, Dicker DT, El-deiry WS. ONC201 kills solid tumor cells by triggering an integrated stress response dependent on ATF4 activation by specific eIF2α kinases. *Sci Signal*. 2016;9(415):1-11. doi:10.1126/scisignal.aac4374

19. Ishizawa J, Kojima K, Chachad D, Ruvolo P, Ruvolo V, Jacamo RO, Borthakur G, Mu H, Zeng Z, Tabe Y, Allen JE, Wang Z, Ma W, Lee HC, Orlowski R, Sarbassov DD, Lorenzi PL, Huang X, Neelapu SS et al. ATF4 induction through an atypical integrated stress response to ONC201 triggers p53-independent apoptosis in hematological malignancies. *Sci Signal*. 2016;9(415):1-15. doi:10.1126/scisignal.aac4380

20. Pakos-zebrucka K, Koryga I, Mnich K, Ljujic M, Samali A, Gorman AM, Pakos-zebrucka K. The Integrated Stress Response. *EMBO Rep*. 2016;17(10):1374-1395. doi: 10.15252/embr.201642195

21. Anderson NS, Haynes CM. Folding the Mitochondrial UPR into the Integrated Stress Response. *Trends Cell Biol*. 2020;30(6):428-439. doi:10.1016/j.tcb.2020.03.001

22. Greer YE, Porat-Shliom N, Nagashima K, Stuelten C, Crooks D, Koparde VN, Gilbert SF, Islam C, Ubaldini A, Ji Y, Gattinoni L, Soheilian F, Wang X, Hafner M, Shetty J, Tran B, Jailwala P, Cam M, Lang M et al. ONC201 kills breast cancer cells in vitro by targeting mitochondria. *Oncotarget*. 2018;9(26):18454-18479. doi:10.18632/oncotarget.24862

23. Vijay V, Morrow S, Rahman A, Carlsen L, Louie A, Oster W, El-Deiry WS. ONC201 and imipridones : Anti-cancer compounds with clinical efficacy. *Neoplasia*. 2020;22(12):725-744. doi:10.1016/j.neo.2020.09.005

24. Anderson PM, Trucco MM, Tarapore RS, Zahler S, Thomas S, Gortz J, Mian O, Stoignew M, Prabhu V, Morrow S, Allen JE. Phase II Study of ONC201 in Neuroendocrine Tumors including Pheochromocytoma-Paraganglioma and Desmoplastic Small Round Cell Tumor. *Clin Cancer Res*. 2022;28(9):1773-1782. doi:10.1158/1078-0432.CCR-21-4030

25. Ekhator C, Rak R, Tadipatri R, Fonkem E, Grewal J. A Single-Center Experience of Dopamine Antagonist ONC201 for Recurrent Histone H3 Lysine 27-to-Methionine (H3K27M)-Mutant Glioblastoma in Adults. *Cureus*. 2022;14(8). doi:10.7759/cureus.28175

26. Arrillaga-Romany I, Odia Y, Prabhu V V., Tarapore RS, Merdinger K, Stogniew M, Oster W, Allen JE, Mehta M, Batchelor TT, Wen PY. Biological activity of weekly ONC201 in adult recurrent glioblastoma patients. *Neuro Oncol*. 2020;22(1):94-102. doi:10.1093/NEUONC/NOZ164

27. Wagner J, Leah Kline C, Zhou L, Campbell KS, MacFarlane AW, Olszanski AJ, Cai KQ, Hensley HH, Ross EA, Ralff MD, Zloza A, Chesson CB, Newman JH, Kaufman H, Bertino J, Stein M, El-Deiry WS. Dose intensification of TRAIL-inducing ONC201 inhibits metastasis and promotes intratumoral NK cell recruitment. *J Clin Invest*. 2018;128(6):2325-2338. doi:10.1172/JCI96711

28. Graves PR, Aponte-Collazo LJ, Fennell EM, Graves AC, Hale AE, Dicheva N, Herring LE, Gilbert TS, East MP, McDonald IM, Lockett MP, Ashamalla H, Moorman NJ, Karanewsky DS, Iwanowicz EJ, Holmuhamedov E, Graves LM. Mitochondrial Protease ClpP is a Target for the Anticancer Compounds ONC201 and Related Analogs. *ACS Chem Biol*. 2019;14(5):1020-1029. doi:10.1021/acschembio.9b00222

29. Ishizawa J, Zarabi SF, Davis RE, Halgas O, Nii T, Jitkova Y, Zhao R, St-Germain J, Hesse LE,

Egan G, Ruvolo VR, Barghout SH, Nishida Y, Hurren R, Ma W, Gronda M, Link T, Wong K, Mabanglo M et al. Mitochondrial ClpP-Mediated Proteolysis Induces Selective Cancer Cell Lethality Article Mitochondrial ClpP-Mediated Proteolysis Induces Selective Cancer Cell Lethality. *Cancer Cell*. 2019;35(5):721-737.e9. doi:10.1016/j.ccell.2019.03.014

30. Seraphim T V., Houry WA. AAA+ proteins. *Curr Biol*. 2020;30(6):R251-R257. doi:10.1016/j.cub.2020.01.044

31. Mabanglo MF, Houry WA. Recent structural insights into the mechanism of ClpP protease regulation by AAA+ chaperones and small molecules. *J Biol Chem*. 2022;298(5):101781. doi:10.1016/j.jbc.2022.101781

32. Alexopoulos JA, Guarné A, Ortega J. ClpP: A structurally dynamic protease regulated by AAA+ proteins. *J Struct Biol*. 2012;179(2):202-210. doi:10.1016/j.jsb.2012.05.003

33. Wong KS, Mabanglo MF, Seraphim T V., Mollica A, Mao YQ, Rizzolo K, Leung E, Moutaoufik MT, Hoell L, Phanse S, Goodreid J, Barbosa LRS, Ramos CHI, Babu M, Mennella V, Batey RA, Schimmer AD, Houry WA. Acyldepsipeptide Analogs Dysregulate Human Mitochondrial ClpP Protease Activity and Cause Apoptotic Cell Death. *Cell Chem Biol*. 2018;25(8):1017-1030.e9. doi:10.1016/j.chembiol.2018.05.014

34. Binepal G, Mabanglo MF, Goodreid JD, Leung E, Barghash MM, Wong KS, Lin F, Cossette M, Bansagi J, Song B, Balasco Serrão VH, Pai EF, Batey RA, Gray-Owen SD, Houry WA. Development of Antibiotics That Dysregulate the Neisserial ClpP Protease. *ACS Infect Dis*. 2020;6(12):3224-3236. doi:10.1021/acsinfecdis.0c00599

35. Stahl M, Korotkov VS, Balogh D, Kick LM, Gersch M, Pahl A, Kielkowski P, Richter K, Schneider S, Sieber SA. Selective Activation of Human Caseinolytic Protease P (ClpP). *Angew Chemie - Int Ed*. 2018;57(44):14602-14607. doi:10.1002/anie.201808189

36. Brötz-Oesterhelt H, Vorbach A. Reprogramming of the Caseinolytic Protease by ADEP Antibiotics: Molecular Mechanism, Cellular Consequences, Therapeutic Potential. *Front Mol Biosci*. 2021;8(May):1-19. doi:10.3389/fmolb.2021.690902

37. Nouri K, Feng Y, Schimmer AD. Mitochondrial ClpP serine protease-biological function and emerging target for cancer therapy. *Cell Death Dis*. 2020;11(10). doi:10.1038/s41419-020-03062-z

38. Seo JH, Rivadeneira DB, Caino MC, Chae YC, Speicher DW, Tang HY, Vaira V, Bosari S, Palleschi A, Rampini P, Kossenkov A V., Languino LR, Altieri DC. The Mitochondrial Unfoldase-Peptidase Complex ClpXP Controls Bioenergetics Stress and Metastasis. *PLoS Biol*. 2016;14(7):1-21. doi:10.1371/journal.pbio.1002507

39. Mabanglo MF, Bhandari V, Houry WA. Substrates and interactors of the ClpP protease in the mitochondria. *Curr Opin Chem Biol*. 2022;66:102078. doi:10.1016/j.cbpa.2021.07.003

40. Mabanglo MF, Wong KS, Barghash MM, Leung E, Chuang SHW, Ardalan A, Majaesic EM, Wong CJ, Zhang S, Lang H, Karanewsky DS, Iwanowicz AA, Graves LM, Iwanowicz EJ, Gingras AC, Houry WA. Potent ClpP agonists with anticancer properties bind with improved structural complementarity and alter the mitochondrial N-terminome. *Structure*. 2023;31(2):185-200.e10. doi:10.1016/j.str.2022.12.002

41. Wong KS, Houry WA. Chemical Modulation of Human Mitochondrial ClpP: Potential Application in Cancer Therapeutics. *ACS Chem Biol*. 2019;(14):2349-2360. doi:10.1021/acschembio.9b00347

42. Haynes CM, Petrova K, Benedetti C, Yang Y, Ron D. ClpP Mediates Activation of a Mitochondrial Unfolded Protein Response in C . elegans. *Dev Cell*. 2007;(October):467-480.

doi:10.1016/j.devcel.2007.07.016

43. Qureshi MA, Haynes CM, Pellegrino MW. The mitochondrial unfolded protein response: Signaling from the powerhouse. *J Biol Chem*. 2017;292(33):13500-13506. doi:10.1074/jbc.R117.791061

44. Cole A, Wang Z, Coyaud E, Voisin V, Gronda M, Mattson R, Hurren R, Babovic S, Maclean N, Restall I, Wang X, Jeyaraju D V, Sukhai MA, Prabha S, Ramakrishnan A, Leung E, Qia YH, Zhang N, Kevin R et al. Inhibition of the mitochondrial protease, ClpP, as a therapeutic strategy for human acute myeloid leukemia. *Cancer Cell*. 2015;27(6):864-876. doi:10.1016/j.ccell.2015.05.004.Inhibition

45. Warburg O. On the Origin of Cancer Cells. *Science (80-)*. 1956;123. doi: 10.1126/science.123.3191.309.

46. Warburg O, Wind F, Negelein E. The Metabolism of Tumors in the Body. *J Gen Physiol*. 1927;8(6):519-530. doi:10.1085/jgp.8.6.519

47. Ward PS, Thompson CB. Metabolic Reprogramming: A Cancer Hallmark Even Warburg Did Not Anticipate. *Cancer Cell*. 2012;21(3):297-308. doi:10.1016/j.ccr.2012.02.014

48. DeBerardinis RJ, Lum JJ, Hatzivassiliou G, Thompson CB. The Biology of Cancer: Metabolic Reprogramming Fuels Cell Growth and Proliferation. *Cell Metab*. 2008;7(1):11-20. doi:10.1016/j.cmet.2007.10.002

49. Lunt SY, Vander Heiden MG. Aerobic glycolysis: Meeting the metabolic requirements of cell proliferation. *Annu Rev Cell Dev Biol*. 2011;27:441-464. doi:10.1146/annurev-cellbio-092910-154237

50. Huang M, Graves LM. De novo synthesis of pyrimidine nucleotides; emerging interfaces with signal transduction pathways. *Cell Mol Life Sci*. 2003;60(2):321-336. doi:10.1007/s000180300027

51. Luengo A, Gui DY, Vander Heiden MG. Targeting Metabolism for Cancer Therapy. *Cell Chem Biol*. 2017;24(9):1161-1180. doi:10.1016/j.chembiol.2017.08.028.

52. McKeehan WL. Glycolysis, glutaminolysis, and cell proliferation. *Cell Biol Int Rep*. 1982;6(7):635-650. doi: 10.1016/0309-1651(82)90125-4

53. Yang C, Ko B, Hensley CT, Jiang L, Wasti AT, Rutter J, Merritt ME, Deberardinis RJ. Glutamine oxidation maintains the TCA cycle and cell survival during impaired mitochondrial pyruvate transport. *Mol Cell*. 2015;56(3):414-424. doi:10.1016/j.molcel.2014.09.025.Glutamine

54. Vander Heiden MG, Deberardinis RJ. Understanding the intersections between metabolism and cancer biology. *Cell*. 2017;168(4):657-669. doi:10.1016/j.cell.2016.12.039

55. Hasin Y, Seldin M, Lusis A. Multi-omics approaches to disease. *Genome Biol*. 2017;18(1):1-15. doi:10.1186/s13059-017-1215-1

56. Fiehn O. Metabolomics - The link between genotypes and phenotypes. *Plant Mol Biol*. 2002;48(1-2):155-171. doi:10.1023/A:1013713905833

57. Krassowski M, Das V, Sahu SK, Misra BB. State of the Field in Multi-Omics Research: From Computational Needs to Data Mining and Sharing. *Front Genet*. 2020;11(December):1-17. doi:10.3389/fgene.2020.610798

58. Ebrahim A, Brunk E, Tan J, O'Brien EJ, Kim D, Szubin R, Lerman JA, Lechner A, Sastry A, Bordbar A, Feist AM, Palsson BO. Multi-omic data integration enables discovery of hidden

biological regularities. *Nat Commun*. 2016;7:1-9. doi:10.1038/ncomms13091

59. Stein MN, Bertino JR, Kaufman HL, Mayer T, Moss R, Silk A, Chan N, Malhotra J, Rodriguez L, Aisner J, Aiken RD, Haffty BG, DiPaola RS, Saunders T, Zloza A, Damare S, Beckett Y, Yu B, Najmi S et al. First-in-human clinical trial of oral ONC201 in patients with refractory solid tumors. *Clin Cancer Res*. 2017;23(15):4163-4169. doi:10.1158/1078-0432.CCR-16-2658

60. Allen JE, Krigsfeld G, Patel L, Mayes PA, Dicker DT, Wu GS, El-Deiry WS. Identification of TRAIL-inducing compounds highlights small molecule ONC201/TIC10 as a unique anti-cancer agent that activates the TRAIL pathway. *Mol Cancer*. 2015;14(1):1-10. doi:10.1186/s12943-015-0346-9

61. Wagner J, Kline CL, Ralff MD, Lev A, Lulla A, Zhou L, Olson GL, Nallaganchu BR, Benes CH, Allen JE, Prabhu V V., Stogniew M, Oster W, El-Deiry WS. Preclinical evaluation of the imipridone family, analogs of clinical stage anti-cancer small molecule ONC201, reveals potent anti-cancer effects of ONC212. *Cell Cycle*. 2017;16(19):1790-1799. doi:10.1080/15384101.2017.1325046

62. Feng Y, Zhou J, Li Z, Jiang Y, Zhou Y. Small Molecular TRAIL Inducer ONC201 Induces Death in Lung Cancer Cells: A Preclinical Study. *PLoS One*. 2016;11(9):1-13. doi:10.1371/journal.pone.0162133

63. Ma Z, Gao G, Fang K, Sun H. Development of Novel Anticancer Agents with a Scaffold of Tetrahydropyrido[4,3- d]pyrimidine-2,4-dione. *ACS Med Chem Lett*. 2019;10(2):191-195. doi:10.1021/acsmedchemlett.8b00531

64. Xu R, Liu Y. Imidazo-Pyrimidone Compounds, And Preparation Method and Application Thereof. 2016.

65. Iwanowicz EJ. Protein Kinase Regulators. 2018:92.

66. Iwanowicz EJ. Protein Kinase Regulators. 2018:81.

67. Quirós PM, Prado MA, Zamboni N, D'Amico D, Williams RW, Finley D, Gygi SP, Auwerx J. Multi-omics analysis identifies ATF4 as a key regulator of the mitochondrial stress response in mammals. *J Cell Biol*. 2017;216(7):2027-2045. doi:10.1083/jcb.201702058

68. Ni X, Zhang X, Hu CH, Langridge T, Tarapore RS, Allen JE, Oster W, Duvic M. ONC201 selectively induces apoptosis in cutaneous T-cell lymphoma cells via activating pro-apoptotic integrated stress response and inactivating JAK/STAT and NF-κB pathways. *Oncotarget*. 2017;8(37):61761-61776. doi:10.18632/oncotarget.18688

69. Lenarcic EM, Ziehr B, De Leon G, Mitchell D, Moorman NJ. Differential Role for Host Translation Factors in Host and Viral Protein Synthesis during Human Cytomegalovirus Infection. *J Virol*. 2014;88(3):1473-1483. doi:10.1128/jvi.02321-13

70. Ziehr B, Vincent HA, Moorman NJ. Human Cytomegalovirus pTRS1 and pIRS1 Antagonize Protein Kinase R To Facilitate Virus Replication. *J Virol*. 2016;90(8):3839-3848. doi:10.1128/jvi.02714-15

71. Baker TA, Sauer RT. ClpXP , an ATP-powered unfolding and protein-degradation machine. *BBA - Mol Cell Res*. 2012;1823(1):15-28. doi:10.1016/j.bbamcr.2011.06.007

72. Maurizi MR, Clark WP, Kim SH, Gottesman S. Clp P Represents a Unique Family of Serine Proteases. *J Biol Chem*. 1990;265(21):12546-12552. doi:10.1016/s0021-9258(19)38379-6

73. Kang SG, Ortega J, Singh SK, Wang N, Huang NN, Steven AC, Maurizi MR. Functional proteolytic complexes of the human mitochondrial ATP-dependent protease, hClpXP. *J Biol Chem*.

2002;277(23):21095-21102. doi:10.1074/jbc.M201642200

74. Matsushima Y, Kaguni LS. Matrix proteases in mitochondrial DNA function. *Biochim Biophys Acta*. 2012;23(1):1-7. doi:10.1016/j.bbagrm.2011.11.008.Matrix

75. Leung E, Datti A, Cossette M, Goodreid J, McCaw SE, Mah M, Nakhamchik A, Ogata K, El Bakkouri M, Cheng YQ, Wodak SJ, Eger BT, Pai EF, Liu J, Gray-Owen S, Batey RA, Houry WA. Activators of Cylindrical Proteases as Antimicrobials: Identification and Development of Small Molecule Activators of ClpP Protease. *Chem Biol*. 2011;18(9):1167-1178. doi:10.1016/j.chembiol.2011.07.023

76. Bhandari V, Wong KS, Zhou JL, Mabanglo MF, Batey RA, Houry WA. The Role of ClpP Protease in Bacterial Pathogenesis and Human Diseases. *ACS Chem Biol*. 2018;13(6):1413-1425. doi:10.1021/acschembio.8b00124

77. Kang SG, Dimitrova MN, Ortega J, Ginsburg A, Maurizi MR. Human Mitochondrial ClpP is a Stable Heptamer That Assembles into a Tetradecamer in the Presence of ClpX. *J Biol Chem*. 2005;280(42):35424-35432. doi:10.1074/jbc.M507240200

78. Li DHS, Ching YS, Gloyd M, Joseph E, Ghrilando R, Wright GD, Cheng Y-Q, Maurizi MR, Guarné A, Ortega J. Acyldepsipeptide Antibiotics Induces the Formation of a Structured Axial Channel in ClpP: a Model for the ClpX/ClpA Bound State of ClpP. *Chem Biol*. 2010;17(9):959-969. doi:10.1016/j.chembiol.2010.07.008.Acyldepsipeptide

79. Okumu DO, East MP, Levine M, Herring LE, Zhang R, Gilbert TSK, Litchfield DW, Zhang Y, Graves LM. BIRC6 mediates imatinib resistance independently of Mcl-1. *PLoS One*. 2017;12(5):1-26. doi:10.1371/journal.pone.0177871

80. Shevchenko A, Wilm M, Vorm O, Mann M. Mass spectrometric Sequencing of Proteins from Silver-Stained Polyacrylamide Gels. *Anal Chem*. 1996;68(5):850-858. doi:10.1021/ac950914h

81. Thompson MW, Maurizi MR. Activity and Specificity of Escherichia coli ClpAP Protease in Cleaving Model Peptide Substrates. *J Biol Chem*. 1994;269(27):18201-18208. doi:10.1016/s0021-9258(17)32435-3

82. Thompson MW, Singh SK, Maurizi MR. Processive Degradation of Proteins by the ATP-dependent Clp Protease from Escherichia coli: Requirement for the Multiple Array of Active Sites in ClpP but not ATP Hydrolysis. *J Biol Chem*. 1994;269(27):18209-18215. doi:10.1016/s0021-9258(17)32436-5

83. Woo KM, Chung WJ, Ha DB, Goldberg AL, Chung CH. Protease Ti from Escherichia coli Requires ATP Hydrolysis for Protein Breakdown but Not for Hydrolysis of Small Peptides. *J Biol Chem*. 1989;264(4):2088-2091. doi:10.1016/s0021-9258(18)94145-1

84. Maurizi MR, Thompson MW, Singh SK, Kim SH. Endopeptidase Clp: ATP-Dependent Clp Protease from Escherichia coli. *Methods Enzymol*. 1994;244(C):314-331. doi:10.1016/0076-6879(94)44025-5

85. Costa RLB, Gradishar WJ. Triple-negative breast cancer: Current practice and future directions. *J Oncol Pract*. 2017;13(5):301-303. doi:10.1200/JOP.2017.023333

86. Dent R, Trudeau M, Pritchard KI, Hanna WM, Kahn HK, Sawka CA, Lickley LA, Rawlinson E, Sun P, Narod SA. Triple-negative breast cancer: Clinical features and patterns of recurrence. *Clin Cancer Res*. 2007;13(15):4429-4434. doi:10.1158/1078-0432.CCR-06-3045

87. Qiu D, Zhang G, Yan X, Xiao X, Ma X, Lin S, Wu J, Li X, Wang W, Liu J, Ma Y, Ma M. Prospects

of Immunotherapy for Triple-Negative Breast Cancer. *Front Oncol*. 2022;11(January):1-10. doi:10.3389/fonc.2021.797092

88. Villacampa G, Tolosa P, Salvador F, Sanchez-Bayona R, Villanueva L, Dienstmann R, Ciruelos E, Pascual T. Addition of immune checkpoint inhibitors to chemotherapy versus chemotherapy alone in first-line metastatic triple-negative breast cancer: A systematic review and meta-analysis. *Cancer Treat Rev*. 2022;104. doi:10.1016/j.ctrv.2022.102352

89. Martínez-Reyes I, Chandel NS. Cancer metabolism: looking forward. *Nat Rev Cancer*. 2021;21(10):669-680. doi:10.1038/s41568-021-00378-6

90. Sun X, Wang M, Wang M, Yu X, Guo J, Sun T, Li X, Yao L, Dong H, Xu Y. Metabolic Reprogramming in Triple-Negative Breast Cancer. *Front Oncol*. 2020;10(March). doi:10.3389/fonc.2020.00428

91. Martinez-Outschoorn UE, Peiris-Pagés M, Pestell RG, Sotgia F, Lisanti MP. Cancer metabolism: A therapeutic perspective. *Nat Rev Clin Oncol*. 2017;14(1):11-31. doi:10.1038/nrclinonc.2016.60

92. Xu Y, Xue D, Bankhead A, Neamati N. Why All the Fuss about Oxidative Phosphorylation (OXPHOS)? *J Med Chem*. 2020;63(23):14276-14307. doi:10.1021/acs.jmedchem.0c01013

93. Bonekamp NA, Peter B, Hillen HS, Felser A, Bergbrede T, Choidas A, Horn M, Unger A, Di Lucrezia R, Atanassov I, Li X, Koch U, Menninger S, Boros J, Habenberger P, Giavalisco P, Cramer P, Denzel MS, Nussbaumer P et al. Small-molecule inhibitors of human mitochondrial DNA transcription. *Nature*. 2020;588(7839):712-716. doi:10.1038/s41586-020-03048-z

94. Gao L, Xu Z, Huang Z, Tang Y, Yang D, Huang J, He L, Liu M, Chen Z, Teng Y. CPI-613 rewires lipid metabolism to enhance pancreatic cancer apoptosis via the AMPK-ACC signaling. *J Exp Clin Cancer Res*. 2020;39(1):1-12. doi:10.1186/s13046-020-01579-x

95. Ellinghaus P, Heisler I, Unterschemmann K, Haerter M, Beck H, Greschat S, Ehrmann A, Summer H, Flamme I, Oehme F, Thierauch K, Michels M, Hess-Stumpp H, Ziegelbauer K. BAY 87-2243, a highly potent and selective inhibitor of hypoxia-induced gene activation has antitumor activities by inhibition of mitochondrial complex I. *Cancer Med*. 2013;2(5):611-624. doi:10.1002/cam4.112

96. Molina JR, Sun Y, Protopopova M, Gera S, Bandi M, Bristow C, McAfoos T, Morlacchi P, Ackroyd J, Agip ANA, Al-Atrash G, Asara J, Bardenhagen J, Carrillo CC, Carroll C, Chang E, Ciurea S, Cross JB, Czako B et al. An inhibitor of oxidative phosphorylation exploits cancer vulnerability. *Nat Med*. 2018;24(7):1036-1046. doi:10.1038/s41591-018-0052-4

97. Tsuji A, Akao T, Masuya T, Murai M, Miyoshi H. IACS-010759, a potent inhibitor of glycolysis-deficient hypoxic tumor cells, inhibits mitochondrial respiratory complex I through a unique mechanism. *J Biol Chem*. 2020;295(21):7481-7491. doi:10.1074/jbc.RA120.013366

98. Talekar MK, Allen JE, El-Deiry WS. ONC201 (TIC10) Induces TRAIL and Cell Death in Pediatric Lymphoma. *Cell Cycle*. 2013;122:1671. doi: 10.1080/15384101.2015.1054086

99. Ralff MD, Kline CLB, Küçükkase OC, Wagner J, Lim B, Dicker DT, Prabhu V V., Oster W, El-Deiry WS. ONC201 demonstrates antitumor effects in both triple-negative and non–triple-negative breast cancers through TRAIL-dependent and TRAIL-independent mechanisms. *Mol Cancer Ther*. 2017;16(7):1290-1298. doi:10.1158/1535-7163.MCT-17-0121

100. Talekar MK, Allen JE, Dicker DT, El-Deiry WS. ONC201 induces cell death in pediatric non-Hodgkin's lymphoma cells. *Cell Cycle*. 2015;14(15):2422-2428. doi:10.1080/15384101.2015.1054086

101. Wagner J, Kline CL, Zhou L, Khazak V, El-Deiry WS. Anti-tumor effects of ONC201 in combination with VEGF-inhibitors significantly impacts colorectal cancer growth and survival in vivo through complementary non-overlapping mechanisms. *J Exp Clin Cancer Res*. 2018;37(1):11. doi:10.1186/s13046-018-0671-0

102. Jacques S, van der Sloot AM, Huard CC, Coulombe-Huntington J, Tsao S, Tollis S, Bertomeu T, Culp EJ, Pallant D, Cook MA, Bonneil E, Thibault P, Wright GD, Tyers M. Imipridone Anticancer Compounds Ectopically Activate Antibiotic Development. *Genetics*. 2020;214(April):1103-1120. doi:10.1534/genetics.119.302851

103. Ye F, Li J, Yang CG. The development of small-molecule modulators for ClpP protease activity. *Mol Biosyst*. 2017;13(1):23-31. doi:10.1039/C6MB00644B

104. Gersch M, Famulla K, Dahmen M, Göbl C, Malik I, Richter K, Korotkov VS, Sass P, Rübsamen-Schaeff H, Madl T, Brötz-Oesterhelt H, Sieber SA. AAA+ chaperones and acyldepsipeptides activate the ClpP protease via conformational control. *Nat Commun*. 2015;6. doi:10.1038/ncomms7320

105. Kirstein J, Hoffmann A, Lilie H, Schmidt R, Ru H, Mogk A. The antibiotic ADEP reprogrammes ClpP , switching it from a regulated to an uncontrolled protease. *EMBO Mol Med*. 2009;1:37-49. doi: 10.1002/emmm.200900002

106. Kafina MD, Paw BH. Intracellular iron and heme trafficking and metabolism in developing erythroblasts. *Metallomics*. 2017;9(9):1193-1203. doi:10.1039/c7mt00103g

107. Kardon JR, Yien YY, Huston NC, Branco DS, Hildick-Smith GJ, Rhee KY, Paw BH, Baker TA. Mitochondrial ClpX activates a key enzyme for heme biozynthesis and erythropoiesis. *Cell*. 2015;161(4):858-867. doi:10.1016/j.cell.2015.04.017

108. Rondelli CM, Perfetto M, Danoff A, Bergonia H, Gillis S, O'Neill L, Jackson L, Nicolas G, Puy H, West R, Phillips JD, Yien YY. The ubiquitous mitochondrial protein unfoldase CLPX regulates erythroid heme synthesis by control of iron utilization and heme synthesis enzyme activation and turnover. *J Biol Chem*. 2021;297(2):100972. doi:10.1016/j.jbc.2021.100972

109. Fischer F, Langer JD, Osiewacz HD. Identification of potential mitochondrial CLPXP protease interactors and substrates suggests its central role in energy metabolism. *Sci Rep*. 2015;5:1-13. doi:10.1038/srep18375

110. Knuppertz L, Osiewacz HD. Autophagy compensates impaired energy metabolism in CLPXP-deficient Podospora anserina strains and extends healthspan. *Aging Cell*. 2017;16(4):704-715. doi:10.1111/acel.12600

111. Luo J, Zeng B, Tao C, Lu M, Ren G. ClpP regulates breast cancer cell proliferation, invasion and apoptosis by modulating the Src/PI3K/Akt signaling pathway. *PeerJ*. 2020;2020(3):1-19. doi:10.7717/peerj.8754

112. Green JE, Shibata M, Yoshidome K, Liu M, Jorcyk C, Anver MR, Wigginton J, Wiltrout R, Shibata E, Kaczmarczyk S, Wang W, Liu Z, Calvo A, Couldrey C. The C3 (1)/ SV40 T-antigen transgenic mouse model of mammary cancer : ductal epithelial cell targeting with multistage progression to carcinoma. Oncogene. 2000;3:1020-1027. doi: 10.1038/sj.onc.1203280

113. Ferrarini I, Louie A, Zhou L, El-Deiry WS. ONC212 is a novel mitocan acting synergistically with glycolysis inhibition in pancreatic cancer. *Mol Cancer Ther*. 2021;20(9):1572-1583. doi:10.1158/1535-7163.MCT-20-0962

114. Meng Q, Li BX, Xiao X. Toward developing chemical modulators of Hsp60 as potential

therapeutics. *Front Mol Biosci*. 2018;5(APR):1-11. doi:10.3389/fmolb.2018.00035

115. Free RB, Cuoco CA, Xie B, Namkung Y, Prabhu V V., Willette BKA, Day MM, Sanchez-Soto M, Lane JR, Laporte SA, Shi L, Allen JE, Sibley DR. Pharmacological characterization of the imipridone anticancer drug onc201 reveals a negative allosteric mechanism of action at the d2 dopamine receptors. *Mol Pharmacol*. 2021;100(4):372-387. doi:10.1124/molpharm.121.000336

116. Faubert B, Solmonson A, DeBerardinis RJ. Metabolic reprogramming and cancer progression. *Science (80-)*. 2020;368(6487). doi:10.1126/science.aaw5473

117. Hanahan D, Weinberg RA. Hallmarks of cancer: The next generation. *Cell*. 2011;144(5):646-674. doi:10.1016/j.cell.2011.02.013

118. Phan LM, Yeung SCJ, Lee MH. Cancer metabolic reprogramming: importance, main features, and potentials for precise targeted anti-cancer therapies. *Cancer Biol Med*. 2014;11(1):1-19. doi:10.7497/j.issn.2095-3941.2014.01.001

119. Ashton TM, Gillies McKenna W, Kunz-Schughart LA, Higgins GS. Oxidative phosphorylation as an emerging target in cancer therapy. *Clin Cancer Res*. 2018;24(11):2482-2490. doi:10.1158/1078-0432.CCR-17-3070

120. Jang M, Kim SS, Lee J. Cancer cell metabolism: Implications for therapeutic targets. *Exp Mol Med*. 2013;45(10):1-8. doi:10.1038/emm.2013.85

121. Kim S. Cancer Energy Metabolism : Shutting Power off Cancer Factory. *Biomol Ther*. 2018;26(1):39-44. doi:10.4062/biomolther.2017.184

122. Vasan K, Werner M, Chandel NS. Mitochondrial Metabolism as a Target for Cancer Therapy. *Cell Metab*. 2020;32(3):341-352. doi:10.1016/j.cmet.2020.06.019

123. Weinberg SE, Chandel NS. Targeting mitochondria metabolism for cancer therapy. *Nat CHem Biol*. 2015;11(1):9-15. doi:10.1038/nchembio.1712

124. Chae YK, Arya A, Malecek M, Shin DS, Carneiro B, Chandra S, Kaplan J, Kalyan A, Altman JK, Platanias L, Giles F. Repurposing metformin for cancer treatment : current clinical studies. *Oncotarget*. 2016;7(26). doi:10.18632/oncotarget.8194

125. Stuani L, Sabatier M, Saland E, Cognet G, Poupin N, Bosc C, Castelli FA, Gales L, Turtoi E, Montersino C, Farge T, Boet E, Broin N, Larrue C, Baran N, Cisse MY, Conti M, Loric S, Kaoma T et al. Mitochondrial metabolism supports resistance to IDH mutant inhibitors in acute myeloid leukemia. *J Exp Med*. 2021;218(5). doi:10.1084/jem.20200924

126. Jhaveri A V., Zhou L, Ralff MD, Lee YS, Navaraj A, Carneiro BA, Safran H, Prabhu V V., Ross EA, Lee S, El-Deiry WS. Combination of ONC201 and TLY012 induces selective, synergistic apoptosis in vitro and significantly delays PDAC xenograft growth in vivo. *Cancer Biol Ther*. 2021;22(10-12):607-618. doi:10.1080/15384047.2021.1976567

127. Ralff MD, Jhaveri A, Ray JE, Zhou L, Lev A, Campbell KS, Dicker DT, Ross EA, El-Deiry WS. TRAIL receptor agonists convert the response of breast cancer cells to ONC201 from anti-proliferative to apoptotic. *Oncotarget*. 2020;11(42):3753-3769. doi:10.18632/oncotarget.27773

128. Ray JE, Ralff MD, Jhaveri A, Zhou L, Dicker DT, Ross EA, El-Deiry WS. Antitumorigenic effect of combination treatment with ONC201 and TRAIL in endometrial cancer in vitro and in vivo. *Cancer Biol Ther*. 2021;22(10-12):554-563. doi:10.1080/15384047.2021.1977067

129. Chang W, Lin C, Liguori N, Honeyman JN, Lorant A. Molecular Targets for Novel Therapeutics in

Pediatric Fusion-Positive Non-CNS Solid Tumors. *Front Pharmacol*. 2022;12(January):1-16. doi:10.3389/fphar.2021.747895

130. Boettcher M, Tian R, Blau JA, Markegard E, Wagner RT, Wu D, Mo X, Biton A, Zaitlen N, Fu H, McCormick F, Kampmann M, McManus MT. Dual gene activation and knockout screen reveals directional dependencies in genetic networks. *Nat Biotechnol*. 2018;36(2):170-178. doi:10.1038/nbt.4062

131. Iwanowicz EJ. Use of Caseinolytic Protease P Function as a Biomarker of Drug Response to Imipridone-like Agents. 2020.

132. Banker MJ, Clark TH, Williams JA. Development and validation of a 96-well equilibrium dialysis apparatus for measuring plasma protein binding. *J Pharm Sci*. 2003;92(5):967-974. doi:10.1002/jps.10332

133. Zu XL, Guppy M. Cancer metabolism: Facts, fantasy, and fiction. *Biochem Biophys Res Commun*. 2004;313(3):459-465. doi:10.1016/j.bbrc.2003.11.136

134. Darzynkiewicz Z, Staiano-Coico L, Melamed MR. Increased mitochondrial uptake of rhodamine 123 during lymphocyte stimulation. *Proc Natl Acad Sci U S A*. 1981;78(4 II):2383-2387. doi:10.1073/pnas.78.4.2383

135. Fogal V, Richardson AD, Karmali PP, Scheffler IE, Smith JW, Ruoslahti E. Mitochondrial p32 Protein Is a Critical Regulator of Tumor Metabolism via Maintenance of Oxidative Phosphorylation. *Mol Cell Biol*. 2010;30(6):1303-1318. doi:10.1128/mcb.01101-09

136. Deberardinis RJ, Chandel NS. Fundamentals of cancer metabolism. *Sci Adv*. 2016;2(5). doi:10.1126/sciadv.1600200

137. Fennell EMJ, Aponte-Collazo LJ, Wynn JD, Drizyte- Miller K, Leung E, Greer YE, Graves PR, Iwanowicz AA, Ashamalla H, Holmuhamedov E, Lang H, Karanewsky DS, Der CJ, Houry WA, Lipkowitz S, Iwanowicz EJ, Graves LM. Characterization of TR-107, a novel chemical activator of the human mitochondrial protease ClpP. *Pharmacol Res Perspect*. 2022;(May):1-17. doi:10.1002/prp2.993

138. Melber A, Haynes CM. UPR mt regulation and output : a stress response mediated by mitochondrial-nuclear communication. *Nat Publ Gr*. 2018;28(3):281-295. doi:10.1038/cr.2018.16

139. Kumar R, Chaudhary AK, Woytash J, Inigo JR, Gokhale AA, Bshara W, Attwood K, Wang J, Spernyak JA, Rath E, Yadav N, Haller D, Goodrich DW, Tang DG, Chandra D. A mitochondrial unfolded protein response inhibitor suppresses prostate cancer growth in mice via HSP60. *J Clin Invest*. 2022;132(13):34-36. doi:10.1172/JCI149906

140. Wang P, Zhang T, Wang X, Xiao H, Li H, Zhou LL, Yang T, Wei B, Zhu Z, Zhou L, Yang S, Lu X, Zhang Y, Huang Y, Gan J, Yang CG. Aberrant human ClpP activation disturbs mitochondrial proteome homeostasis to suppress pancreatic ductal adenocarcinoma. *Cell Chem Biol*. 2022;29(9):1396-1408.e8. doi:10.1016/j.chembiol.2022.07.002

141. Nguyen TTT, Shang E, Schiffgens S, Torrini C, Shu C, Akman HO, Prabhu V V., Allen JE, Westhoff MA, Karpel-Massler G, Siegelin MD. *Induction of Synthetic Lethality by Activation of Mitochondrial ClpP and Inhibition of HDAC1/2 in Glioblastoma*. Vol 28.; 2022. doi:10.1158/1078-0432.CCR-21-2857

142. Greer YE, Hernandez L, Fennell EMJ, Kundu M, Voeller D, Chari R, Gilbert SF, Gilbert TSK, Ratnayake S, Tang B, Hafner M, Chen Q, Meerzaman D, Iwanowicz EJ, Annunziata CM, Graves LM, Lipkowitz S. Mitochondrial Matrix Protease ClpP Agonists Inhibit Cancer Stem Cell Function in

Breast Cancer Cells by Disrupting Mitochondrial Homeostasis. Cancer Res Commun. 2022. doi: 10.1158/2767-9764.CRC-22-0142

143. Yılmaz S, Ayati M, Schlatzer D, Çiçek AE, Chance MR, Koyutürk M. Robust inference of kinase activity using functional networks. *Nat Commun*. 2021;12(1):1-12. doi:10.1038/s41467-021-21211-6

144. Cooper MJ, Cox NJ, Zimmerman EI, Dewar BJ, Duncan JS, Whittle MC, Nguyen TA, Jones LS, Ghose Roy S, Smalley DM, Kuan PF, Richards KL, Christopherson RI, Jin J, Frye S V., Johnson GL, Baldwin AS, Graves LM. Application of Multiplexed Kinase Inhibitor Beads to Study Kinome Adaptations in Drug-Resistant Leukemia. *PLoS One*. 2013;8(6). doi:10.1371/journal.pone.0066755

145. Losman JA, Kaelin WG. What a difference a hydroxyl makes: Mutant IDH, (R)-2-hydroxyglutarate, and cancer. *Genes Dev*. 2013;27(8):836-852. doi:10.1101/gad.217406.113

146. Wang S, Chen XA, Hu J, Jiang J, Li Y, Chan- KY, Gu Y, Chen G, Thomas C, Pugh BF, Wang Y. ATF4 Gene Network Mediates Cellular Response to the Anticancer PAD Inhibitor YW3-56 in Triple Negative Breast Cancer Cells. *Mol Cancer Ther*. 2015;14(4):877-888. doi:10.1158/1535-7163.MCT-14-1093-T.ATF4

147. Su N, Kilberg MS. C/EBP homology protein (CHOP) interacts with activating transcription factor 4 (ATF4) and negatively regulates the stress-dependent induction of the asparagine synthetase gene. *J Biol Chem*. 2008;283(50):35106-35117. doi:10.1074/jbc.M806874200

148. Pacold ME, Brimacombe KR, Ham Chan S, Rohde JM, Lewis CA, JYM Swier L, Possemato R, Chen WW, Sullivan LB, Fiske BP, Won Cho S, Freinkman E, Birsoy K, Abu-Remaileh M, Shaul YD, Min Liu C, Zhou M, Jung Koh M, Chung H et al. A PHGDH inhibitor reveals coordination of serine synthesis and 1-carbon unit fate HHS Public Access Author manuscript. *Nat Chem Biol*. 2016;12(6):452-458. doi:10.1038/nchembio.2070.A

149. Kubota Y, Nomura K, Katoh Y, Yamashita R, Kaneko K, Furuyama K. Novel mechanisms for heme-dependent degradation of ALAS1 protein as a component of negative feedback regulation of heme biosynthesis. *J Biol Chem*. 2016;291(39):20516-20529. doi:10.1074/jbc.M116.719161

150. Yien YY, Perfetto M. Regulation of Heme Synthesis by Mitochondrial Homeostasis Proteins. *Front Cell Dev Biol*. 2022;10(June):1-16. doi:10.3389/fcell.2022.895521

151. Tian Q, Li T, Hou W, Zheng J, Schrum LW, Bonkovsky HL. Lon peptidase 1 (LONP1)-dependent breakdown of mitochondrial 5-aminolevulinic acid synthase protein by heme in human liver cells. *J Biol Chem*. 2011;286(30):26424-26430. doi:10.1074/jbc.M110.215772

152. Lee J, Pandey AK, Venkatesh S, Thilagavathi J, Honda T, Singh K, Suzuki CK. Inhibition of mitochondrial LonP1 protease by allosteric blockade of ATP binding and hydrolysis via CDDO and its derivatives. *J Biol Chem*. 2022;298(3):101719. doi:10.1016/j.jbc.2022.101719

153. Csizmadia V, Hales P, Tsu C, Ma J, Chen J, Shah P, Fleming P, Senn JJ, Kadambi VJ, Dick L, Wolenski FS. Proteasome inhibitors bortezomib and carfilzomib used for the treatment of multiple myeloma do not inhibit the serine protease HtrA2/Omi. *Toxicol Res (Camb)*. 2016;5(6):1619-1628. doi:10.1039/c6tx00220j

154. Lu B, Lee J, Nie X, Li M, Morozov YI, Venkatesh S, Bogenhagen DF, Temiakov D, Suzuki CK. Phosphorylation of human TFAM in mitochodnria impairs DNA binding and promotes degradation by the AAA+ Lon protease. *Mol Cell*. 2013;49(1):121-132. doi:10.1016/j.molcel.2012.10.023.Phosphorylation

155. Cheng CT, Qi Y, Wang YC, Chi KK, Chung Y, Ouyang C, Chen YR, Oh ME, Sheng X, Tang Y, Liu YR, Lin HH, Kuo CY, Schones D, Vidal CM, Chu JCY, Wang HJ, Chen YH, Miller KM et al. Arginine starvation kills tumor cells through aspartate exhaustion and mitochondrial dysfunction. *Commun Biol*. 2018;1(1):1-15. doi:10.1038/s42003-018-0178-4

156. Qiu F, Chen Y-R, Liu X, Chi C-Y, Shen L-J, Xu J, Guar S, Forman HJ, Zhang H, Zheng S, Yen Y, Huang J, Kung H-J, Ann DK. Arginine Starvation Impairs Mitochondrial Respiratory Function in ASS1-Deficient Breast Cancer Cells. *Sci Signal*. 2015;7(319). doi:10.1126/scisignal.2004761

157. Chen CL, Hsu SC, Ann DK, Yen Y, Kung HJ. Arginine signaling and cancer metabolism. *Cancers (Basel)*. 2021;13(14):1-29. doi:10.3390/cancers13143541

158. Yuan X, Kho D, Xu J, Gajan A, Wu K, Wu GS. ONC201 activates ER stress to inhibit the growth of triplenegative breast cancer cells. *Oncotarget*. 2017;8(13):21626-21638. doi:10.18632/oncotarget.15451

159. Whitman JC, Paw BH, Chung J. The role of ClpX in erythropoietic protoporphyria. *Hematol Transfus Cell Ther*. 2018;40(2):182-188. doi:10.1016/j.htct.2018.03.001

160. Lin KH, Xie A, Rutter JC, Ahn Y, Lloyd-cowden JM, Nichols AG, Soderquist RS, Koves TR, Muoio D, Nancie J, Lamba J, Pardee TS, Mccall CM, Rizzieri DA, Wood KC. Systematic dissection of the metabolic-apoptotis interface in AML reveals heme biosynthesis to be a regulator of drug sensitivity. *Cell Metab*. 2020;29(5):1217-1231. doi:10.1016/j.cmet.2019.01.011.Systematic

161. Mertins P, Tang LC, Krug K, Clark DJ, Gritsenko MA, Chen L, Clauser KR, Clauss TR, Shah P, Gillette MA, Petyuk VA, Thomas SN, Mani DR, Mundt F, Moore RJ, Hu Y, Zhao R, Schnaubelt M, Keshishian H et al. Reproducible workflow for multiplexed deep-scale proteome and phosphoproteome analysis of tumor tissues by liquid chromatography-mass spectrometry. *Nat Protoc*. 2018;13(7):1632-1661. doi:10.1038/s41596-018-0006-9

162. Wass AB, Krishna BA, Herring LE, Gilbert TSK, Nukui M, Groves IJ, Dooley AL, Kulp KH, Matthews SM, Rotroff DM, Graves LM, O'Connor CM. Cytomegalovirus US28 regulates cellular EphA2 to maintain viral latency. *Sci Adv*. 2022;8(43):eadd1168. doi:10.1126/sciadv.add1168

163. McAlister GC, Nusinow DP, Jedrychowski MP, Wühr M, Huttlin EL, Erickson BK, Rad R, Haas W, Gygi SP. MultiNotch MS3 enables accurate, sensitive, and multiplexed detection of differential expression across cancer cell line proteomes. *Anal Chem*. 2014;86(14):7150-7158. doi:10.1021/ac502040v

164. Klann K, Bojkova D, Tascher G, Ciesek S, Münch C, Cinatl J. Growth Factor Receptor Signaling Inhibition Prevents SARS-CoV-2 Replication. *Mol Cell*. 2020;80(1):164-174.e4. doi:10.1016/j.molcel.2020.08.006

165. Hogrebe A, Von Stechow L, Bekker-Jensen DB, Weinert BT, Kelstrup CD, Olsen J V. Benchmarking common quantification strategies for large-scale phosphoproteomics. *Nat Commun*. 2018;9(1). doi:10.1038/s41467-018-03309-6

166. Winnike JH, Stewart DA, Pathmasiri WW, McRitchie SL, Sumner SJ. Stable Isotope-Resolved Metabolomic Differences between Hormone-Responsive and Triple-Negative Breast Cancer Cell Lines. *Int J Breast Cancer*. 2018;2018. doi:10.1155/2018/2063540

167. Stewart DA, Winnike JH, McRitchie SL, Clark RF, Pathmasiri WW, Sumner SJ. Metabolomics Analysis of Hormone-Responsive and Triple-Negative Breast Cancer Cell Responses to Paclitaxel Identify Key Metabolic Differences. *J Proteome Res*. 2016;15(9):3225-3240. doi:10.1021/acs.jproteome.6b00430

168. Välikangas T, Suomi T, Elo LL. A systematic evaluation of normalization methods in quantitative label-free proteomics. *Brief Bioinform*. 2018;19(1):1-11. doi:10.1093/bib/bbw095

169. Hulsen T, de Vlieg J, Alkema W. BioVenn - A web application for the comparison and visualization of biological lists using area-proportional Venn diagrams. *BMC Genomics*. 2008;9:1-6. doi:10.1186/1471-2164-9-488

170. Goedhart J, Luijsterburg MS. VolcaNoseR is a web app for creating, exploring, labeling and sharing volcano plots. *Sci Rep*. 2020;10(1):1-5. doi:10.1038/s41598-020-76603-3

171. Bender R, Lange S. Adjusting for multiple testing-when and how? *J Clin Epidemiol*. 2001;54:343-349. doi:https://doi.org/10.1016/S0895-4356(00)00314-0

172. Huang DW, Sherman BT, Lempicki RA. Systematic and integrative analysis of large gene lists using DAVID bioinformatics resources. *Nat Protoc*. 2009;4(1):44-57. doi:10.1038/nprot.2008.211

173. Salvesen GS, Marcin D. Emerging principles in protease-based drug discovery. *Nat Rev Drug Discov*. 2010;9(9):690-701. doi:10.1038/nrd3053.Emerging

174. Turk B. Targeting proteases: Successes, failures and future prospects. *Nat Rev Drug Discov*. 2006;5(9):785-799. doi:10.1038/nrd2092

175. Bleuez C, Koch WF, Urbach C, Hollfelder F, Jermutus L. Exploiting protease activation for therapy. *Drug Discov Today*. 2022;27(6):1743-1754. doi:10.1016/j.drudis.2022.03.011

176. Eroglu Z, Ribas A. Combination therapy with BRAF and MEK inhibitors for melanoma: Latest evidence and place in therapy. *Ther Adv Med Oncol*. 2016;8(1):48-56. doi:10.1177/1758834015616934

177. Coupe N, Corrie P, Hategan M, Larkin J, Gore M, Gupta A, Wise A, Suter S, Ciria C, Love S, Collins L, Middleton MR. PACMEL: A phase 1 dose escalation trial of trametinib (GSK1120212) in combination with paclitaxel. *Eur J Cancer*. 2015;51(3):359-366. doi:10.1016/j.ejca.2014.11.018

178. Cori CF, Cori GT. The Carbohydrate Metabolism of Tumors: II. Changes in the Sugar, Lactic Acid, and Co-combining Power of Blood Passing Through a Tumor. *J Biol Chem*. 1925;65(2):397-405. doi:10.1016/s0021-9258(18)84849-9

179. Fiorito V, Chiabrando D, Petrillo S, Bertino F, Tolosano E. The Multifaceted Role of Heme in Cancer. *Front Oncol*. 2020;9(January):1-15. doi:10.3389/fonc.2019.01540

180. Patra KC, Hay N. The pentose phosphate pathway and cancer. *Trends Biochem Sci*. 39(8):347-354. doi:10.1016/j.tibs.2014.06.005

181. Walter M, Herr P. Re-Discovery of Pyrimidine Salvage as Target in Cancer Therapy. *Cells*. 2022;11(4). doi:10.3390/cells11040739

182. Taanman JW. The mitochondrial genome: Structure, transcription, translation and replication. *Biochim Biophys Acta - Bioenerg*. 1999;1410(2):103-123. doi:10.1016/S0005-2728(98)00161-3

183. Bogenhagen DF, Rousseau D, Burke S. The layered structure of human mitochondrial DNA nucleoids. *J Biol Chem*. 2008;283(6):3665-3675. doi:10.1074/jbc.M708444200

184. Guo Y, Gu R, Gan D, Hu F, Li G, Xu G. Mitochondrial DNA drives noncanonical inflammation activation via cGAS–STING signaling pathway in retinal microvascular endothelial cells. *Cell Commun Signal*. 2020;18(1):1-12. doi:10.1186/s12964-020-00637-3

185. Zhang W, Li G, Luo R, Lei J, Song Y, Wang B, Ma L, Liao Z, Ke W, Liu H, Hua W, Zhao K, Feng X, Wu X, Zhang Y, Wang K, Yang C. Cytosolic escape of mitochondrial DNA triggers cGAS-STING-NLRP3 axis-dependent nucleus pulposus cell pyroptosis. *Exp Mol Med*. 2022;54(2):129-142. doi:10.1038/s12276-022-00729-9

186. West AP, Khoury-Hanold W, Staron M, Tal MC, Pineda CM, Lang SM, Bestwick M, Duguay BA, Raimundo N, MacDuff DA, Kaech SM, Smiley JR, Means RE, Iwasaki A, Shadel GS. Mitochondrial DNA stress primes the antiviral innate immune response. *Nature*. 2015;520(7548):553-557. doi:10.1038/nature14156

187. Decout A, Katz JD, Venkatraman S, Ablasser A. The cGAS–STING pathway as a therapeutic target in inflammatory diseases. *Nat Rev Immunol*. 2021;21(9):548-569. doi:10.1038/s41577-021-00524-z

188. Stein MN, Malhotra J, Tarapore RS, Malhotra U, Silk AW, Chan N, Rodriguez L, Aisner J, Aiken RD, Mayer T, Haffty BG, Newman JH, Aspromonte SM, Bommareddy PK, Estupinian R, Chesson CB, Sadimin ET, Li S, Medina DJ et al. Safety and enhanced immunostimulatory activity of the DRD2 antagonist ONC201 in advanced solid tumor patients with weekly oral administration. *J Immunother Cancer*. 2019;7(1):1-9. doi:10.1186/s40425-019-0599-8

189. Feng M, Marjon KD, Zhu F, Weissman-Tsukamoto R, Levett A, Sullivan K, Kao KS, Markovic M, Bump PA, Jackson HM, Choi TS, Chen J, Banuelos AM, Liu J, Gip P, Cheng L, Wang D, Weissman IL. Programmed cell removal by calreticulin in tissue homeostasis and cancer. *Nat Commun*. 2018;9(1):1-15. doi:10.1038/s41467-018-05211-7

190. Gardai SJ, McPhillips KA, Frasch SC, Janssen WJ, Starefeldt A, Murphy-Ullrich JE, Bratton DL, Oldenborg PA, Michalak M, Henson PM. Cell-surface calreticulin initiates clearance of viable or apoptotic cells through trans-activation of LRP on the phagocyte. *Cell*. 2005;123(2):321-334. doi:10.1016/j.cell.2005.08.032